NASA Technical Paper 1301

A Correlation of Mixing Noise From Coannular Jets With Inverted Flow Profiles

S. Paul Pao

APRIL 1979

NASA

NASA Technical Paper 1301

A Correlation of Mixing Noise From Coannular Jets With Inverted Flow Profiles

S. Paul Pao
Langley Research Center
Hampton, Virginia

National Aeronautics
and Space Administration

**Scientific and Technical
Information Office**

1979

CONTENTS

SUMMARY

This report correlates data for jet mixing noise from coannular jets with inverted flow velocity profiles (IVP's). The acoustic performance of coannular jets is measured against a hypothetical single jet with the same mass flow, thrust, and total enthalpy flow as the coannular jet. Coannular jets with velocity ratios greater than 1.2 were found to have lower overall sound power levels than their equivalent jets. The study shows that the magnitude of the sound power reduction was a function of both equivalent jet velocity and velocity ratio and that optimum noise reduction of coannular jets in the data set occurs within a range of equivalent velocities between 500 and 700 meters per second and velocity ratios between 1.6 and 2.3. If the expected sound power level of the single equivalent jet is used as the basis for comparison, the maximum sound power reduction is about 4 decibels.

The jet mixing noise data have been analyzed for directivity and spectra. Directivity indices for coannular jets in different equivalent jet velocity ranges were derived from the data correlation. A special set of spectral curves have been developed to describe the characteristic double peak spectra of coannular jet noise. These spectral curves depend on directivity angle, equivalent jet velocity, and velocity ratio. The combination of empirical curves for overall acoustic power, directivity, and spectra is used to develop a prediction method for aircraft noise from coannular jets. The temperature ratio between the inner and outer streams has not been found to be important in this acoustic correlation. However, the mean temperature effect has been included in the computations of sound pressure levels.

Since the nozzles under consideration are limited in variety, effects of geometric parameters such as radius ratio and area ratio on the acoustic properties of coannular jets are not covered in this study.

INTRODUCTION

Variable-cycle engine designs have been proposed for the advanced supersonic transport. These engine concepts are intended for achieving high efficiency in both subsonic and supersonic flight operations. For a typical design, the jet temperature and velocity in the secondary (outer) stream may be substantially higher than those in the primary (inner) stream at take-off conditions. Such an exhaust flow system is different from that for a conventional coaxial jet where the primary stream has a higher velocity than the fan stream; thus, this system has acquired the name of coannular jet with an inverted velocity profile (IVP).

The NASA Lewis Research Center has sponsored a sequence of experimental programs to establish the acoustic properties of the coannular jet. In references 1 and 2, extensive acoustic measurements are presented for several basic coannular jet nozzle configurations over a large matrix of flow conditions.

The size and quality of these data sets are comparable to the best available data sets on single circular jets.

The original data analyses reported in references 1 and 2 showed that coannular jets with IVP's produce less noise than expected; however, the amount of noise reduction and its dependence on jet operating parameters remain controversial. The controversy is due, in part, to the basis for noise comparison which was used in these earlier data analyses.

The purpose of this report is to correlate the data from references 1 and 2 from a unified point of view. Recent publications (refs. 3, 4, and 5) agree that the noise characteristics of the coannular jet should be compared to those of a fully mixed equivalent jet. This equivalence is a hypothetical single circular jet which has the same mass flow, thrust, and total enthalpy flow as the coannular jet. The equivalent jet is uniquely defined for a given coannular jet flow condition and is a reasonable standard for noise comparison.

Several objectives are accomplished by this data correlation. First, the dependence of noise reduction, measured here in terms of overall acoustic power, on key parameters (such as the equivalent jet velocity and the velocity ratio) is established. This objective may be achieved with confidence because of the large size of the data sets. Second, this correlation provides the basis for an interim noise prediction procedure for coannular jets. Third, key trends are useful in understanding the origin and dynamic process of coannular jet noise emission.

The analysis of the data begins with the static data sets, and correlation curves are developed for the overall acoustic power generated by a coannular jet on a static test stand. Then the directivity index and spectral shapes are developed. After equations for the noise from a nonmoving jet source are established, wind-tunnel data are analyzed for the effect of forward velocity on the coannular jet noise.

SYMBOLS

A	area, m^2
A_e	nozzle exit area defined for equivalent jet, m^2
A_{ref}	reference area for sound power correlation, 1.00 m^2
C_1	convection factor, equation (17)
C_2	convection factor, equation (18)
c_a	ambient speed of sound, m/s
D_e	diameter of equivalent jet, m
$D(\theta)$	directivity factor

f	one-third-octave band center frequency, Hz
I	acoustic intensity, W/m^2
I_{av}	average acoustic intensity, W/m^2
m	forward velocity exponent
$\dot{m}$	mass flow rate, kg/s
$\dot{m}_e$	mass flow rate of equivalent jet, kg/s
$\dot{m}_1$	mass flow rate of primary stream, kg/s
$\dot{m}_2$	mass flow rate of secondary stream, kg/s
$N_{S,e}$	Strouhal number as defined in equation (15)
$N_{S,peak}$	peak Strouhal number for a given spectrum
OASPL	overall sound pressure level, dB re 2×10^{-5} N/m^2
PWL	sound power level, dB re 10^{-12} W
p	acoustic pressure, N/m^2
$\overline{p^2}$	mean-square sound pressure, N^2/m^4
p_a	atmospheric pressure, N/m^2
$p_{t,1}$	total pressure of primary stream, N/m^2
$p_{t,2}$	total pressure of secondary stream, N/m^2
R	spherical radius, m
$N_{S,1}$	peak Strouhal number for first spectral component
$N_{S,2}$	peak Strouhal number for second spectral component
SPL	one-third-octave band sound pressure level, dB re 2×10^{-5} N/m^2
T_a	atmospheric temperature, K
T_e	total temperature of equivalent single jet, K
T_1	total temperature of primary stream, K
T_2	total temperature of secondary stream, K
V	velocity, m/s

V_a forward velocity, m/s

V_e velocity of equivalent single jet, m/s

V_1 velocity of primary stream, m/s

V_2 velocity of secondary stream, m/s

V_θ jet velocity as defined in equation (14), m/s

W corrected sound power, W

W_o sound power, W

γ ratio of specific heats

θ directivity angle from inlet axis, deg

ρ density of air, kg/m^3

ρ_a density of ambient air, kg/m^3

ρ_e density of equivalent single jet, kg/m^3

ω jet density exponent

STATIC MIXING NOISE

Static Data Base

The research programs described in references 1 and 2 were initiated under NASA Lewis Research Center sponsorship to determine noise characteristics of duct-burning turbofan engines. Nozzle configurations studied in these programs included the basic coannular nozzles and a large variety of coannular nozzles with noise suppression devices. The present report correlates the acoustic data for the basic coannular nozzle configurations shown in figures 1 to 5 only (these configurations are named in this report as models 1 to 5, respectively).

Models 1 to 3 were used in reference 1. Model 1, a circular convergent nozzle, was used for calibration throughout the test series. The primary duct fairing (illustrated in fig. 1) within the nozzle did not have any adverse effect on the performance of the convergent nozzle. Models 2 and 3 are coannular nozzles with area ratios 0.75 and 1.20, respectively. The secondary or fan stream and the primary stream exit planes were offset in the axial direction. In both models 2 and 3, the secondary nozzle was convergent and the primary nozzle was convergent-divergent.

The total temperature for both streams was limited to 1100 K or less. The maximum nozzle pressure ratio was approximately 4.0, while the primary stream nozzle pressure ratio was fixed at 1.53 for most run conditions. The acoustic data obtained with models 1, 2, and 3 covered 30 one-third-octave bands, from

100 Hz to 80 kHz, and nine (nominal) directivity angles ranging from 60° to 165° relative to the inlet axis. The acoustic data were corrected to remove atmospheric attenuation effects in accordance with the SAE ARP 866 procedure (ref. 6). The acoustic tests were conducted in an outdoor facility with a polar array of microphones at a radius of 4.57 m away from the primary nozzle exit. Ground effect was not significant for directivity angles greater than 90° in this test facility because the jets exited vertically upward with respect to the ground.

Models 4 and 5 (figs. 4 and 5) were used in reference 2. Model 4 is coannular and has a centerbody within the primary nozzle. Model 5 is a simple coannular nozzle with coplanar fan and primary stream exits. The total temperature for either stream was again limited to 1100 K or less. The primary jet pressure ratio was fixed at either 1.55 or 1.75, while the fan pressure ratio varied from approximately 1.2 to 3.9. The acoustic data obtained with models 4 and 5 covered 30 one-third-octave bands, from 50 Hz to 40 kHz, and covered nominal directivity angles in 10° increments from 30° to 160° relative to the inlet axis. The acoustic tests were conducted in an outdoor facility with a polar array of microphones at a radius of 12.2 m from the nozzle exit reference point. The data have been corrected for atmospheric attenuation effects according to SAE ARP 866 and for ground effects using a method described in reference 2. The published data have also been adjusted for spherical divergence to show sound pressure levels at a reference radius of 45.7 m from the nozzle exit. Over 200 flow conditions are included in these static model acoustic measurements from references 1 and 2. The flow conditions for models 1 to 5 are summarized in tables I to V, respectively.

Equivalent Jet

In replacing the coannular jet with a single equivalent jet, quantities to be conserved are mass flow, thrust, and total enthalpy flow. The total base area of the jet exhaust is also an important consideration in aircraft performance. However, only three constraints can be imposed for constructing a single equivalent jet. Conditions of equal mass flow, thrust, and exit area are often chosen (refs. 3 and 4). In the present report, the conditions selected for constructing the single equivalent jet are equal mass flow, thrust, and total enthalpy flow. In most of the jet exhaust flow conditions covered in this report, the change of total computed nozzle exit area as a result of the conversion is much less than 10 percent. The single jet thus defined is sometimes referred to as the fully mixed equivalent jet because, in theory (assuming no wall friction losses), it can be obtained by actually mixing together the secondary stream and the primary stream by mechanical devices.

For a given coannular jet, the condition of mass flow equivalence gives

$$\dot{m}_e = \dot{m}_1 + \dot{m}_2 \tag{1}$$

The conditions of equivalence of mass flow and thrust give

$$V_e = \frac{\dot{m}_1 V_1 + \dot{m}_2 V_2}{\dot{m}_e} \tag{2}$$

where

$$\dot{m} = \rho A V \tag{3}$$

and the equivalence of mass flow and energy flow gives

$$T_e = \frac{T_1 \dot{m}_1 + T_2 \dot{m}_2}{\dot{m}_e} \tag{4}$$

where the specific heat for constant pressure is assumed to be a constant. The equivalent jet density is then found by the condition that the jet static pressure is equal to the ambient static pressure. The perfect gas law gives

$$\rho_e = \rho_a \left[\frac{T_e}{T_a} - \frac{1}{2}(\gamma - 1)\left(\frac{V_e}{c_a}\right)^2 \right]^{-1} \tag{5}$$

The equivalent jet exit area is then found from

$$A_e = \frac{\dot{m}_e}{\rho_e V_e} \tag{6}$$

and the diameter is

$$D_e = 2\sqrt{\frac{A_e}{\pi}} \tag{7}$$

This single equivalent jet and its acoustic properties provide a reference basis for correlating the overall jet noise power, directivity, and spectral properties of coannular jets.

Typical acoustic spectral data for each of the five model configurations are shown in figures 6 to 10. In each case the measured one-third-octave sound pressure levels are shown at four different angles. The data are shown by symbols for easy identification. Predicted sound pressure levels for the corresponding single equivalent jets, computed according to the SAE ARP 876 procedure (ref. 7), are shown as continuous curves. The acoustic data shown in figure 6 are obtained from model 1. It can be seen that the measured data and the prediction agree with each other because model 1 is a single circular jet. The acoustic data in figures 7 to 10 are typical of coannular jets. The measured sound pressure level is, in general, lower than the predicted equivalent jet sound pressure level. At large angles from the inlet, the coannular jet noise spectrum exhibits a double hump structure which is quite different from a typical circular jet noise spectrum. Hence, it is clear that the SAE circular jet noise prediction method is not capable of describing the acoustic properties of coannular jets.

Analysis of Sound Power

Comparison of the noise level of a coannular jet with that of its single equivalent jet is done on the basis of overall sound power in this report. The noise levels can also be compared on the basis of maximum sound pressure level (refs. 3, 4, and 5). Comparison on the basis of maximum sound pressure level is convenient because the maximum sound pressure level can be obtained directly from the measured data record and can be directly related to perceived noise level for full-scale conditions. However, the sound pressure level comparison is more sensitive to error because its maximum occurs at different directions for different jets; in addition, the maximum level is more susceptible to error due to data scatter than is the case with overall sound power.

The overall sound power can be expressed as an integral of the mean-square sound pressure divided by $\rho_a c_a$ over a reference spherical surface, as follows:

$$W_o = 2\pi R^2 \int_0^{\pi} \frac{\overline{p^2(\theta)}}{\rho_a c_a} \sin\theta \, d\theta \tag{8}$$

For each test condition in references 1 and 2, the mean-square sound pressure is given at approximately 10^o intervals so that an accurate value of overall sound power can be obtained from equation (8). For convenience in comparing different size nozzles, the overall sound power is further normalized with respect to jet density effect and unit nozzle exit area by the equation

$$W = W_o \left(\frac{\rho_e}{\rho_a}\right)^{-\omega} \left(\frac{A_{ref}}{A_e}\right) \tag{9}$$

where the density exponent ω (fig. 11) is taken from reference 8, and the reference area is chosen to be 1 m^2. The standard reference sound power of 10^{-12} W is used to convert the overall sound power to overall sound power level; that is,

$$PWL = 10 \log_{10} W - 120 \tag{10}$$

Figure 12 shows the variation of normalized overall power level with equivalent jet velocity for the single jet cases for model 1. Also shown in figure 12 is the SAE normalized power correlation curve for conical jets from reference 7. It can be seen that the data from model 1 matches the SAE power correlation curve very well. Since the SAE curve is known to be accurate in the prediction of single jet noise, the comparison of the model 1 data validates the entire acoustic test series reported in reference 1. Figures 13 and 14 show the variation of normalized overall sound power level with equivalent jet velocity for all test conditions for models 2 and 3, respectively. Although some of the coannular jet noise data in these figures lie above the SAE curve, indicating a noise increase, these data are associated with those cases where the fan jet velocity is less than 1.2 times the primary jet velocity. Figures 15 to 19 show the normalized power level variation with equivalent jet velocity for five different nominal jet velocity ratios ranging from about 1.2 to 2.3. None of the data points in these figures is above the SAE sound power reference curve.

Figures 20 and 21 show the variation of normalized overall sound power level with equivalent jet velocity for models 4 and 5, respectively, for all test conditions as given in tables IV and V. Only two data points for a single circular jet are included (fig. 20), and both of these are less than 0.5 dB away from the SAE reference curve. Figure 20 shows that the coannular jet noise data of model 4 lie above the SAE power level at the low equivalent jet velocities and below the SAE power level at the high equivalent jet velocities. Again, most of the coannular jet noise data which lie above the SAE curve are for cases where the fan velocity is less than 1.2 times the primary velocity. Of particular interest is a group of data for model 4 where the exhaust flow is from the fan stream only. The data lie significantly below the reference sound power level of the equivalent single jet. Figure 21 shows that most of the data of model 5 lie above the SAE reference.

The overall sound power level comparison confirms that the coannular jet configuration has some noise reduction in comparison to the equivalent single jet configuration. The sound power level reduction is defined as the difference between the equivalent jet noise power level and the measured coannular jet noise power level, with a positive value indicating a noise reduction. The sound power level reduction is dependent upon the coannular jet flow condition for a given nozzle configuration. The equivalent jet velocity and the velocity ratio are assumed to be the most important parameters. Table VI shows these parameters and the power level reduction for models 2, 3, and 4. An analysis of this sound power reduction for these coannular jets is given in the following discussion. The effect of geometrical variation of nozzle configuration on sound power reduction has not been taken into account in this study.

The coannular jet noise data with velocity ratios approximately 1.0 and greater are divided into four groups of different equivalent jet velocities. The variation of sound power level reduction with the velocity ratio for each group is shown in figure 22 for data from models 2 and 3 and in figure 23 for data from model 4. The noise reduction trends of data from model 5 indicate that this nozzle configuration is not in the optimal range for applications. Hence, a detailed analysis of sound power reduction characteristics for this model is not included in this report. A least-square parabolic fit for each group of data points is also shown in these figures. The least-square-fit curves show a consistent trend of sound power level reduction as a function of velocity ratio in each equivalent jet velocity range. There appears to be an optimum velocity ratio for maximum noise reduction with respect to the equivalent single jet, and the optimum value of velocity ratio increases with the increase of equivalent jet velocity. For each equivalent velocity range, the trend of noise reduction as a function of velocity ratio is similar for both data sets from references 1 and 2.

The sound power level data can be analyzed in a somewhat different way. According to the definition of an equivalent single jet, a coannular jet with a velocity ratio of 1.0 should have the same total mass flow and velocity profiles as its equivalent single jet. However, the density distributions in these two jets are different. If effects of density distribution on noise emission are ignored, one may expect that the coannular jet with a velocity ratio of 1.0 will exhibit no noise reduction with respect to the single equivalent jet. With this consideration in mind, the data groups can be analyzed again with the constraints as follows:

(a) The parabolic least-square-fit curve should pass through the point where velocity ratio equals 1.0 and sound power level reduction equals 0.

(b) Only data points with a velocity ratio greater than 1.2 are to be included in the data analysis.

These new curves are shown in figures 22 and 23 as dashed lines. The values of optimum velocity ratio and the corresponding maximum value of sound power reduction are tabulated as follows for models 2, 3, and 4:

Equivalent velocity, m/s	Maximum PWL reductions for -			
	Models 2 and 3		Model 4	
	Velocity ratio	Maximum ΔPWL, dB	Velocity ratio	Maximum ΔPWL, dB
300 to 400	1.4	3.9	1.3	4.1
400 to 500	1.6	3.5	1.6	2.5
500 to 600	1.9	3.9	1.9	3.3
Over 600	2.2	4.0	2.0	2.5

Note that in the 300 to 400 m/s equivalent velocity range only a few data points are available in each data set. When data in the 300 to 400 m/s and the 400 to 500 m/s equivalent velocity ranges are analyzed together using the least-square fit, the results for models 2 and 3 and the results for model 4 agree with each other. In both sets the optimum velocity ratio is near 1.6 and the maximum sound power level reduction is approximately 3.5 dB. At higher velocity ranges, results from model 4 tests show a general optimization at a slightly lower velocity ratio with a smaller sound power level reduction, compared with the corresponding results for models 2 and 3. The data sample size for model 4 is much smaller than the combined data sample size for models 2 and 3, and data scattering may be accountable for some of the differences in the results just mentioned.

The entire data set for models 2 and 3 is plotted in figure 24 where the sound power reduction is shown as a function of both velocity ratio and equivalent jet velocity. The contours in figure 24 are constructed with the aid of the least-square-fit analysis as shown in figure 22. The trends of sound power level reduction as shown by the contours are surprisingly regular. The average value of deviation of data points with respect to the contours is less than 0.7 dB. Data represented in figure 24 fall within the following limits: the velocity ratio is between 1.20 and 2.77; the equivalent single jet velocity is between 250 and 800 m/s; and the sound power level reduction is between 1.5 and 4.8 dB. The trends observable from this figure are summarized as follows:

(1) For each equivalent jet velocity, there is an optimum velocity ratio where the overall sound power level reduction is a maximum.

(2) In order to maintain a given level of sound power reduction, a higher velocity ratio is required for a higher equivalent jet velocity.

(3) The contours of the highest noise reduction level appear to be closed. There is a sufficient data density at the lower end of the closed contours. In the region of high velocity ratio and high equivalent single jet velocity, data points are insufficient to confirm whether contours are actually closed. Hence, this part of the contour is shown as dashed lines in figure 24. It is desirable to obtain more experimental data in the region bounded by velocity ratio of greater than 1.8 and equivalent jet velocity of greater than 600 m/s.

Directivity

The directivity is assumed to be a function of the equivalent single jet velocity. Hence, the data points in a given equivalent single jet velocity range are collected and an empirical directivity for this velocity range is determined from these data points.

The directivity pattern can be normalized in the form of a directivity factor which is defined as

$$D(\theta) = \frac{I(R,\theta)}{I_{av}} \tag{11}$$

where $I(R,\theta)$ is the overall intensity at a given point in the far field and

$$I_{av} = \frac{W}{4\pi R^2} \tag{12}$$

The value of the directivity factor is commonly represented in terms of the directivity index, $10 \log_{10} D(\theta)$, which is a decibel measure.

The directivity index is computed for each of the data cases with a velocity ratio of greater than 1.2. The cases associated with models 2 and 3 are evaluated separately from the cases associated with model 4. Figure 25 shows the variation of directivity index with directivity angle for models 2 and 3 in eight different equivalent jet velocity ranges. Figure 26 shows the corresponding information for model 4 in seven different velocity ranges. The empirical directivity patterns are shown as faired in figures 25 and 26. It can be seen that the peak noise for all models is near a directivity angle of 150°. The peak directivity index increases with increasing equivalent jet velocity. At directivity angles less than 90° from the inlet axis, the original acoustic data are often dominated by the shock noise of the fan stream, and therefore the directivity pattern for angles less than 90° is not determined. An analysis of shock noise from coannular jets is given in a report by Stone (ref. 9). The Stone formulas are known to provide shock noise predictions with reasonable accuracy. The directivity indices for models 2, 3, and 4 in different equivalent jet velocity ranges are presented in table VII. For comparison purposes, the SAE circular jet directivity patterns from reference 7 are also shown in figures 25 and 26.

It should be noted that the position and directivity angle of the acoustic microphones are computed from the center of the nozzle exit plane. However, the dominant jet noise source is often located 8 to 10 nozzle diameters downstream from the nozzle exit plane. The acoustic measurements of models 1, 2, and 3 were made at a distance of 36 diameters away from the nozzle exit plane center, and the measurements of models 4 and 5 were taken at a distance of 80 diameters. If the true source noise location is on the nozzle center line 8 diameters downstream from the nozzle exit plane, the 130° microphone directivity is actually 118.8° for models 1, 2, and 3, and 125.3° for models 4 and 5.

Spectral Characteristics

A special feature of coannular jet noise is that its spectrum in direction near the downstream jet axis contains two peaks, as shown in figure 27. According to reference 3, one can associate the first (low frequency) peak with noise emission from the merged portion of the exhaust flow and the second (high fre-

quency) peak with noise emission from the premerged segment of the fan stream. The observed abrupt transition from the premerged region to the merged region (ref. 1) in the exhaust flow may be the cause for the distinct separation of the spectrum in two parts. The fan stream is supersonic in many of the run conditions in the data set, and shock noise is present. The empirical prediction method proposed by Stone (ref. 9) and the theoretical and experimental work by Harper-Bourne and Fisher (ref. 10) provide a clear description of shock noise. Hence, efforts of data correlation in this report concentrated upon the understanding of the mixing noise.

An empirical procedure is employed here to analyze the spectral properties of the data. Each spectrum is normalized with respect to its own overall spectral level, and the Strouhal number is based upon the equivalent jet velocity with a temperature correction factor recommended by Stone (ref. 11)

$$N_{S,e} = \frac{fD_e}{V_e}\left(\frac{T_e}{T_a}\right)^{0.4} \tag{13}$$

Since the geometry of models 2 and 3 is different from that of model 4, the corresponding data sets are analyzed separately, although the same method of analysis is used.

Spectral data for models 2 and 3 are shown in figure 28. The spectra for directivity angles between 90° and 120° have a single peak. The double-peak characteristic is clearly shown for angles greater than 120°. A single-peak spectrum can be characterized by the shape of the spectral distribution and the value of the peak Strouhal number. A double-peak spectrum is assumed to be the sum of two partial spectral distributions with identical shape. Such a spectrum can be specified by the values of the first and the second peak Strouhal number, the relative sound pressure level between these peaks, and the shape of the partial spectral distribution. In order to analyze the data set according to this empirical scheme, the normalized spectrum is collected according to emission angle and equivalent jet velocity groups. The following empirical relations are observed:

(1) The shapes of spectral distributions for a single-peak spectrum and the shapes of partial spectral distribution for a double-peak spectrum vary with angle. These shapes are, however, independent of either the equivalent jet velocity or the velocity ratio.

(2) The value of the peak Strouhal number for each spectral distribution is a function of angle, equivalent jet velocity, and secondary stream velocity.

(3) The relative sound pressure level of the first and the second peak of a double-peak spectrum is a function of angle, equivalent jet velocity, and the velocity ratio.

The shapes of the spectral distribution are summarized in figure 29. The spectral distribution remains essentially unchanged between 90° and 110°.

Beyond 110°, the distribution becomes narrower with increasing values of θ. It appears from the data that noise from the high-velocity premerged region is radiated primarily to the side, while noise from the lower velocity merged region is radiated toward the aft arc. Therefore, an attempt is made to correlate the spectral data by defining a Strouhal number with the velocity as a function of angle. The velocity varies from the secondary stream velocity at 120° to the mixed velocity at 150°. The equation for this velocity is

$$\left.\begin{aligned} V_\theta &= V_2 && (\theta \leq 120^\circ) \\ V_\theta &= \frac{30V_e + (V_2 - V_e)(150 - \theta)}{30} && (120^\circ < \theta < 150^\circ) \\ V_\theta &= V_e && (\theta \geq 150^\circ) \end{aligned}\right\} \tag{14}$$

and the corresponding Strouhal number is

$$N_{S,e} = \frac{fD_e}{V_\theta}\left(\frac{T_e}{T_a}\right)^{0.4} \tag{15}$$

The values of the first and second peak Strouhal number as functions of the inlet angle and the equivalent jet velocity are shown in figures 30 and 31. In general, the first peak Strouhal number varies slowly with the equivalent velocity while the second peak Strouhal number is very sensitive to changes in V_e. At angles smaller than 120° the first and the second peaks merge to the same value. Figure 31 shows that the value of the second peak Strouhal number decreases rapidly with increasing inlet angle for cases with high equivalent jet velocities. When the high-frequency part of the spectrum is associated with noise emission from the premerged segment of the fan stream, this rapid shift in peak Strouhal number may be a result of fluid dynamic shielding as described by Pao (ref. 12) and Balsa (ref. 13). According to these theories, the pressure fluctuations which originate in the fan stream must pass through a long segment of the merged stream before they emerge as acoustic waves. The attenuation of high-frequency sound through this process is substantial. As the angle increases, the attenuation to the high-frequency portion of the spectrum increases dramatically, and the result is a rapid shift of the observed second peak to lower Strouhal numbers.

The relative sound pressure level of the second peak with respect to the first peak in a double-peak spectrum for various angles is shown in figure 32. At 120° the SPL's for the two peaks are almost the same for all values of V_e and the velocity ratio. Hence, the double-peak spectrum should merge smoothly into the single-peak spectrum for lower angles. At angles larger than 120°, the relative SPL depends strongly on both the equivalent jet velocity and the velocity ratio.

The data set associated with model 4 is analyzed in the same manner. A sample set of normalized spectra is shown in figure 33. Finally, the normalized shapes of the spectral distribution for all angles between 120° and 160° are shown in figure 34. In general, the typical values of all the spectral parameters of model 4 are different from those associated with models 2 and 3. The trends of the data, however, are quite similar among all these models. A spectrum measured in directions between 90° and 120° has only a single peak, and the double-peak structure of the spectrum appears at angles 120° or greater. The values of the first and the second peak Strouhal number as a function of V_e are shown in figures 35 and 36. The relative SPL between the second and the first peak is shown in figure 37.

FORWARD FLIGHT EFFECTS

Wind-Tunnel Data Base

In view of the potential noise reduction characteristics of the coannular jet configuration, it is important to investigate whether the coannular jet retains its acoustic advantage over a single circular jet under flight conditions. The data considered in this report are obtained from references 14 and 15. This simulated forward flight experiment was performed in a free-jet wind tunnel with model scale coannular jets. These models are referred to as models 6 and 7 in this report, and their configurations are shown in figures 38 and 39. Essentially, these models are scaled down versions of models 2 and 3. A single circular jet nozzle model serving a purpose similar to that of model 1 was also used in a simulated flight test series to provide a reference for the acoustic data.

The test conditions are listed in tables VIII and IX. Owing to facility limitations, a cold primary jet (394 K) was used. Furthermore, the maximum fan jet temperature was 708 K which is considerably less than the maximum fan jet temperature of 1100 K for the corresponding static test series with models 2 and 3. The microphones were located at a distance of 36 diameters from the center of the nozzle exit, and the range of acoustic recording was between 50 Hz and 80 kHz. The measured data were corrected for atmospheric attenuation and refraction effects of the free shear layer at the boundary of the free jet flow.

Typical acoustic spectra for models 6 and 7 at various free-jet tunnel velocities are presented in figures 40 to 45. The expected sound pressure levels for the equivalent single jet based on the SAE ARP 876 (ref. 7) prediction method are included in these figures. At tunnel velocities below 30 m/s, the spectra are similar to those observed in the static test series. However, the sound pressure level at the high-frequency end of the spectrum appears to be higher than expected. For free-jet velocities greater than 60 m/s, some irregularities in the spectrum can be observed at the lower end of the spectrum. These low-frequency irregularities can be attributed to tunnel interference effects. In the data analysis of the present report, the low-frequency portion of the spectrum has been corrected according to the expected SAE spectral shape in order to remove the irregularities in the measured data.

Owing to the presence of irregularities in the spectrum in addition to the presence of shock noise, it is difficult to analyze the simulated flight acoustic data with respect to directivity and spectral characteristics. Hence, only relations of the overall sound power level under flight conditions were investigated. The computation of overall sound power follows the same procedure presented in an earlier section. Figure 46 shows the overall power levels for test cases using models 6 and 7 (see tables VIII and IX) as well as the single jet test cases. The summary of computed sound power of the single jet equivalent in static environment is indicated as a curve in the same figure. Furthermore, the variations of measured overall sound power with five different tunnel velocities are shown in figure 47. Note that the decrease of overall sound power of the coannular jets with increasing tunnel velocity is consistent with the trends of a single circular jet under the same simulated flight conditions.

Correlation Methods

Two different methods of correlating the simulated forward flight jet noise data are investigated in the present report. The main objective is to relate the acoustic characteristics in flight to the corresponding acoustic estimates in a static environment. Note that the changes in flow interaction between the coannular jet exhaust and the ambient air under forward flight conditions are very complex. These empirical methods of correlation are adequate only for obtaining an interim understanding of the observed trends of noise emission.

Method I.- As Stone (ref. 11) suggests, forward motion affects both the source strength and convective amplification in jet noise emission. Hence, the following formula was chosen to correlate the forward flight effect:

$$\overline{p^2}_{static} = \overline{p^2}_{flight}\left(\frac{V_\theta}{V_\theta - V_a}\right)^m\left(\frac{C_2}{C_1}\right)^{2.5} \tag{16}$$

Here, V_θ varies with directivity angle according to equation (14), m is an index governing the variation in source strength, and C_1 and C_2 are convection factors based on the Lighthill theory:

$$C_1 = \left(1 + 0.6\,\frac{V_\theta}{c_a}\cos\theta\right)^2 + 0.06\left(\frac{V_\theta}{c_a}\right)^2 \tag{17}$$

$$C_2 = \left(1 + 0.6\,\frac{V_\theta - V_a}{c_a}\cos\theta\right)^2 + 0.06\left(\frac{V_\theta - V_a}{c_a}\right)^2 \tag{18}$$

The index m was chosen to be a function of θ as shown in figure 48. Note that these values are different from those recommended by Stone for applications to single circular jets. In addition, the choice of a variable index deviates from Stone's original line of thought where coefficients and exponents in the formulas are always kept constant. With equation (16), the measured mean-square overall sound pressure in the simulated flight data set can be converted to static conditions. The overall sound power level under static conditions is then computed according to equation (10). The results are summarized in figure 49. It can be seen in figure 49 that equation (16) produced a slight overcorrection for the forward flight acoustic data.

Method II.- The recommended procedure according to SAE ARP 876 (ref. 7) is used in this case. Essentially, it is a simplified approach compared to method I in which all of the flight effects, including changes in source strength and convection, are represented by a power function of the flight-to-static relative velocity ratio:

$$\overline{p^2}_{static} = \overline{p^2}_{flight}\left(\frac{V_e}{V_e - V_a}\right)^m \left(1 - \frac{V_a}{c_a}\cos\theta\right) \tag{19}$$

A Doppler factor is also included in this formula. The power index m varies with θ and a curve representing this function is shown in figure 50 which is proposed by Hoch of Société National d'Etude et de Construction de Moteurs d'Aviation, France (SNECMA). Based on this formula, the mean-square sound pressure at each angle is converted to its static value and the overall sound power level is computed according to equation (10). Results of the sound power converted to static condition shown in figure 51 are similar to the results of method I. Individual sets of results for each tunnel velocity are shown in figure 52. These figures illustrate that the flight-to-static data correlation by this method is uniformly valid for all the tunnel velocities within the range of the acoustic test conditions. Also, according to recent discussions in the SAE A-21 committee, comparisons of various methods of flight effect corrections in the industry indicate that the Hoch-proposed power index should be modified.

Some preliminary investigation of forward flight effects on the acoustic spectrum indicated that data correction using either method I or method II produces unsatisfactory results in the spectrum. An alternative is to apply the flight effect correction to the high-frequency and the low-frequency portions of the spectrum separately. According to previous discussions, the high- and low-frequency portions of the spectrum are associated with the fan stream and the merged stream, respectively. Hence, the forward flight effect on these partial spectra can be assumed to scale with the relative velocity ratio of their corresponding flow segments in the jet exhaust.

From the results of references 14 and 15 as well as from the analyses of this section, one may conclude that the effects of forward flight on coannular jets are similar to those applicable to single circular jets. Hence, the coannular jet retains its relative acoustic advantage over its single equivalent jet in forward flight. The methods currently available to account for the for-

ward flight effects on coannular jets are, however, not sufficiently accurate. Further research is needed to understand the complex dynamic interaction between the dual flow jet exhaust and the ambient so that better acoustic scaling rules can be defined.

For the purpose of an interim noise prediction procedure, use of method II is recommended since the measured data trends can be described adequately by this method. The high-frequency and the low-frequency portions of the spectrum should be, however, dealt with separately using the relative velocity ratio of the fan stream and the merged stream.

CONCLUDING REMARKS

According to results of this data review, important trends of basic acoustic properties of coannular jets can be summarized as follows:

1. The temperature effect on coannular jet noise is incorporated into the data correlation in the same manner as that adopted for single jets. The density exponent originally proposed by Hoch was used for the normalization of sound power, and a temperature correction factor proposed by Stone was adopted for the normalization of Strouhal numbers.

2. The coannular jets with a velocity ratio greater than 1.2 are quieter than their corresponding single equivalent jets, and the sound power level reduction with respect to the single equivalent jet appears to be a smooth continuous function of both the equivalent jet velocity and the velocity ratio.

3. At each given equivalent jet velocity, there is an optimum velocity ratio at which the noise reduction level is a maximum. At the lower equivalent velocity range of less than 400 meters per second the optimum velocity ratio is approximately 1.6, and at equivalent velocities beyond 600 meters per second the optimum velocity ratio can exceed 2.0.

4. There are an insufficient number of data points in the areas of velocity ratio greater than 1.8 and equivalent jet velocity greater than 600 meters per second to define clearly the trends of sound power reduction. Since this region is important for engineering design applications, further data should be obtained in this domain.

5. The variation of spectral shape of coannular jet noise follows a complex pattern. In general, the spectrum has a single peak for angles less than 120° from the inlet and has a recognizable double peak for angles equal to or greater than 120°. Use of an empirical method of correlation shows the spectral shape to follow a consistent pattern of dependence upon direction, equivalent jet velocity, and the velocity ratio. The noise radiation characteristics are different for coannular jets with a center plug and those without a center plug.

6. The forward flight effects were reviewed very briefly in this report. There is a lack of understanding of the dynamic interaction between the coannular jet and the ambient atmosphere in forward flight conditions. Further theoretical and experimental studies should be performed so that a scaling law can

be established. The existing empirical methods of data correlation, however, seem adequate for the description of observed forward flight effects.

7. Because this data review has encompassed sufficient details of the expected acoustic properties of coannular jets, an interim noise prediction procedure can be established directly from these results. Such an interim prediction procedure has been adopted in the NASA Aircraft Noise Prediction Program system. This method differs from a method proposed recently by Stone (NASA TM-73838) and other methods in the industry. Comparison among these methods should offer an opportunity for investigating the basic properties of coannular jet noise from different points of view.

Langley Research Center
National Aeronautics and Space Administration
Hampton, VA 23665
February 6, 1979

REFERENCES

1. Kozlowski, Hilary; and Packman, Allan B.: Aerodynamic and Acoustic Tests of Duct-Burning Turbofan Exhaust Nozzles. NASA CR-2628, 1976.

2. Knott, P. R.; Stringas, E. J.; Brausch, J. F.; Staid, P. S.; Heck, P. H.; and Latham, D.: Acoustic Tests of Duct-Burning Turbofan Jet Noise Simulation. NASA CR-2966, 1978.

3. Packman, A. B.; Kozlowski, H.; and Gutierrez, O.: Jet Noise Characteristics of Unsuppressed Duct Burning Turbofan Exhaust System. J. Aircraft, vol. 14, no. 3, Mar. 1977, pp. 227-232.

4. Crouch, R. W.; Coughlin, C. L.; and Paynter, G. C.: Nozzle Exit Flow Profile Shaping for Jet Noise Reduction. AIAA Paper No. 76-511, July 1976.

5. Cargill, A. M.; and Duponchel, J. P.: The Noise Characteristics of Inverted Velocity Profile Coannular Jets. AIAA Paper 77-1263, Oct. 1977.

6. Standard Values of Atmospheric Absorption as a Function of Temperature and Humidity for Use in Evaluating Aircraft Flyover Noise. ARP 866, Soc. Automot. Eng., Aug. 31, 1964.

7. Gas Turbine Jet Exhaust Noise Prediction. ARP 876, Soc. Automot. Eng., Mar. 1978.

8. Hoch, R. G.; Duponchel, J. P.; Cocking, B. J.; and Bryce, W. D.: Studies of the Influence of Density on Jet Noise. SNECMA and NGTE paper presented at the First International Symposium on Air Breathing Engines (Marseille, France), June 19-23, 1972.

9. Stone, James R.: An Empirical Model for Inverted-Velocity-Profile Jet Noise Prediction. Paper presented at the Ninety-Fourth Meeting of the Acoustical Society of America (Miami, Fla.), Dec. 13-16, 1977. (Available as NASA TM-73838.)

10. Harper-Bourne, M.; and Fisher, M. J.: The Noise From Shock Waves in Supersonic Jets. Noise Mechanisms, AGARD-CP-131, Mar. 1974, pp. 11-1 - 11-13.

11. Stone, James R.: Interim Prediction Method for Jet Noise. NASA TM X-71618, 1974.

12. Pao, S. P.: Aerodynamic Noise Emission From Turbulent Shear Layers. J. Fluid Mech., vol. 59, pt. 3, July 1973, pp. 451-479.

13. Balsa, T. F.: The Acoustic Field of Sources in Shear Flow With Application to Jet Noise: Convective Amplification. J. Fluid Mech., vol. 79, pt. 1, Jan. 1977, pp. 33-47.

14. Packman, A. B.; Ng, K. W.; and Chen, C. Y.: Effect of Simulated Forward Speed on the Jet Noise of Inverted Velocity Profile Coannular Nozzles. AIAA 4th Aeroacoustics Conference, CP-77-1329, American Inst. Aeronaut. & Astronaut., Oct. 1977.

15. Kozlowski, Hilary; and Packman, Allan B.: Flight Effects on the Aero/ Acoustic Characteristics of Inverted Profile Coannular Nozzles. NASA CR-3018, 1978.

TABLE I.- STATIC TEST CONDITIONS FOR MODEL 1

Test	$p_{t,1}/p_a$	T_1, K	$\dot{m}_1$, kg/s	V_1, m/s
1	1.150	388.7	1.909	173.7
2	1.160	914.8	1.333	274.0
3	1.290	1091.5	1.656	395.0
4	1.300	695.9	2.058	316.4
5	1.300	885.4	1.876	361.2
6	1.310	395.9	2.832	244.4
7	1.530	699.5	2.763	401.7
8	1.530	812.6	2.580	433.4
9	1.530	1086.5	2.254	502.9
10	1.540	894.3	2.479	456.6
11	1.540	403.2	3.710	305.7
12	1.800	413.2	4.495	357.8
13	1.800	900.9	3.029	531.9
14	1.800	1072.6	2.751	580.0
15	1.820	704.8	3.485	474.9
16	2.010	816.5	3.630	547.1
17	2.420	425.9	6.119	437.4
18	2.500	1060.9	3.948	707.7
19	2.520	824.3	4.492	624.8
20	2.530	895.9	4.383	652.9
21	2.540	702.0	4.940	577.6
22	2.640	414.8	6.645	450.2
23	3.000	904.3	5.496	702.3
24	3.150	719.3	6.094	640.1
25	3.210	1060.4	4.908	816.3

TABLE II.- STATIC TEST CONDITIONS FOR MODEL 2

Test	$p_{t,1}/p_a$	$p_{t,2}/p_a$	T_1, K	T_2, K	$\dot{m}_1$, kg/s	$\dot{m}_2$, kg/s	V_1, m/s	V_2, m/s
1	1.540	1.140	380.9	369.8	2.313	0.818	297.5	167.9
2	1.530	1.290	384.3	688.7	2.316	.886	297.5	310.3
3	1.520	1.290	389.8	903.7	2.304	.785	297.2	358.4
4	1.520	1.780	380.9	377.6	2.280	1.969	293.5	340.2
5	1.520	1.800	387.1	705.4	2.297	1.481	296.6	468.8
6	1.530	2.480	382.1	379.8	2.302	2.815	296.6	418.2
7	1.520	1.770	402.1	885.9	2.256	1.319	301.8	521.5
8	1.530	1.800	407.6	1077.1	2.277	1.212	306.3	582.5
9	1.520	2.480	403.7	705.9	2.244	2.094	302.7	573.0
10	1.520	2.510	407.6	892.6	2.248	1.897	304.2	648.9
11	1.540	2.490	413.7	1065.9	2.263	1.725	310.0	708.4
12	1.530	3.230	395.4	389.8	2.190	3.460	301.8	473.0
13	1.530	3.220	399.8	702.6	2.253	2.715	303.9	637.6
14	1.530	3.160	400.9	893.7	2.247	2.411	303.6	716.3
15	1.530	3.210	413.2	1077.1	2.249	2.233	309.7	793.1
16	1.530	4.080	422.6	1090.4	2.243	2.820	311.5	864.1
17	1.540	1.310	692.6	385.9	1.725	1.164	402.9	238.7
18	1.520	1.290	697.1	683.2	1.725	.868	399.3	312.7
19	1.520	1.290	693.7	904.8	1.746	.762	399.6	358.1
20	1.540	1.800	695.9	393.2	1.714	1.921	402.6	349.6
21	1.510	1.780	694.8	703.7	1.704	1.442	396.2	464.2
22	1.520	1.800	693.2	906.5	1.694	1.280	397.5	534.0
23	1.550	1.800	696.5	1082.6	1.759	1.188	406.9	582.8
24	1.540	2.510	708.7	399.8	1.684	2.711	409.0	431.3
25	1.530	2.500	695.9	704.3	1.718	2.096	400.8	573.9
26	1.530	2.490	699.8	898.2	1.725	1.864	402.3	648.6
27	1.520	2.550	700.9	1093.7	1.711	1.716	399.9	724.8
28	1.530	3.190	700.9	394.3	1.658	3.497	401.7	473.4
29	1.530	3.170	704.8	705.4	1.681	2.655	402.6	635.2
30	1.530	3.190	704.8	901.5	1.679	2.376	402.3	721.8
31	1.510	4.110	713.2	1100.4	1.687	2.820	399.9	870.5
32	1.560	1.320	810.9	388.7	1.611	1.163	441.7	243.8
33	1.530	1.300	806.5	897.7	1.613	.855	431.0	320.6
34	1.520	1.290	811.5	888.2	1.612	.772	431.0	357.2
35	1.540	1.810	820.9	395.9	1.594	1.916	440.1	353.0
36	1.530	1.790	803.7	699.3	1.594	1.456	429.8	465.7
37	1.520	1.810	805.4	887.1	1.625	1.302	429.2	534.0
38	1.520	1.810	808.7	897.1	1.625	1.302	429.2	534.0
39	1.530	1.780	808.7	1089.3	1.612	1.177	433.1	579.7
40	1.530	2.500	810.9	400.9	1.574	2.710	431.6	431.6
41	1.520	2.500	806.5	702.6	1.567	2.098	429.5	573.0
42	1.530	2.500	808.7	907.1	1.569	1.846	431.3	653.2

TABLE II.- Concluded

Test	$p_{t,1}/p_a$	$p_{t,2}/p_a$	T_1, K	T_2, K	$\dot{m}_1$, kg/s	$\dot{m}_2$, kg/s	V_1, m/s	V_2, m/s
43	1.520	2.460	805.4	1094.8	1.594	1.684	429.8	713.8
44	1.540	3.210	814.3	398.7	1.789	3.491	437.4	477.3
45	1.520	3.150	812.6	703.2	1.532	2.637	429.5	632.5
46	1.520	3.190	807.1	907.6	1.562	2.381	428.2	724.5
47	1.520	3.180	808.7	1097.1	1.589	2.165	431.0	797.1
48	1.510	4.030	819.3	1088.7	1.563	2.747	428.2	860.1
49	1.520	1.300	1085.9	378.7	1.393	1.088	499.3	236.2
50	1.530	1.290	1093.2	692.1	1.381	.839	502.3	312.7
51	1.520	1.300	1086.5	899.8	1.388	.750	499.6	361.2
52	1.530	1.790	1053.7	395.9	1.392	1.868	495.9	349.0
53	1.520	1.810	1094.3	706.5	1.360	1.432	499.9	472.1
54	1.540	1.790	1087.1	879.8	1.387	1.278	507.5	523.3
55	1.530	1.800	1083.2	1080.4	1.398	1.178	502.3	583.4
56	1.520	2.510	1053.2	401.5	1.363	2.704	490.7	432.2
57	1.540	2.500	1096.5	690.9	1.355	2.067	506.6	568.1
58	1.540	2.530	1094.3	904.8	1.374	1.862	508.4	655.9
59	1.540	2.530	1099.8	1133.2	1.372	1.711	508.1	735.8
60	1.520	3.210	1058.7	397.6	1.353	3.475	492.6	477.0
61	1.530	3.230	1087.1	719.8	1.352	2.679	502.9	646.5
62	1.510	3.130	1088.7	929.8	1.309	2.299	494.4	727.9
63	1.540	3.190	1077.1	1082.6	1.366	2.185	504.1	792.5
64	1.530	4.080	1098.2	1108.7	1.333	2.792	504.1	872.0
65	2.000	1.300	808.2	708.2	2.118	.856	543.5	323.4
66	2.020	1.790	809.8	705.4	2.136	1.443	547.7	468.8
67	2.020	1.790	808.7	1087.1	2.142	1.176	546.5	582.2
68	1.990	2.470	810.4	1085.4	2.084	1.674	541.6	711.4
69	2.010	3.120	810.9	705.4	2.078	2.629	545.6	631.2
70	2.010	4.120	789.3	1093.2	2.128	2.859	538.0	867.8
71	2.500	1.310	805.9	694.3	2.665	.829	614.8	320.3
72	2.500	1.790	809.3	701.5	2.656	1.420	616.0	467.3
73	2.480	1.780	808.7	1084.3	2.632	1.144	613.0	578.2
74	2.450	2.480	812.1	1093.2	2.609	1.684	610.8	715.7
75	2.500	3.190	820.9	708.2	2.581	2.662	620.9	637.9
76	2.500	4.040	829.3	1099.3	2.376	2.784	624.2	865.3
77	2.720	.000	694.3	515.9	3.016	.000	592.2	623.9
78	2.710	1.260	700.4	1092.6	3.039	.672	594.1	377.6
79	2.710	1.300	703.2	899.3	3.004	.766	595.0	363.9
80	2.720	1.430	698.7	701.5	3.007	1.030	594.7	372.5
81	2.720	1.950	478.2	351.5	2.973	2.130	595.6	361.5

TABLE III.- STATIC TEST CONDITIONS FOR MODEL 3

Test	$p_{t,1}/p_a$	$p_{t,2}/p_a$	T_1, K	T_2, K	$\dot{m}_1$, kg/s	$\dot{m}_2$, kg/s	V_1, m/s	V_2, m/s
1	1.530	1.300	389.3	702.0	1.823	1.089	299.0	318.8
2	1.520	1.800	396.5	702.0	1.782	1.842	301.1	468.8
3	1.530	1.810	397.6	1084.8	1.774	1.516	303.0	586.1
4	1.520	2.460	398.7	704.3	1.755	2.584	298.4	570.3
5	1.540	2.500	419.8	1088.7	1.704	2.165	312.4	716.9
6	1.530	3.180	414.3	707.0	1.745	3.347	308.8	637.0
7	1.520	3.450	448.7	1094.3	1.617	2.963	319.7	820.8
8	1.530	1.300	807.0	708.2	1.282	1.048	432.5	323.4
9	1.540	1.820	812.6	698.7	1.204	1.896	435.9	470.6
10	1.530	1.820	807.6	1082.0	1.212	1.515	431.0	587.3
11	1.530	2.510	809.3	700.9	1.151	2.703	432.8	573.9
12	1.540	2.500	807.0	1088.7	1.192	2.156	434.0	716.6
13	1.530	3.200	810.9	701.5	1.123	3.461	434.0	635.5
14	1.530	4.060	843.7	1079.8	1.230	3.414	441.7	858.9

TABLE IV.- STATIC TEST CONDITIONS FOR MODEL 4

Test	$p_{t,1}/p_a$	$p_{t,2}/p_a$	T_1, K	T_2, K	$\dot{m}_1$, kg/s	$\dot{m}_2$, kg/s	V_1, m/s	V_2, m/s
1	1.510	0.000	808.3	0.0	2.289	0.000	426.1	0.0
2	1.564	.000	549.4	.0	2.931	.000	364.2	.0
3	1.369	1.524	557.8	398.3	2.345	2.120	310.3	301.4
4	1.377	2.074	557.2	551.7	2.372	2.503	313.0	456.9
5	1.389	2.734	551.1	752.2	2.423	2.807	315.5	616.9
6	1.555	1.176	552.2	281.7	2.875	1.478	363.0	160.0
7	1.574	1.274	562.8	363.9	2.894	1.616	371.2	221.0
8	1.581	1.504	557.8	393.3	2.924	2.090	371.2	294.7
9	1.583	1.738	556.7	463.3	2.931	2.315	371.2	368.8
10	1.552	2.897	552.8	573.9	2.813	3.363	362.4	549.9
11	1.597	2.456	555.6	666.7	2.968	2.684	374.3	552.0
12	1.566	2.902	557.2	1006.1	2.917	2.581	367.3	734.0
13	1.552	2.657	556.7	1097.2	2.883	2.260	363.6	739.4
14	1.580	3.275	557.8	916.1	2.919	3.027	370.9	732.1
15	1.539	1.341	680.0	371.1	2.497	1.750	398.7	245.1
16	1.532	1.849	676.7	487.8	2.530	2.408	395.6	397.5
17	1.525	2.640	678.9	730.0	2.514	2.753	394.4	598.3
18	1.536	3.552	677.2	1000.0	2.542	3.136	397.2	787.6
19	1.528	3.188	689.4	1076.1	2.527	2.738	398.4	787.9
20	1.513	1.204	811.1	282.2	2.265	1.587	427.6	171.3
21	1.506	1.417	806.7	377.8	2.257	1.947	424.3	268.5
22	1.509	1.631	808.9	437.2	2.260	2.208	425.8	338.6
23	1.518	1.953	808.9	523.3	2.283	2.423	428.9	427.9
24	1.513	2.873	810.6	776.1	2.267	2.900	427.6	640.1
25	1.509	3.877	804.4	1087.2	2.322	3.276	424.6	845.5
26	1.630	1.226	426.7	297.8	3.419	1.730	334.4	197.5
27	1.632	1.612	423.3	425.0	3.494	2.206	333.5	330.1
28	1.634	2.254	428.9	608.3	3.476	2.583	335.9	504.1
29	1.641	2.577	247.2	523.9	3.503	3.190	336.8	499.6
30	1.619	2.604	426.7	930.0	3.488	2.415	332.2	673.0
31	1.651	3.025	428.9	456.7	3.521	4.022	339.2	498.7

TABLE IV.- Concluded

Test	$p_{t,1}/p_a$	$p_{t,2}/p_a$	T_1, K	T_2, K	$\dot{m}_1$, kg/s	$\dot{m}_2$, kg/s	V_1, m/s	V_2, m/s
32	1.642	2.980	430.6	832.8	3.498	2.900	338.3	673.3
33	1.768	1.176	277.2	281.1	4.739	1.477	289.6	160.0
34	1.764	1.335	280.6	371.7	4.700	1.760	290.8	243.2
35	1.777	1.508	285.6	391.7	4.702	2.104	295.0	295.4
36	1.782	2.048	282.2	543.2	4.739	2.484	293.8	449.3
37	1.790	2.601	284.4	437.2	4.736	3.541	296.0	458.4
38	1.779	2.712	283.9	753.3	4.715	2.780	294.1	615.1
39	1.796	3.179	288.9	648.9	4.717	3.524	299.0	606.9
40	1.755	1.494	814.4	392.2	2.715	2.072	494.7	292.3
41	1.757	2.171	806.1	583.3	2.732	2.542	492.6	483.1
42	1.736	3.873	808.9	1091.1	2.724	3.302	488.6	846.7
43	1.871	1.947	551.1	520.0	3.564	2.421	426.4	425.8
44	1.869	2.861	557.2	786.1	3.539	2.866	428.5	643.1
45	1.860	3.864	556.7	1091.7	3.564	3.293	426.7	846.4
46	2.066	1.589	810.6	426.7	3.165	2.160	554.5	325.8
47	2.056	2.426	816.7	668.3	3.138	2.646	555.0	549.6
48	2.043	3.696	811.7	1033.9	3.166	3.243	551.1	811.7
49	2.560	1.750	808.9	467.2	3.927	2.319	621.5	372.5
50	2.460	2.725	802.2	742.2	3.833	2.846	607.5	611.7
51	2.461	3.401	806.7	953.9	3.827	3.110	609.3	757.4
52	0	2.410	0	665.6	0	2.684	0	546.5
53	0	2.832	0	783.3	0	2.875	0	639.2
54	0	2.866	0	786.1	0	2.875	0	643.4
55	0	3.012	0	827.8	0	2.937	0	673.6
56	0	3.565	0	993.3	0	3.160	0	785.8
57	0	2.907	0	1000.0	0	2.567	0	732.4
58	0	3.721	0	1036.7	0	3.225	0	814.4
59	0	2.091	0	1056.1	0	1.795	0	639.5
60	0	3.819	0	1076.7	0	3.245	0	837.3
61	0	3.843	0	1080.0	0	3.290	0	840.0

TABLE V.- STATIC TEST CONDITIONS FOR MODEL 5

Test	$p_{t,1}/p_a$	$p_{t,2}/p_a$	T_1, K	T_2, K	$\dot{m}_1$, kg/s	$\dot{m}_2$, kg/s	V_1, m/s	V_2, m/s
1	1.352	1.533	527.8	393.9	2.348	2.128	296.3	301.8
2	1.365	2.732	551.1	738.9	2.305	2.800	306.9	610.8
3	1.363	2.058	547.2	552.2	2.310	2.458	305.4	455.1
4	1.536	1.174	549.4	301.7	2.787	1.408	357.2	164.9
5	1.567	1.252	552.8	363.9	2.855	1.538	366.1	213.4
6	1.558	1.496	550.0	388.3	2.840	2.070	363.0	291.4
7	1.590	1.589	425.0	423.9	3.336	2.163	325.5	325.2
8	1.560	1.728	552.2	452.8	2.838	2.304	364.2	363.0
9	1.576	2.858	547.8	562.8	2.888	3.380	366.7	541.6
10	1.568	2.424	553.3	664.4	2.854	2.629	366.7	547.7
11	1.566	2.886	551.7	980.6	2.860	2.556	365.5	722.7
12	1.566	2.658	559.4	1093.3	2.841	2.223	368.2	737.9
13	1.590	3.269	552.2	890.6	2.913	3.042	371.6	721.2
14	1.535	1.337	673.3	359.4	2.504	1.781	395.6	239.9
15	1.549	2.654	671.7	717.8	2.544	2.766	399.3	594.4
16	1.537	3.565	682.8	995.0	2.497	3.132	399.0	786.4
17	1.524	3.199	681.7	1083.9	2.469	2.686	394.7	791.6
18	1.481	1.159	806.1	301.7	2.171	1.348	415.7	158.5
19	1.504	1.433	816.1	356.7	2.204	2.022	426.4	264.9
20	1.513	1.646	802.8	428.3	2.240	2.235	425.5	338.0
21	1.523	1.945	791.7	512.8	2.278	2.413	425.8	422.5
22	1.518	2.859	807.2	788.9	2.251	2.837	428.2	643.7
23	1.497	3.888	812.8	1093.3	2.200	3.251	423.1	848.6
24	1.612	1.223	422.8	302.8	3.390	1.589	329.2	184.7

TABLE V.- Concluded

Test	$p_{t,1}/p_a$	$p_{t,2}/p_a$	T_1, K	T_2, K	$\dot{m}_1$, kg/s	$\dot{m}_2$, kg/s	V_1, m/s	V_2, m/s
25	1.621	2.252	425.0	606.7	3.403	2.574	331.9	503.2
26	1.626	2.584	422.8	510.0	3.437	3.232	331.9	493.8
27	1.627	2.591	426.7	915.0	3.417	2.378	333.8	666.0
28	2.638	3.013	425.6	458.3	3.460	3.980	335.6	499.0
29	1.637	2.983	421.7	826.1	3.471	2.893	333.8	670.6
30	1.770	1.160	292.8	308.3	4.546	1.337	297.5	160.6
31	1.763	1.337	286.1	354.4	4.597	1.799	293.5	238.0
32	1.771	1.503	279.4	401.7	4.673	2.056	291.1	298.1
33	1.767	2.024	288.9	554.4	4.577	2.422	295.0	451.4
34	1.792	2.586	283.9	429.4	4.691	3.539	296.0	453.2
35	1.769	2.699	288.3	753.9	4.593	2.746	295.4	613.9
36	1.772	3.153	290.6	646.1	4.584	3.482	296.9	603.5
37	1.777	1.506	806.1	385.6	2.729	2.101	497.1	292.6
38	1.748	2.191	812.2	593.9	2.671	2.524	492.6	490.1
39	1.742	3.883	807.2	1106.7	2.670	3.228	489.5	853.7
40	1.862	1.950	552.2	517.8	3.486	2.408	425.2	425.2
41	1.878	2.853	553.3	777.8	3.511	2.849	428.2	638.9
42	1.852	3.884	570.0	1083.9	3.418	3.264	430.4	844.6
43	2.051	1.595	807.2	421.1	3.106	2.173	550.8	325.2
44	2.035	2.467	811.1	667.2	3.075	2.674	549.6	553.5
45	2.032	3.720	797.8	1056.1	3.098	3.170	544.4	822.4
46	2.460	1.725	811.7	462.2	3.718	2.279	611.1	366.1
47	2.469	2.733	832.8	751.7	3.555	2.785	609.6	616.6
48	2.458	3.418	807.2	953.9	3.725	2.235	609.0	758.6

TABLE VI.- EQUIVALENT SINGLE JET FLOW PROPERTIES AND SOUND POWER REDUCTIONS

Test	$\dot{m}_e$, kg/s	T_e, K	ρ_e, kg/m^3	A_e, m^2	V_e, m/s	V_2/V_1	Measured PWL	Ideal PWL	ΔPWL
Model 2									
1	3.131	378.0	1.027	0.01157	263.6	0.56	144.91	144.74	-0.17
2	3.202	468.5	.831	.01280	301.0	1.04	146.94	150.12	3.18
3	3.089	520.4	.746	.01324	312.7	1.20	148.30	151.90	3.60
4	4.249	379.4	1.068	.01262	315.1	1.15	150.29	152.11	1.82
5	3.778	511.8	.788	.01317	364.1	1.58	155.15	158.56	3.42
6	5.117	380.8	1.118	.01259	363.5	1.41	160.21	158.35	-1.86
7	3.574	580.6	.691	.01351	382.8	1.72	158.06	160.88	2.82
8	3.490	640.2	.628	.01385	402.3	1.90	161.13	163.16	2.03
9	4.339	549.6	.768	.01304	433.2	1.89	164.81	166.69	1.89
10	4.146	629.6	.668	.01343	462.0	2.13	167.89	169.66	1.77
11	3.988	695.8	.602	.01374	482.3	2.28	169.64	171.39	1.75
12	5.649	392.0	1.136	.01223	406.6	1.56	165.39	163.89	-1.50
13	4.968	565.3	.781	.01308	486.3	2.09	170.36	171.74	1.38
14	4.658	656.0	.667	.01351	517.2	2.35	172.21	174.51	2.30
15	4.483	743.9	.586	.01390	550.5	2.56	174.24	177.16	2.92
16	5.063	794.6	.573	.01428	619.3	2.77	177.04	180.81	3.77
17	2.889	569.0	.686	.01251	336.7	.59	154.65	154.87	.22
18	2.592	692.4	.562	.01246	370.3	.78	157.80	159.51	1.71
19	2.508	757.9	.513	.01264	387.0	.89	159.09	161.61	2.53
20	3.635	535.9	.753	.01288	374.6	.86	157.72	159.80	2.08
21	3.146	698.9	.576	.01279	427.4	1.17	173.89	176.65	2.76
22	2.973	785.0	.513	.01272	456.2	1.34	165.64	169.28	3.64
23	2.947	852.1	.472	.01306	477.8	1.43	167.54	171.22	3.69
24	4.395	518.2	.817	.01272	422.8	1.05	165.18	165.57	.39
25	3.814	700.5	.603	.01275	495.9	1.43	168.81	172.63	3.82
26	3.590	802.8	.525	.01291	530.2	1.61	171.27	175.51	4.23
27	3.427	897.6	.469	.01300	562.6	1.81	173.49	178.00	4.51
28	5.155	492.9	.894	.01280	450.3	1.17	168.26	168.52	.26
29	4.336	705.2	.624	.01275	545.0	1.57	173.28	176.69	3.41
30	4.055	820.1	.535	.01285	589.5	1.79	175.58	179.28	3.70
31	4.507	955.4	.479	.01355	694.3	2.17	180.10	184.41	4.31
32	2.775	633.9	.616	.01256	358.7	.55	158.56	157.72	-.83
33	2.468	769.1	.506	.01242	392.7	.74	162.35	162.41	.06
34	2.384	836.3	.464	.01262	407.1	.82	163.03	164.21	1.18
35	3.510	588.9	.685	.01306	392.5	.80	160.33	162.03	1.70
36	3.051	753.9	.534	.01278	446.9	1.08	165.99	168.47	2.48
37	2.927	846.2	.475	.01294	475.8	1.24	168.01	171.12	3.11
38	2.927	848.0	.474	.01297	475.8	1.24	168.19	171.24	3.06
39	2.789	927.1	.432	.01303	495.0	1.33	169.26	172.79	3.52
40	4.283	551.6	.764	.01299	431.6	1.00	164.57	166.56	2.00

TABLE VI.- Continued

Test	$\dot{m}_e$, kg/s	T_e, K	ρ_e, kg/m^3	A_e, m^2	V_e, m/s	V_2/V_1	Measured PWL	Ideal PWL	ΔPWL
Model 2 - Concluded									
41	3.665	747.0	0.565	0.01268	511.6	1.33	170.66	174.29	3.63
42	3.414	861.9	.488	.01268	551.2	1.51	173.51	177.44	3.93
43	3.278	954.1	.439	.01297	575.7	1.66	174.41	178.76	4.35
44	5.280	539.5	.809	.01407	463.8	1.09	169.53	169.75	.22
45	4.169	743.4	.590	.01266	557.9	1.47	174.69	177.74	3.05
46	3.944	867.8	.505	.01286	607.1	1.69	177.17	180.37	3.20
47	3.754	975.0	.447	.01307	642.1	1.84	178.55	182.07	3.52
48	4.310	991.0	.460	.01332	703.5	2.00	181.15	184.67	3.51
49	2.481	775.8	.499	.01295	383.9	.47	164.97	161.10	3.87
50	2.219	941.6	.411	.01253	430.7	.62	169.21	166.72	-2.49
51	2.139	1021.0	.379	.01250	451.0	.72	170.35	163.71	-1.64
52	3.260	676.8	.591	.01340	411.7	.70	164.91	164.27	-.64
53	2.792	895.3	.448	.01284	485.6	.94	171.31	171.96	.66
54	2.665	987.7	.406	.01273	515.1	1.03	173.34	174.42	1.07
55	2.576	1081.9	.370	.01290	539.4	1.16	174.26	176.40	2.14
56	4.067	620.0	.675	.01334	451.8	.88	167.48	168.59	1.11
57	3.422	851.6	.493	.01277	543.8	1.12	175.21	176.98	1.78
58	3.236	985.3	.427	.01278	593.3	1.29	177.57	179.59	2.02
59	3.083	1118.3	.375	.01295	634.5	1.44	179.39	181.63	2.24
60	4.828	582.9	.748	.01341	481.4	.96	170.11	171.35	1.24
61	4.031	843.0	.520	.01294	598.3	1.28	179.37	179.93	.56
62	3.608	987.5	.441	.01273	643.2	1.47	179.86	182.07	2.21
63	3.551	1080.5	.404	.01290	681.5	1.57	180.90	183.80	2.91
64	4.125	1105.3	.414	.01324	753.2	1.72	183.67	185.76	2.09
65	2.974	779.4	.525	.01180	480.1	.59	173.02	171.39	-1.62
66	3.579	767.7	.548	.01266	515.9	.85	173.26	174.48	1.22
67	3.318	907.3	.461	.01286	559.1	1.06	176.33	178.07	1.74
68	3.758	932.9	.465	.01311	617.3	1.31	178.49	181.07	2.59
69	4.707	752.0	.601	.01320	593.4	1.15	176.84	179.62	2.78
70	4.986	963.5	.488	.01406	727.0	1.61	183.17	185.32	2.15
71	3.494	779.5	.550	.01165	544.9	.52	178.58	177.20	-1.38
72	4.076	771.7	.566	.01277	564.2	.75	178.38	178.31	-.07
73	3.776	892.2	.486	.01290	602.4	.94	180.10	180.14	.04
74	4.295	922.3	.484	.01359	652.0	1.17	181.83	182.54	.71
75	5.243	763.7	.610	.01365	629.5	1.02	179.64	181.67	2.03
76	5.160	974.9	.493	.01389	754.3	1.38	184.52	185.93	1.41
77	3.016	694.3	.667	.00763	592.2	1.05	182.18	179.50	-2.68
78	3.711	771.4	.562	.01191	554.9	.63	182.53	177.52	-5.01
79	3.770	743.0	.586	.01175	548.0	.61	182.16	177.04	-5.12
80	4.037	699.4	.626	.01198	538.0	.62	180.03	176.25	-3.78
81	5.103	425.3	1.162	.00882	497.9	.60	175.42	172.91	-2.51

TABLE VI.- Continued

Test	$\dot{m}_e$, kg/s	T_e, K	ρ_e, kg/m^3	A_e, m^2	V_e, m/s	V_2/V_1	Measured PWL	Ideal PWL	ΔPWL
Model 3									
1	2.912	506.3	0.766	0.01241	306.4	1.06	149.51	151.95	2.44
2	3.624	551.8	.735	.01276	386.4	1.55	159.37	162.62	3.25
3	3.290	714.2	.563	.01347	433.4	1.93	165.55	167.16	1.61
4	4.339	580.7	.736	.01280	460.3	1.91	168.00	170.68	2.67
5	3.870	794.1	.535	.01343	538.8	2.29	173.61	176.63	3.02
6	5.092	606.7	.742	.01308	524.5	2.06	174.12	175.39	1.28
7	4.579	866.4	.522	.01362	643.9	2.56	179.38	182.30	2.93
8	2.330	762.6	.508	.01195	383.4	.74	161.12	161.26	.14
9	3.100	743.0	.547	.01240	457.1	1.07	166.82	169.36	2.54
10	2.727	960.1	.421	.01252	517.8	1.36	171.48	174.61	3.13
11	3.855	733.3	.587	.01234	531.8	1.32	171.97	175.79	3.82
12	3.348	988.4	.432	.01259	616.0	1.65	177.18	180.70	3.52
13	4.584	728.3	.622	.01257	586.2	1.46	175.88	179.22	3.34
14	4.644	1017.3	.462	.01344	748.4	1.94	183.25	185.83	2.57
Model 4									
1	2.289	1455.0	0.477	0.01127	426.1	0.00	167.46	167.53	0.07
2	2.931	989.0	.716	.01124	364.2	.00	158.88	160.03	1.16
3	4.465	867.7	.792	.01841	306.1	.97	152.49	152.20	-.29
4	4.875	997.9	.713	.01767	386.9	1.45	159.71	162.96	3.25
5	5.230	1186.3	.619	.01772	477.3	1.95	169.58	172.31	2.74
6	4.353	828.7	.828	.01788	294.1	.44	150.43	150.98	.55
7	4.510	884.7	.781	.01819	317.4	.59	161.17	153.99	-7.18
8	5.014	880.6	.797	.01854	339.4	.79	161.83	156.93	-4.90
9	5.246	927.9	.767	.01847	370.2	.99	163.82	161.09	-2.73
10	6.176	1015.7	.729	.01824	464.5	1.51	167.25	170.61	3.36
11	5.652	1095.0	.673	.01831	458.7	1.47	167.46	170.57	3.10
12	5.498	1382.3	.540	.01886	539.4	1.99	174.30	177.67	3.37
13	5.143	1429.5	.515	.01890	528.8	2.03	173.65	176.93	3.28
14	5.946	1332.4	.566	.01892	554.8	1.97	175.89	178.35	2.46
15	4.247	994.9	.679	.01864	335.4	.61	158.85	155.50	-3.35
16	4.938	1052.2	.674	.01849	396.5	1.00	162.74	163.81	1.07
17	5.267	1270.1	.578	.01817	501.0	1.51	171.50	174.36	2.86
18	5.678	1539.9	.490	.01891	612.8	1.98	178.94	181.32	2.38
19	5.265	1602.9	.467	.01877	600.9	1.97	178.77	180.93	2.16
20	3.852	1067.7	.634	.01886	322.0	.40	155.11	154.92	-.20
21	4.204	1094.5	.627	.01905	352.2	.63	161.97	158.56	-3.41
22	4.468	1125.4	.618	.01889	382.7	.79	163.61	162.54	-1.07
23	4.706	1191.3	.595	.01845	428.4	.99	167.08	167.67	.59
24	5.167	1424.2	.517	.01826	546.9	1.49	174.98	177.86	2.88
25	5.598	1745.9	.432	.01930	670.9	1.99	182.10	184.07	1.97

TABLE VI.- Continued

Test	$\dot{m}_e$, kg/s	T_e, K	ρ_e, kg/m^3	A_e, m^2	V_e, m/s	V_2/V_1	Measured PWL	Ideal PWL	ΔPWL
Model 4 - Concluded									
26	5.149	690.1	0.994	0.01796	288.4	0.59	151.04	148.94	-2.09
27	5.700	763.2	.933	.01839	332.2	.98	154.81	156.13	1.33
28	6.059	909.7	.808	.01839	407.6	1.50	160.42	165.78	5.36
29	6.693	851.9	.881	.01833	414.4	1.48	163.97	166.57	2.60
30	5.903	1138.7	.655	.01912	471.6	2.02	169.11	172.02	2.91
31	7.543	798.7	.966	.01840	424.2	1.46	165.82	167.67	1.86
32	6.398	1103.1	.684	.01908	490.2	1.99	171.68	173.71	2.04
33	6.216	500.7	1.417	.01695	258.8	.55	148.11	145.62	-2.52
34	6.460	549.7	1.298	.01791	277.8	.83	148.59	148.51	-.08
35	6.806	573.1	1.261	.01829	295.1	1.00	150.70	150.75	.05
36	7.223	669.6	1.106	.01880	347.3	1.52	156.37	157.94	1.57
37	8.277	629.7	1.217	.01860	365.5	1.54	159.02	160.81	1.79
38	7.495	824.4	.918	.01976	413.2	2.09	165.23	166.24	1.01
39	8.241	797.1	.975	.01962	430.7	2.02	166.91	168.40	1.51
40	4.787	1137.1	.620	.01898	407.1	.59	168.94	165.58	-3.36
41	5.274	1257.7	.579	.01865	488.0	.98	172.90	173.57	.67
42	6.026	1734.4	.445	.01977	684.9	1.73	182.53	184.68	2.15
43	5.985	969.3	.760	.01848	426.2	.99	165.39	167.26	1.86
44	6.405	1187.3	.640	.01907	524.6	1.50	173.11	176.21	3.10
45	6.857	1464.5	.535	.02038	628.3	1.98	179.23	182.31	3.08
46	5.325	1178.7	.616	.01873	461.7	.58	173.97	171.19	-2.79
47	5.784	1347.9	.557	.01881	552.5	.99	177.40	178.47	1.06
48	6.409	1663.4	.470	.01996	682.9	1.47	182.65	184.63	1.99
49	6.246	1227.7	.616	.01917	529.0	.59	178.13	177.04	-1.09
50	6.679	1398.0	.561	.01953	609.3	1.00	179.78	181.29	1.51
51	6.937	1570.8	.506	.02031	675.7	1.24	182.58	184.42	1.84
52	2.684	1198.0	.653	.00752	546.5	∞	170.73	177.98	7.26
53	2.875	1410.0	.569	.00790	639.2	∞	176.84	182.74	5.91
54	2.875	1415.0	.558	.00801	643.4	∞	177.27	181.91	4.65
55	2.937	1490.0	.534	.00817	673.6	∞	179.22	183.56	4.34
56	3.160	1788.0	.451	.00892	785.8	∞	184.48	186.43	1.95
57	2.567	1801.0	.429	.00818	732.4	∞	181.49	185.24	3.75
58	3.225	1866.0	.433	.00915	814.4	∞	185.71	187.01	1.30
59	1.795	1901.0	.378	.00743	639.5	∞	176.48	181.73	5.25
60	3.245	1938.0	.417	.00929	837.3	∞	186.46	187.48	1.02
61	3.290	1944.0	.424	.00924	840.0	∞	186.41	188.11	1.70

TABLE VI.- Continued

Test	$\dot{m}_e$, kg/s	T_e, K	ρ_e, kg/m^3	A_e, m^2	V_e, m/s	V_2/V_1	Measured PWL	Ideal PWL	ΔPWL
Model 5									
1	4.476	835.4	0.823	0.01820	298.9	1.01	151.52	151.16	-0.36
2	5.105	1177.4	.622	.01732	473.6	1.99	172.79	172.11	-.68
3	4.768	989.6	.717	.01737	382.6	1.49	160.62	162.42	1.80
4	4.195	839.3	.816	.01757	292.7	.46	155.26	150.30	-4.96
5	4.393	876.0	.788	.01784	312.6	.58	156.47	153.11	-3.36
6	4.910	867.3	.807	.01827	332.8	.80	156.87	155.84	-1.03
7	5.499	764.2	.931	.01815	325.4	.99	156.16	155.20	-.96
8	5.142	913.8	.777	.01819	363.7	.99	159.61	160.01	.40
9	6.268	1000.6	.754	.01803	461.0	1.47	170.41	170.95	.54
10	5.483	1091.9	.672	.01798	453.5	1.49	168.70	170.24	1.54
11	5.416	1357.3	.547	.01856	534.0	1.97	176.59	177.58	1.00
12	5.064	1428.9	.512	.01866	530.5	2.00	176.85	177.37	.52
13	5.955	1305.1	.580	.01865	550.1	1.94	177.43	178.18	.76
14	4.285	977.2	.704	.01840	330.9	.60	159.13	155.63	-3.50
15	5.310	1252.2	.589	.01799	500.9	1.48	173.32	174.56	1.24
16	5.629	1541.7	.491	.01864	614.5	1.97	181.15	181.85	.70
17	5.155	1604.3	.463	.01852	601.5	2.00	180.62	181.17	.55
18	3.519	1103.2	.612	.01814	317.2	.38	160.51	153.79	-6.72
19	4.226	1073.3	.640	.01892	349.1	.62	162.60	158.10	-4.50
20	4.475	1108.4	.629	.01864	381.8	.79	164.67	162.38	-2.29
21	4.691	1166.8	.608	.01819	424.1	.99	167.57	167.39	-.17
22	5.088	1434.6	.515	.01802	548.4	1.50	179.07	178.36	-.71
23	5.451	1764.2	.429	.01876	676.8	2.00	184.53	184.60	.06
24	4.979	692.1	1.005	.01750	283.1	.56	152.59	148.85	-3.74

TABLE VI.- Concluded

Test	$\dot{m}_e$, kg/s	T_e, K	ρ_e, kg/m^3	A_e, m^2	V_e, m/s	V_2/V_1	Measured PWL	Ideal PWL	ΔPWL
Model 5 - Concluded									
25	5.977	905.8	0.815	0.01808	405.7	1.51	164.88	165.61	0.72
26	6.669	837.1	.902	.01803	410.4	1.48	166.43	166.15	-.28
27	5.795	1128.7	.655	.01883	470.1	1.99	172.16	171.75	-.41
28	7.440	797.6	.971	.01812	423.0	1.48	169.23	167.59	-1.64
29	6.364	1089.9	.695	.01881	486.9	2.00	173.44	173.59	.15
30	5.883	533.4	1.333	.01657	266.4	.54	149.42	146.26	-3.16
31	6.396	549.6	1.305	.01763	277.9	.81	150.87	148.44	-2.43
32	6.729	570.2	1.270	.01807	293.2	1.02	152.24	150.81	-1.43
33	6.999	685.4	1.082	.01853	349.2	1.53	158.30	158.53	.23
34	8.230	623.7	1.236	.01832	363.6	1.53	161.89	160.51	-1.37
35	7.339	832.6	.911	.01943	414.5	2.07	167.78	166.78	-1.00
36	8.066	799.3	.975	.01927	429.2	2.03	169.17	168.39	-.77
37	4.830	1121.7	.632	.01872	408.2	.58	170.29	165.94	-4.35
38	5.195	1271.1	.575	.01838	491.4	.99	174.04	174.08	.03
39	5.898	1748.0	.438	.01955	688.9	1.74	184.68	184.90	.22
40	5.894	968.7	.761	.01822	425.2	1.00	167.04	167.47	.43
41	6.360	1177.0	.647	.01880	522.6	1.49	174.25	176.30	2.05
42	6.682	1477.9	.527	.02005	632.7	1.96	181.73	182.71	.98
43	5.279	1166.9	.624	.01848	457.9	.59	174.80	171.04	-3.75
44	5.749	1339.5	.562	.01854	551.4	1.00	178.24	178.55	.32
45	6.268	1671.2	.464	.01972	685.0	1.51	174.83	184.80	-.03
46	5.997	1222.0	.616	.01879	518.0	.59	180.08	176.34	-3.74
47	6.340	1434.9	.539	.01919	612.7	1.01	182.58	181.76	-.83
48	5.960	1552.0	.506	.01772	665.1	1.24	184.94	184.22	-.72

TABLE VII.- DIRECTIVITY INDEX FOR COANNULAR JET

θ, deg	$\log_{10} D(\theta)$ for V_e/c_a of -							
	1.18	1.36	1.44	1.53	1.62	1.76	1.94	2.11
Models 2 and 3								
90	-0.33	-0.46	-0.46	-0.53	-0.56	-0.65	-0.69	-0.75
105	-.09	-.17	-.24	-.30	-.26	-.36	-.41	-.44
120	.16	.15	.10	0	.13	-.01	-.06	-.07
130	.31	.33	.27	.26	.33	.25	.26	.24
140	.43	.51	.52	.54	.57	.56	.60	.58
150	.45	.60	.71	.71	.70	.72	.76	.71
165	.37	.31	.36	.26	.23	.22	.23	.16
Model 4								
90	-0.49	-0.44	-0.49	-0.52	-0.46	-0.59	-0.67	
100	-.37	-.34	-.40	-.37	-.40	-.42	-.51	
110	-.20	-.06	-.08	-.10	-.07	-.19	-.29	
120	.04	.17	.15	.11	.16	.08	.01	
130	.19	.35	.33	.33	.39	.35	.40	
140	.50	.49	.51	.52	.54	.58	.67	
150	.53	.56	.61	.61	.57	.67	.69	
160	.61	.50	.57	.54	.41	.50	.41	

TABLE VIII.- FLIGHT TEST CONDITIONS FOR MODEL 6

Test	$p_{t,1}/p_a$	$p_{t,2}/p_a$	T_1, K	T_2, K	$\dot{m}_1$, kg/s	$\dot{m}_2$, kg/s	V_1, m/s	V_2, m/s	V_a, m/s
1	1.513	1.301	360.4	403.7	0.445	0.222	284.1	242.6	6.4
2	1.523	1.298	371.5	418.2	.440	.204	290.8	245.7	29.6
3	1.537	1.307	372.6	617.6	.422	.159	294.1	302.7	30.2
4	1.525	1.305	375.4	633.2	.390	.159	292.6	305.4	103.6
5	1.528	1.299	378.2	404.8	.422	.209	294.1	242.3	60.4
6	1.527	1.301	383.2	623.2	.435	.159	296.0	301.4	6.4
7	1.509	1.295	396.5	394.3	.404	.209	297.2	237.4	101.5
8	1.525	1.305	399.3	555.4	.404	.163	301.4	286.2	101.2
9	1.528	1.302	402.6	575.9	.417	.177	303.9	290.2	6.7
10	1.529	1.304	404.8	613.2	.413	.159	304.8	300.5	61.3
11	1.534	1.305	405.9	574.3	.417	.177	306.3	290.8	31.1
12	1.561	1.302	409.3	569.3	.426	.186	313.6	306.0	61.6
13	1.525	1.537	384.8	403.7	.417	.195	296.6	306.3	60.4
14	1.527	1.532	389.3	408.2	.426	.290	298.7	306.9	30.5
15	1.529	1.534	391.5	399.3	.417	.290	299.6	308.2	6.4
16	1.531	1.533	392.6	393.7	.399	.281	300.5	301.4	101.8
17	1.529	1.810	377.6	695.4	.435	.245	294.4	467.9	9.4
18	1.526	1.802	380.4	596.5	.431	.263	295.0	431.6	61.0
19	1.522	1.801	382.6	681.5	.404	.227	294.7	461.5	103.3
20	1.524	1.802	387.6	680.9	.426	.263	297.2	461.5	30.8
21	1.526	1.802	393.2	409.8	.422	.367	299.9	357.2	6.4
22	1.529	1.803	394.8	407.1	.422	.363	301.1	356.0	30.2
23	1.527	1.800	396.5	389.3	.395	.354	301.1	347.8	101.5
24	1.529	1.804	396.5	404.3	.413	.358	301.4	355.1	60.4
25	1.508	1.799	398.7	610.4	.395	.263	297.8	435.9	101.8
26	1.523	1.797	402.1	674.3	.408	.254	302.4	458.1	61.6
27	1.527	1.804	404.3	598.7	.417	.295	304.5	432.8	6.7

TABLE VIII.- Concluded

Test	$p_{t,1}/p_a$	$p_{t,2}/p_a$	T_1, K	T_2, K	$\dot{m}_1$, kg/s	$\dot{m}_2$, kg/s	V_1, m/s	V_2, m/s	V_a, m/s
28	1.517	1.787	410.4	599.8	0.413	0.290	304.2	429.8	31.1
29	1.516	2.515	375.9	390.9	.426	.531	291.1	426.7	6.4
30	1.530	2.495	382.1	691.5	.390	.322	296.6	567.5	129.5
31	1.517	2.493	386.5	605.4	.417	.386	295.4	530.0	61.0
32	1.517	2.501	386.5	705.4	.395	.331	295.4	573.9	103.6
33	1.519	2.510	388.2	706.5	.422	.358	296.6	575.2	9.4
34	1.529	2.497	388.7	399.3	.422	.526	299.0	429.8	30.5
35	1.519	2.501	392.1	604.8	.413	.408	297.8	530.7	30.8
36	1.533	2.503	394.3	703.7	.417	.352	301.8	573.3	30.2
37	1.531	2.509	396.5	404.3	.408	.517	302.1	433.4	60.4
38	1.508	2.505	397.6	391.5	.390	.494	297.5	426.1	101.8
39	1.490	2.494	397.6	592.1	.413	.422	293.2	524.3	6.7
40	1.515	2.511	401.5	701.5	.417	.349	300.5	573.3	61.6
41	1.524	2.506	406.5	603.7	.390	.322	304.5	530.7	101.8
42	1.518	3.187	383.2	710.4	.386	.417	294.1	637.6	100.9
43	1.542	3.209	384.3	403.2	.422	.676	299.9	479.1	6.4
44	1.524	3.198	387.6	400.4	.408	.658	297.2	477.0	60.4
45	1.522	3.209	387.6	400.9	.408	.753	296.9	477.9	30.5
46	1.514	3.212	388.7	705.9	.381	.413	295.4	637.6	129.5
47	1.530	3.199	389.3	590.4	.413	.503	299.3	580.9	61.3
48	1.527	3.203	389.8	595.4	.390	.481	298.7	583.7	101.8
49	1.530	3.207	292.6	388.7	.390	.649	300.2	470.6	101.5
50	1.514	3.200	394.3	695.9	.413	.485	297.5	632.2	9.4
51	1.533	3.201	402.1	692.6	.417	.490	304.8	630.3	31.1
52	1.539	3.214	402.6	577.6	.413	.544	306.3	575.5	31.1
53	1.523	3.215	408.2	698.7	.408	.472	304.8	634.3	61.9
54	1.519	3.207	409.3	595.9	.413	.549	304.2	584.3	11.6

TABLE IX.- FLIGHT TEST CONDITIONS FOR MODEL 7

Test	$p_{t,1}/p_a$	$p_{t,2}/p_a$	T_1, K	T_2, K	$\dot{m}_1$, kg/s	$\dot{m}_2$, kg/s	V_1, m/s	V_2, m/s	V_a, m/s
1	1.521	1.303	370.4	653.7	0.327	0.168	289.9	309.7	104.2
2	1.526	1.306	382.6	673.7	.349	.191	295.7	315.8	11.3
3	1.527	1.303	384.3	669.8	.349	.191	296.6	313.6	30.8
4	1.527	1.302	385.9	670.9	.349	.191	297.2	313.3	61.3
5	1.525	1.307	388.7	399.8	.331	.281	297.8	243.2	60.4
6	1.528	1.304	390.4	395.4	.345	.281	299.3	241.1	9.1
7	1.525	1.304	390.4	395.9	.345	.281	298.4	241.1	29.6
8	1.527	1.306	393.2	598.7	.345	.195	300.2	297.2	30.8
9	1.522	1.309	393.2	601.5	.340	.209	299.0	299.3	60.7
10	1.527	1.310	393.7	398.2	.331	.263	300.2	243.8	102.1
11	1.533	1.304	393.7	592.6	.358	.222	301.4	295.0	9.1
12	1.528	1.304	395.9	596.5	.318	.195	301.1	296.0	103.9
13	1.529	1.537	383.2	393.2	.345	.381	296.6	302.4	9.1
14	1.528	1.529	384.8	392.6	.345	.381	297.2	300.2	31.1
15	1.533	1.543	387.1	397.1	.345	.372	299.0	305.1	60.4
16	1.525	1.537	394.3	397.1	.331	.358	299.9	303.9	101.8
17	1.513	1.799	380.4	690.4	.327	.286	292.0	464.2	102.1
18	1.524	1.813	383.2	397.6	.345	.472	295.7	353.6	9.1
19	1.524	1.806	384.8	395.9	.336	.463	296.3	351.7	60.4
20	1.535	1.812	384.8	397.6	.354	.467	298.4	353.6	29.6
21	1.523	1.809	388.7	700.4	.331	.322	297.5	469.7	31.1
22	1.523	1.805	389.3	704.8	.340	.322	297.5	470.3	6.7
23	1.525	1.805	391.5	698.2	.354	.318	299.0	467.9	61.3
24	1.523	1.813	396.5	393.7	.331	.449	300.5	351.7	101.8
25	1.526	1.813	397.1	589.3	.358	.376	301.4	431.0	6.7
26	1.528	1.805	398.2	595.4	.340	.367	302.4	431.6	29.9
27	1.534	1.810	399.3	607.1	.349	.354	303.9	436.8	60.4

TABLE IX.- Concluded

Test	$p_{t,1}/p_a$	$p_{t,2}/p_a$	T_1, K	T_2, K	$\dot{m}_1$, kg/s	$\dot{m}_2$, kg/s	V_1, m/s	V_2, m/s	V_a, m/s
28	1.528	1.800	400.4	605.9	0.331	0.331	303.0	434.6	103.9
29	1.529	2.516	384.8	395.4	.349	.653	297.5	429.2	60.4
30	1.530	2.510	385.4	396.5	.340	.671	297.5	429.2	31.1
31	1.530	2.519	385.4	400.4	.354	.676	297.5	432.2	9.1
32	1.525	2.511	388.7	709.3	.299	.390	297.8	576.4	129.8
33	1.527	2.503	390.4	396.5	.318	.630	299.0	428.5	101.8
34	1.528	2.518	392.6	702.1	.340	.463	299.9	574.2	6.7
35	1.526	2.466	393.7	707.1	.308	.404	299.9	570.6	103.9
36	1.519	2.507	394.3	699.8	.340	.458	298.7	572.1	30.8
37	1.519	2.506	395.4	708.7	.331	.454	299.3	575.8	61.3
38	1.521	2.524	395.9	589.3	.345	.535	299.6	525.8	6.7
39	1.529	2.507	397.6	589.3	.340	.531	302.1	524.3	31.1
40	1.527	2.514	398.7	594.3	.349	.517	302.1	527.3	61.0
41	1.524	2.507	402.1	596.5	.318	.485	302.7	527.6	103.6
42	1.523	3.214	384.8	399.8	.336	.839	296.0	477.6	60.4
43	1.527	3.205	379.3	585.9	.349	.676	294.7	579.1	61.3
44	1.522	3.200	384.8	710.4	.331	.585	296.0	638.6	9.4
45	1.530	3.210	385.4	399.3	.354	.862	297.8	477.0	30.5
46	1.530	3.220	385.4	399.3	.354	.862	297.8	477.6	9.1
47	1.533	3.215	387.1	595.4	.345	.685	299.0	584.3	29.9
48	1.538	3.206	389.3	702.6	.340	.594	300.8	635.5	31.1
49	1.530	3.209	392.1	590.9	.345	.694	300.2	581.9	6.7
50	1.522	3.203	393.2	698.2	.354	.585	299.0	633.4	61.6
51	1.518	3.226	399.3	395.9	.327	.812	300.2	475.8	101.5
52	1.530	3.206	402.1	702.6	.304	.526	304.2	635.5	103.6
53	1.526	3.200	403.2	589.8	.304	.640	303.6	580.6	103.6
54	1.536	3.201	407.1	705.4	.295	.508	307.5	636.4	130.5

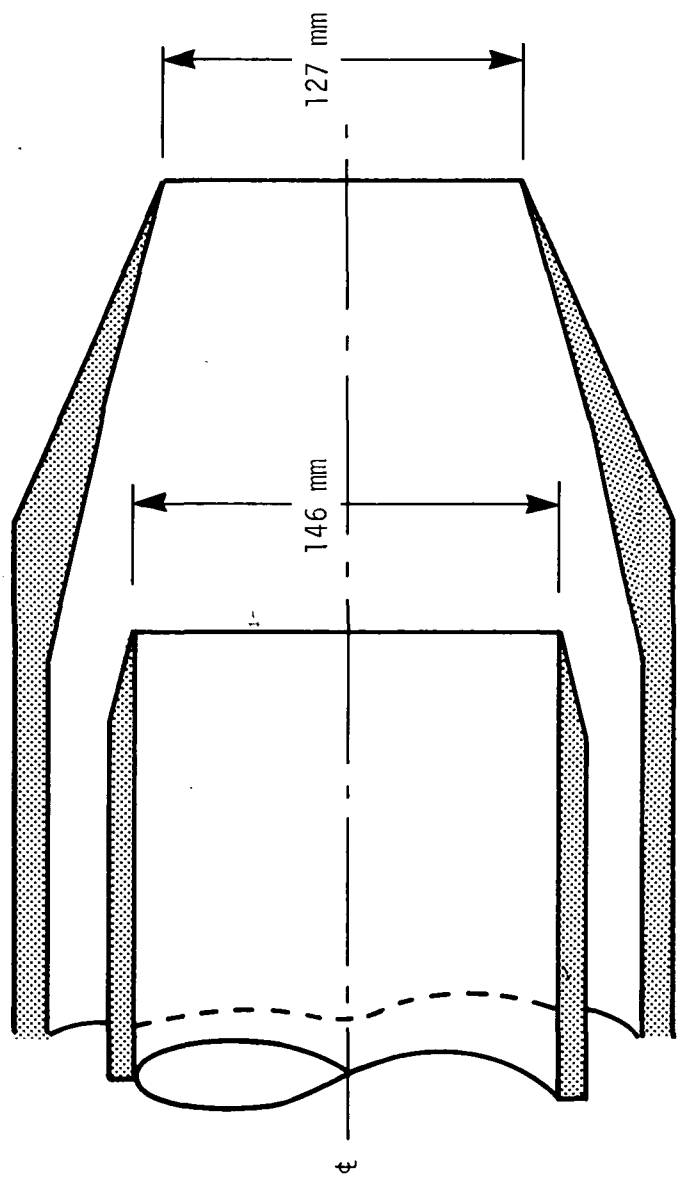

Figure 1.- Model 1, convergent nozzle.

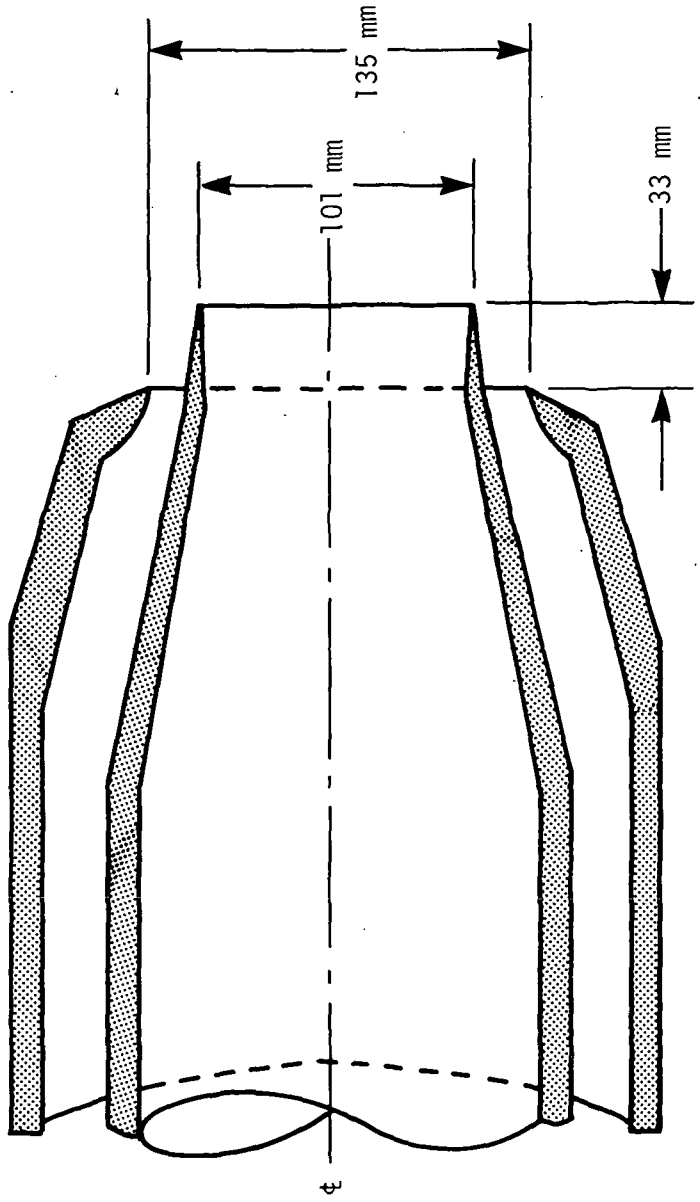

Figure 2.- Model 2, 0.75-area-ratio coannular nozzle.

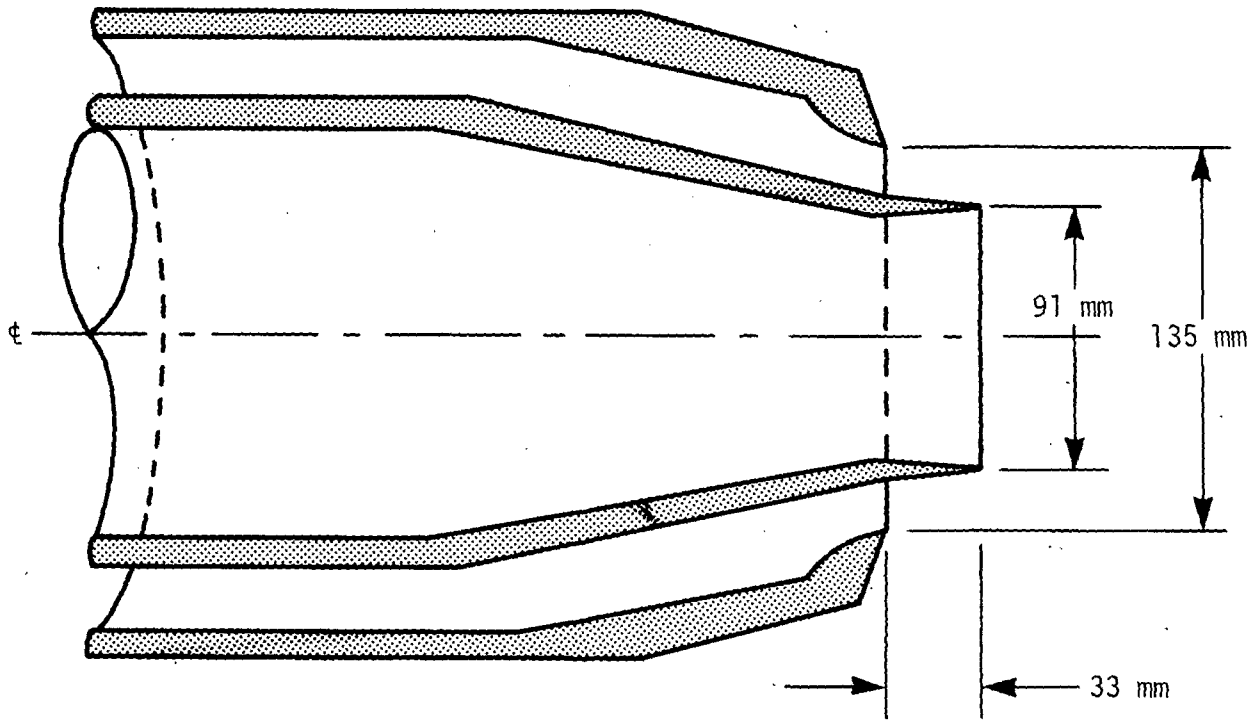

Figure 3.- Model 3, 1.20-area-ratio coannular nozzle.

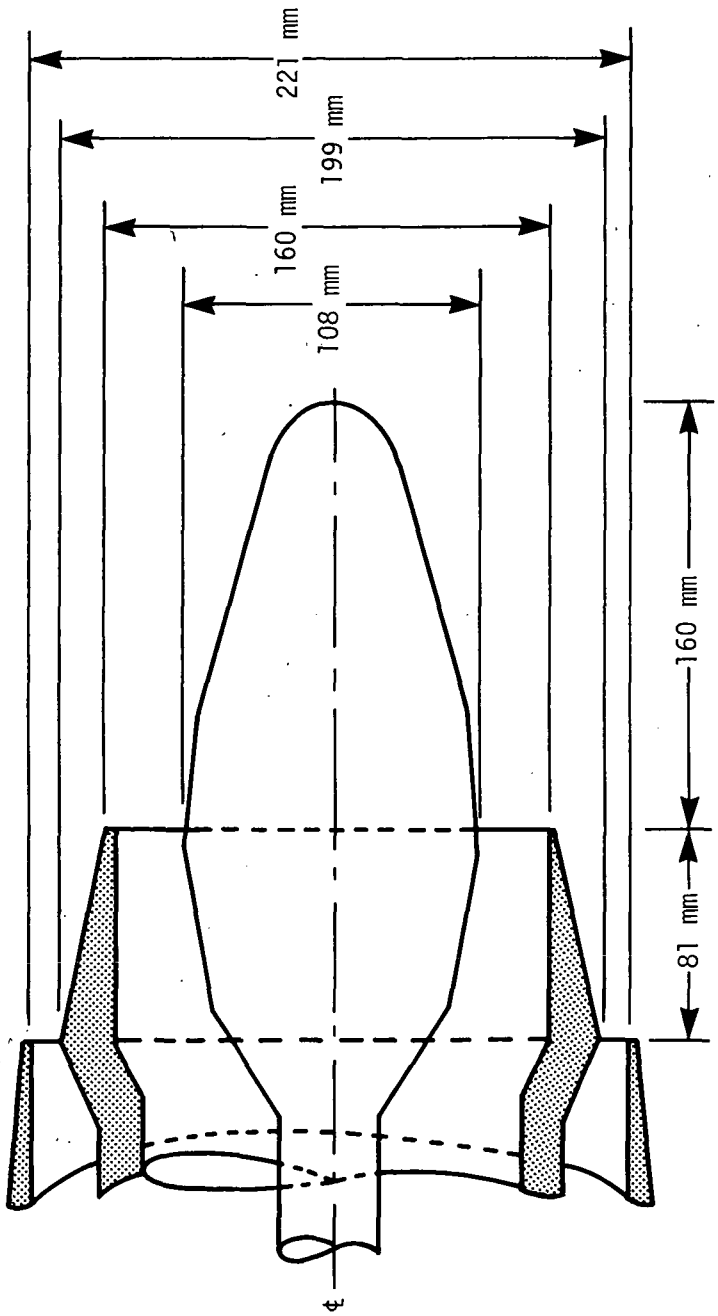

Figure 4.- Model 4, 0.643-area-ratio coannular plug nozzle.

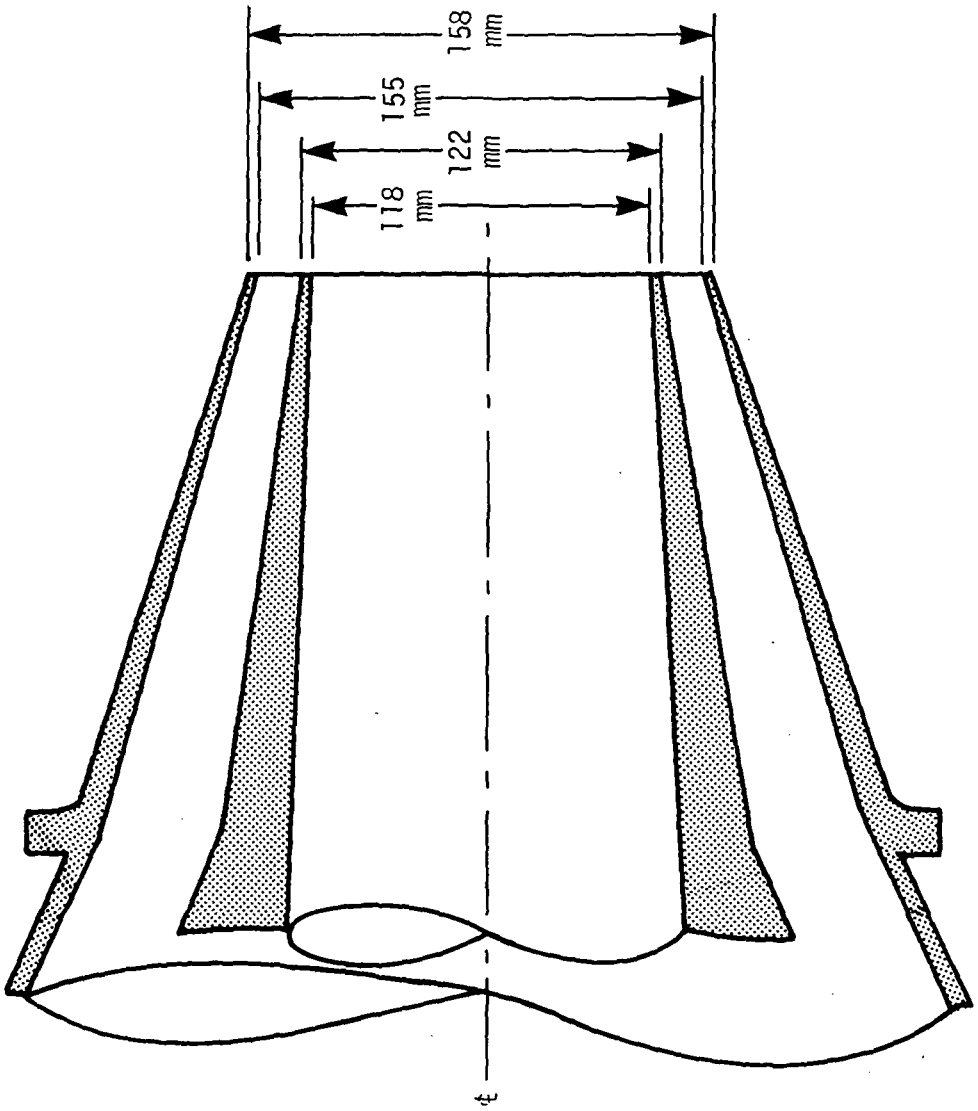

Figure 5.- Model 5, 0.647-area-ratio coannular nozzle.

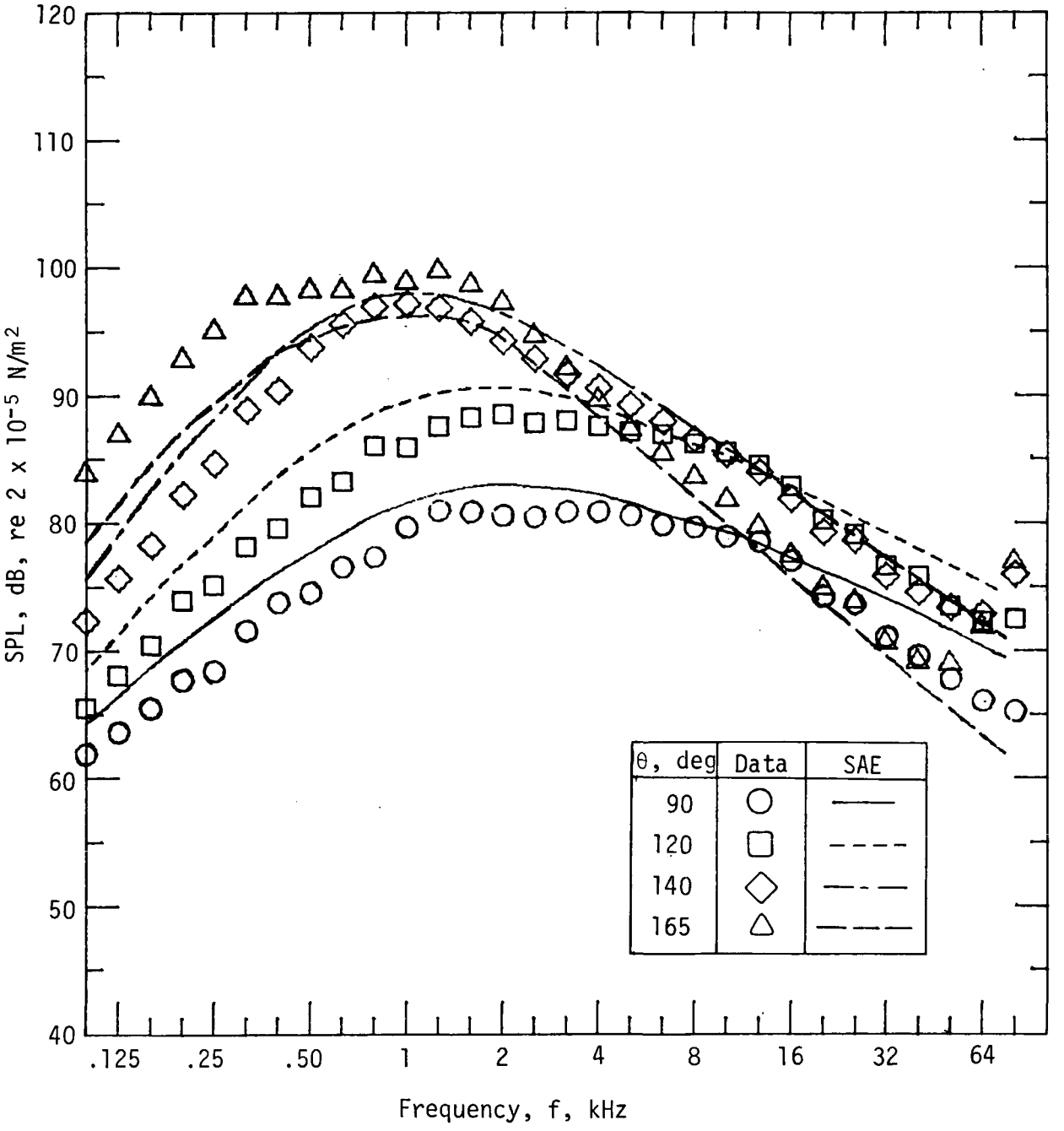

Figure 6.- Typical model 1 spectral data scaled to 45.7-m radius (test 15, table I).

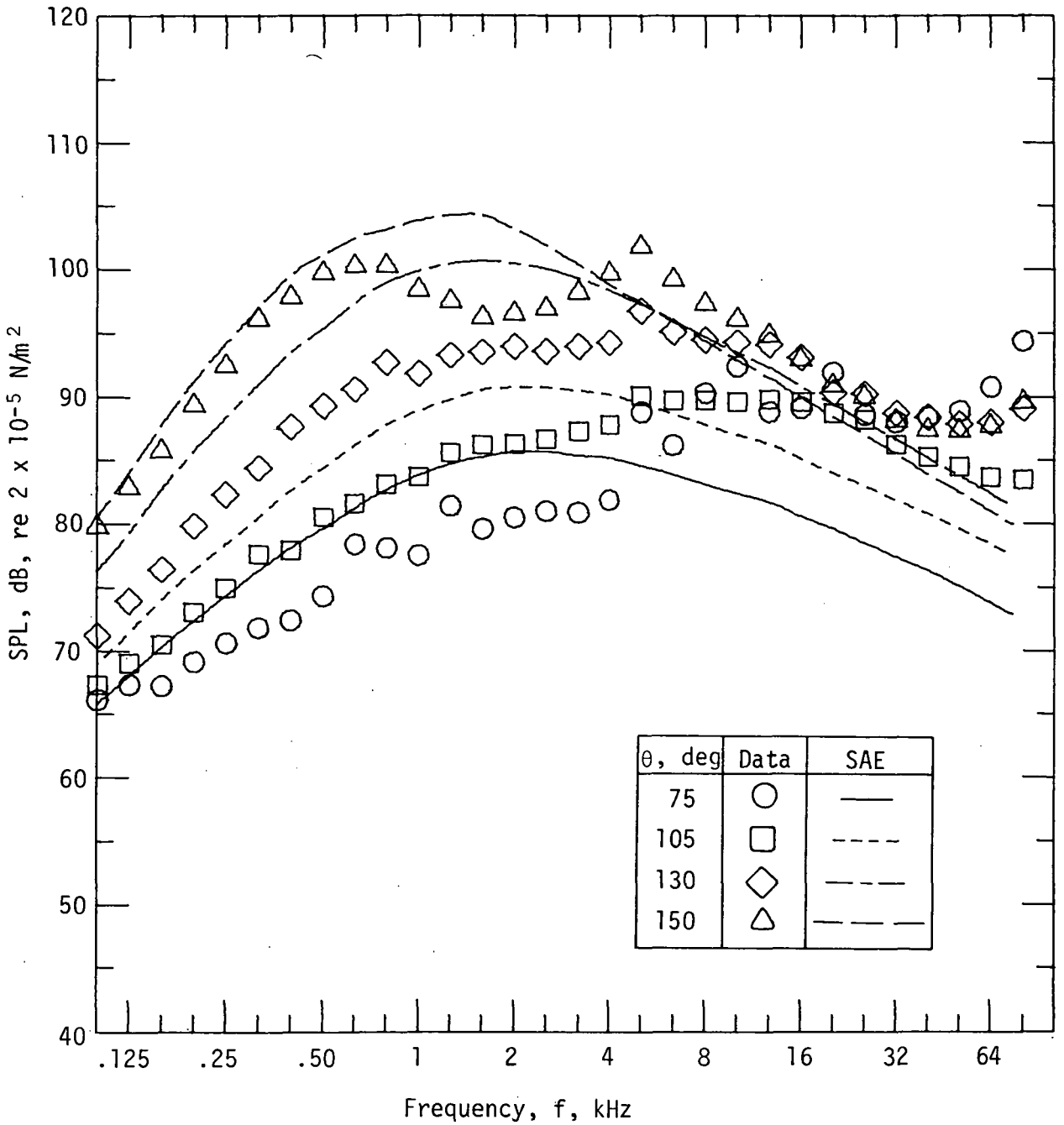

Figure 7.- Typical model 2 spectral data scaled to 45.7-m radius (test 29, table II).

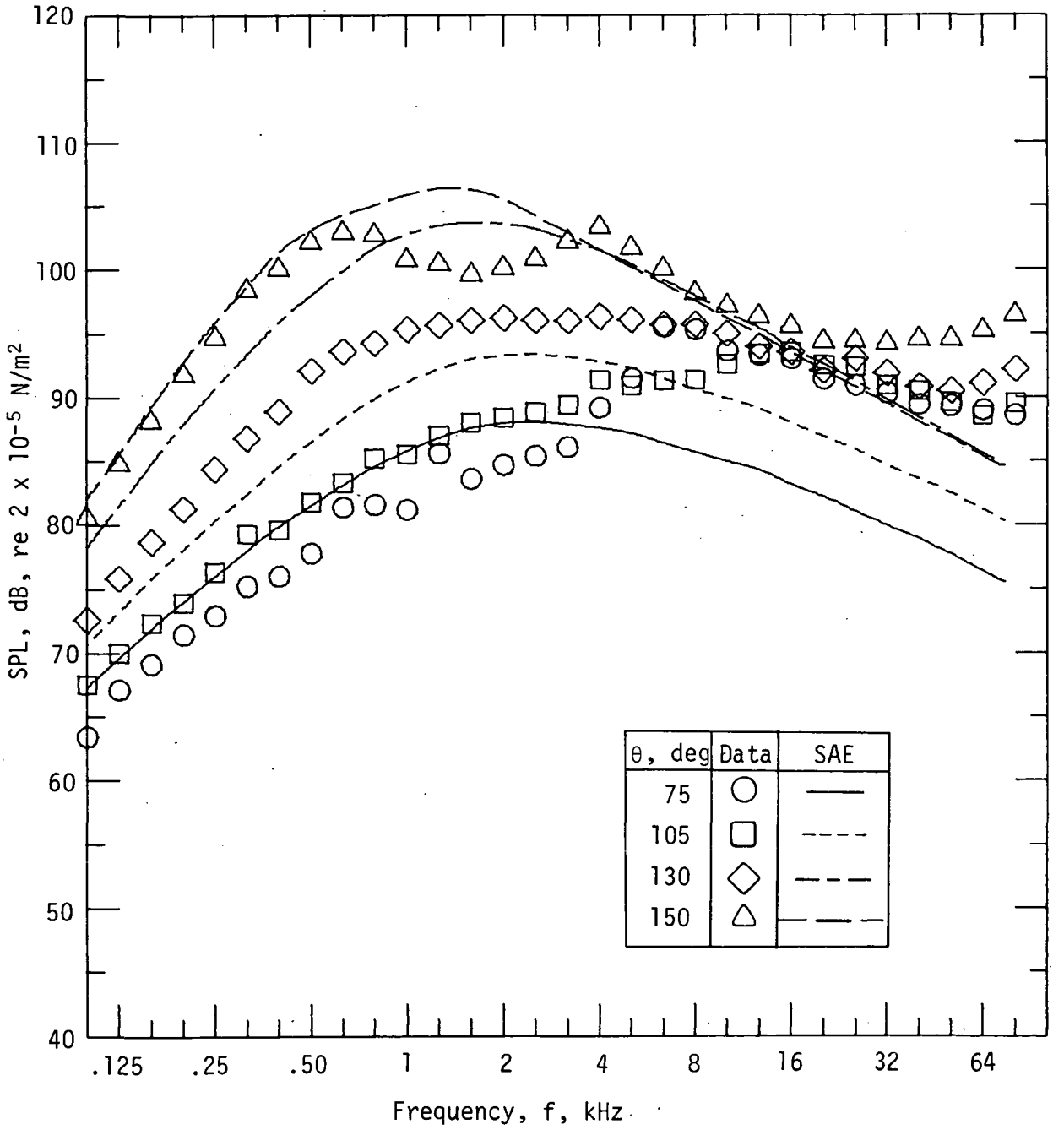

Figure 8.- Typical model 3 spectral data scaled to 45.7-m radius (test 13, table III).

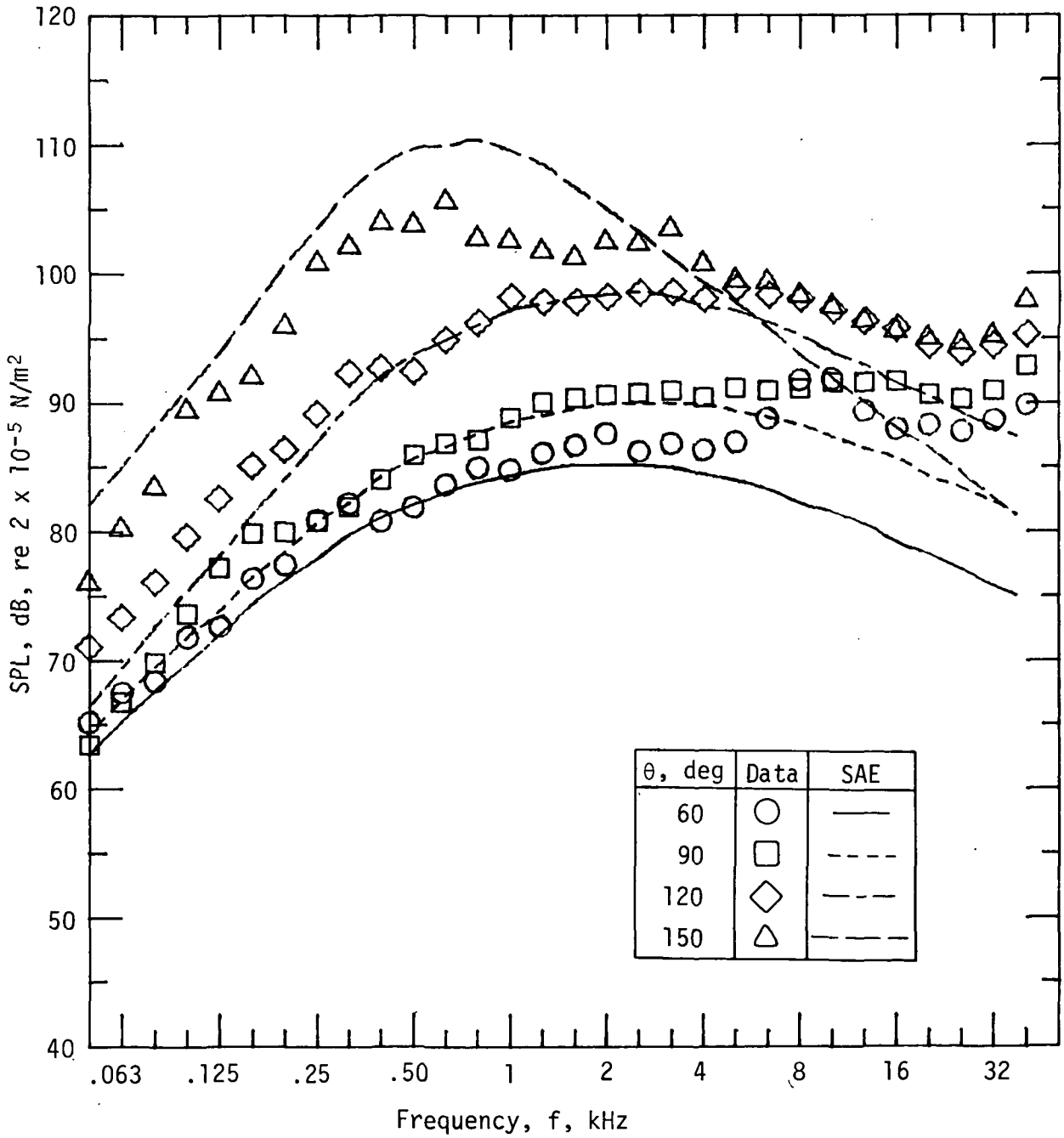

Figure 9.- Typical model 4 spectral data scaled to 45.7-m radius (test 19, table IV).

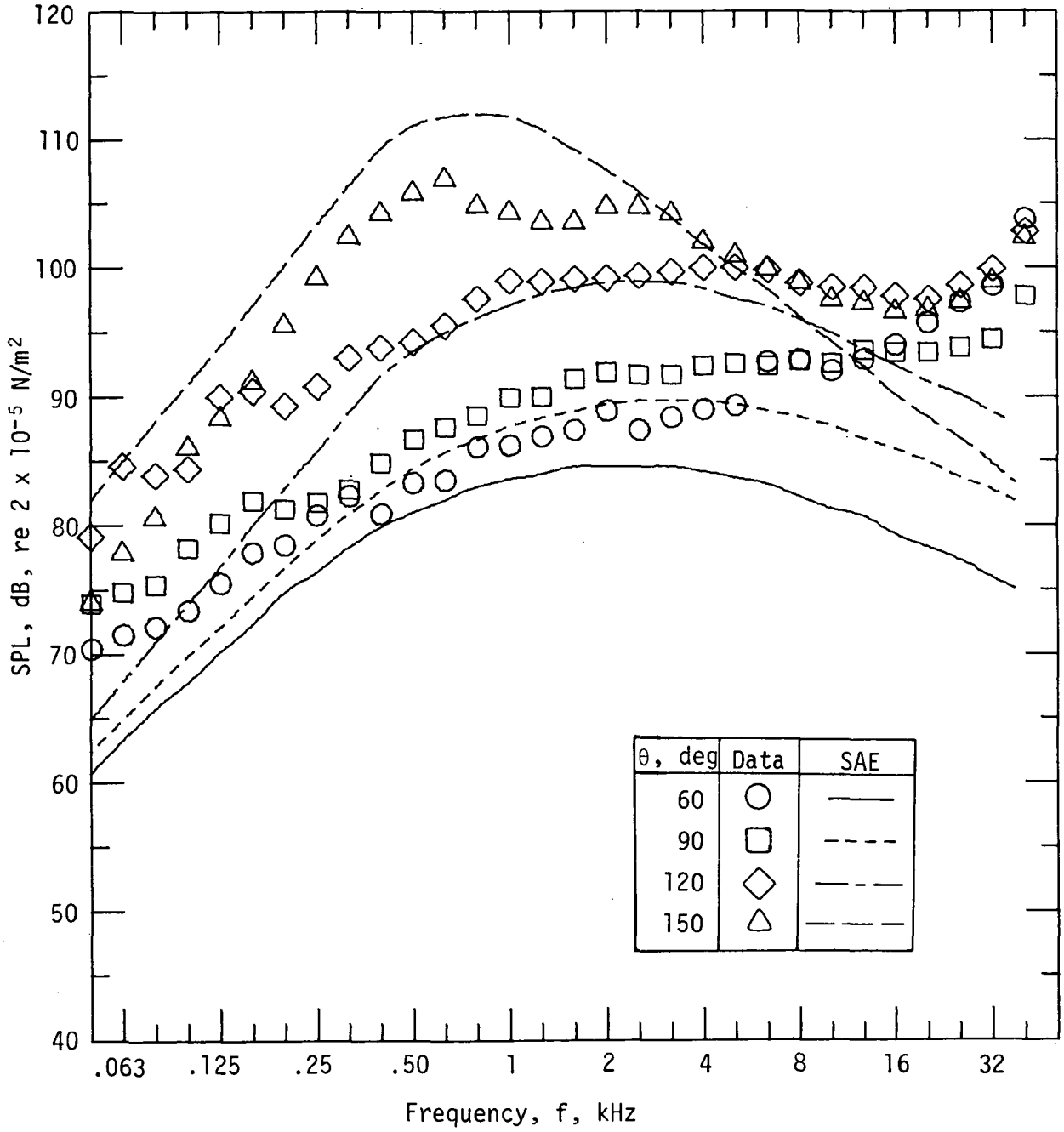

Figure 10.- Typical model 5 spectral data scaled to 45.7-m radius (test 17, table V).

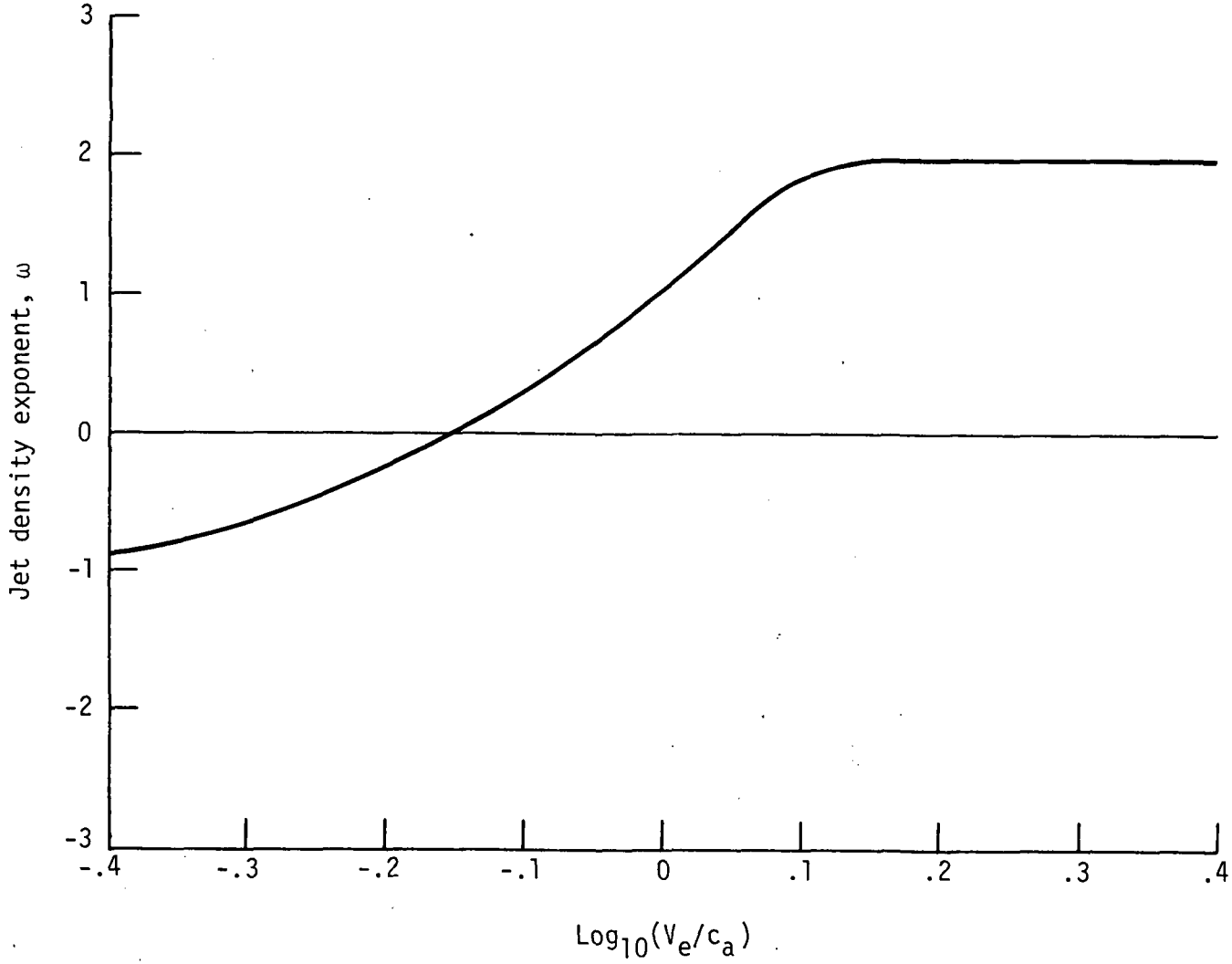

Figure 11.- Jet density exponent ω.

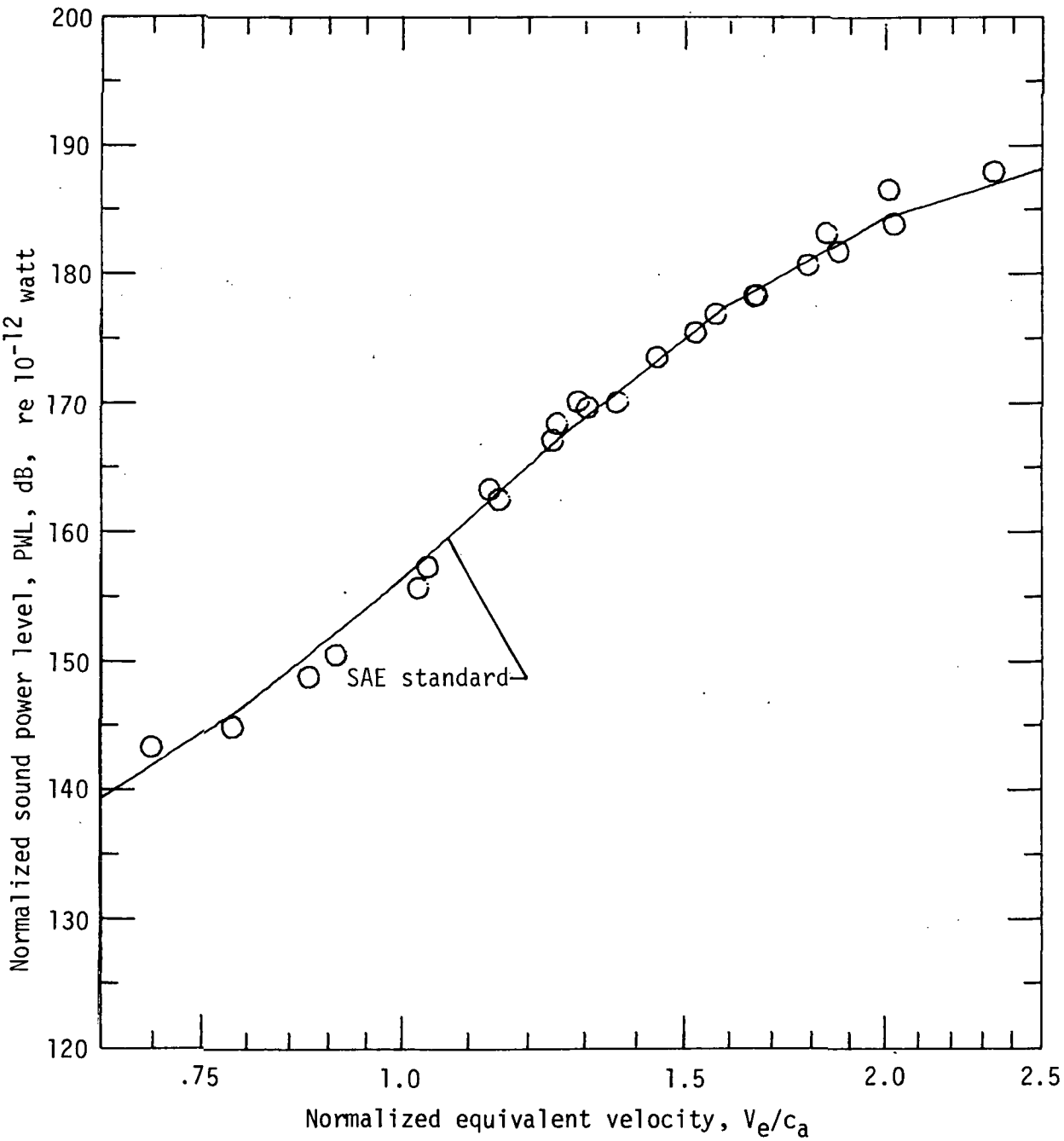

Figure 12.- Model 1 overall acoustic power levels.

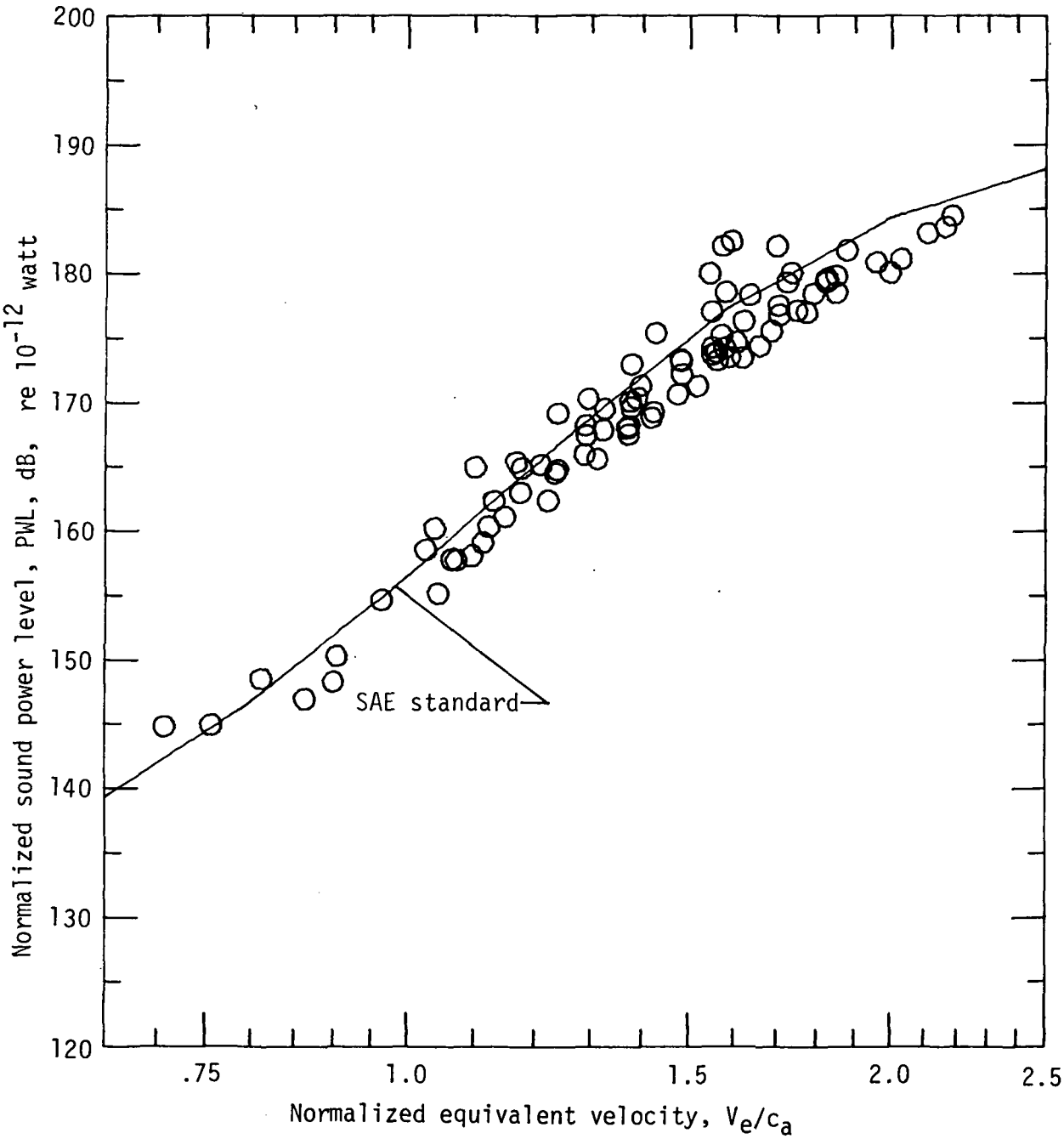

Figure 13.- Model 2 overall acoustic power levels.

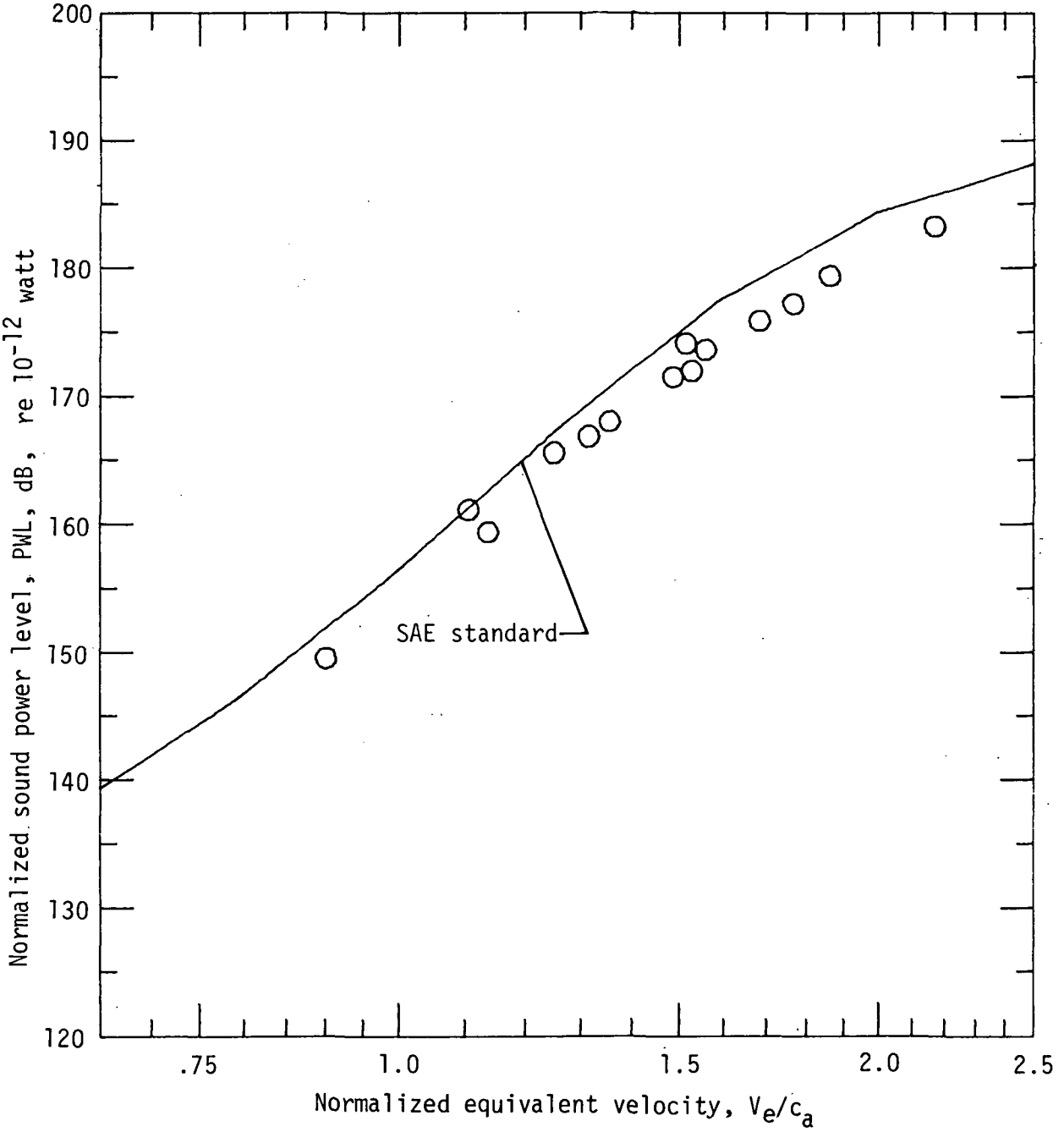

Figure 14.- Model 3 overall acoustic power levels.

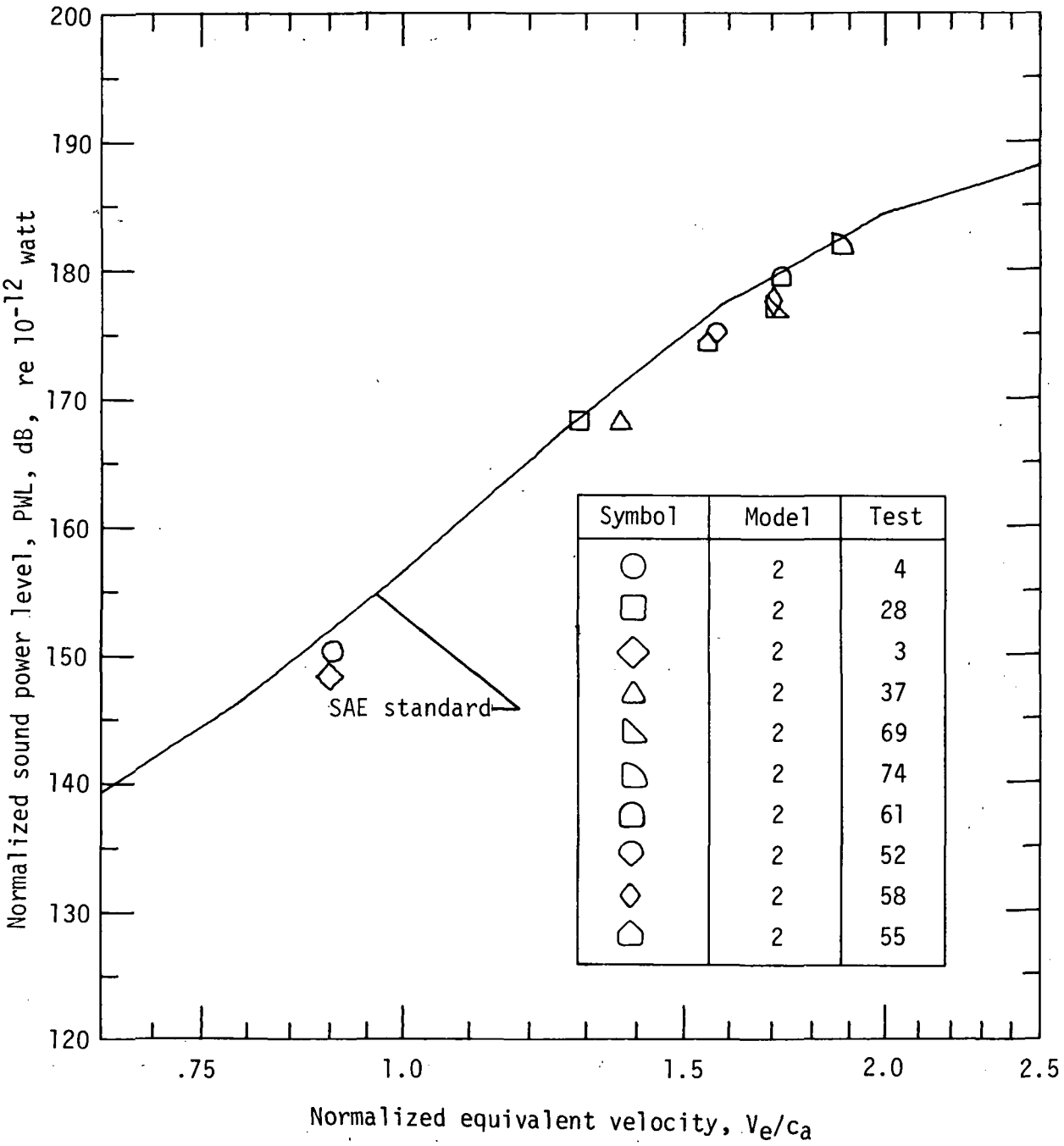

Figure 15.- Models 2 and 3 overall acoustic power levels for velocity ratios near 1.2.

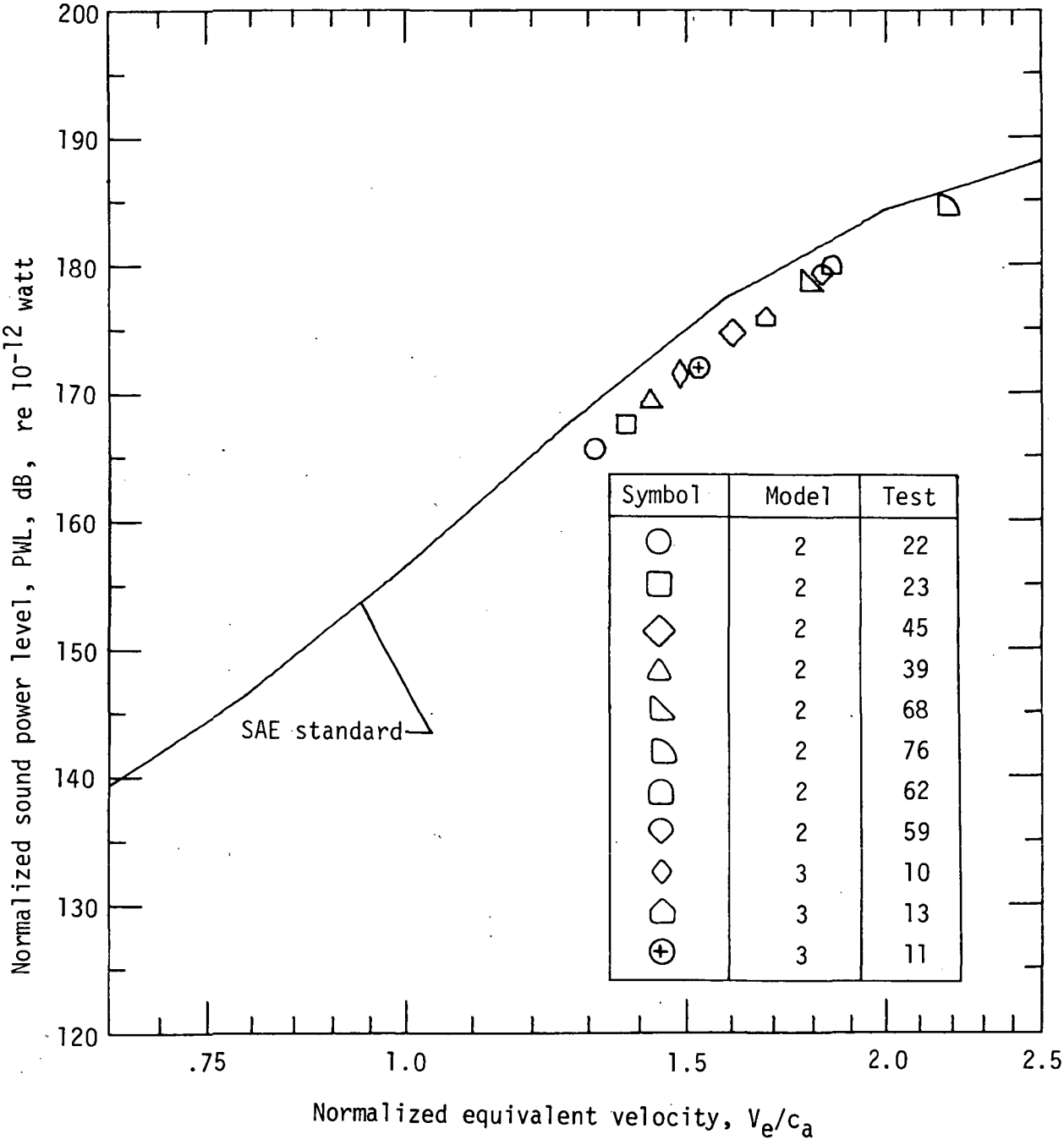

Figure 16.- Models 2 and 3 overall acoustic power levels for velocity ratios near 1.4.

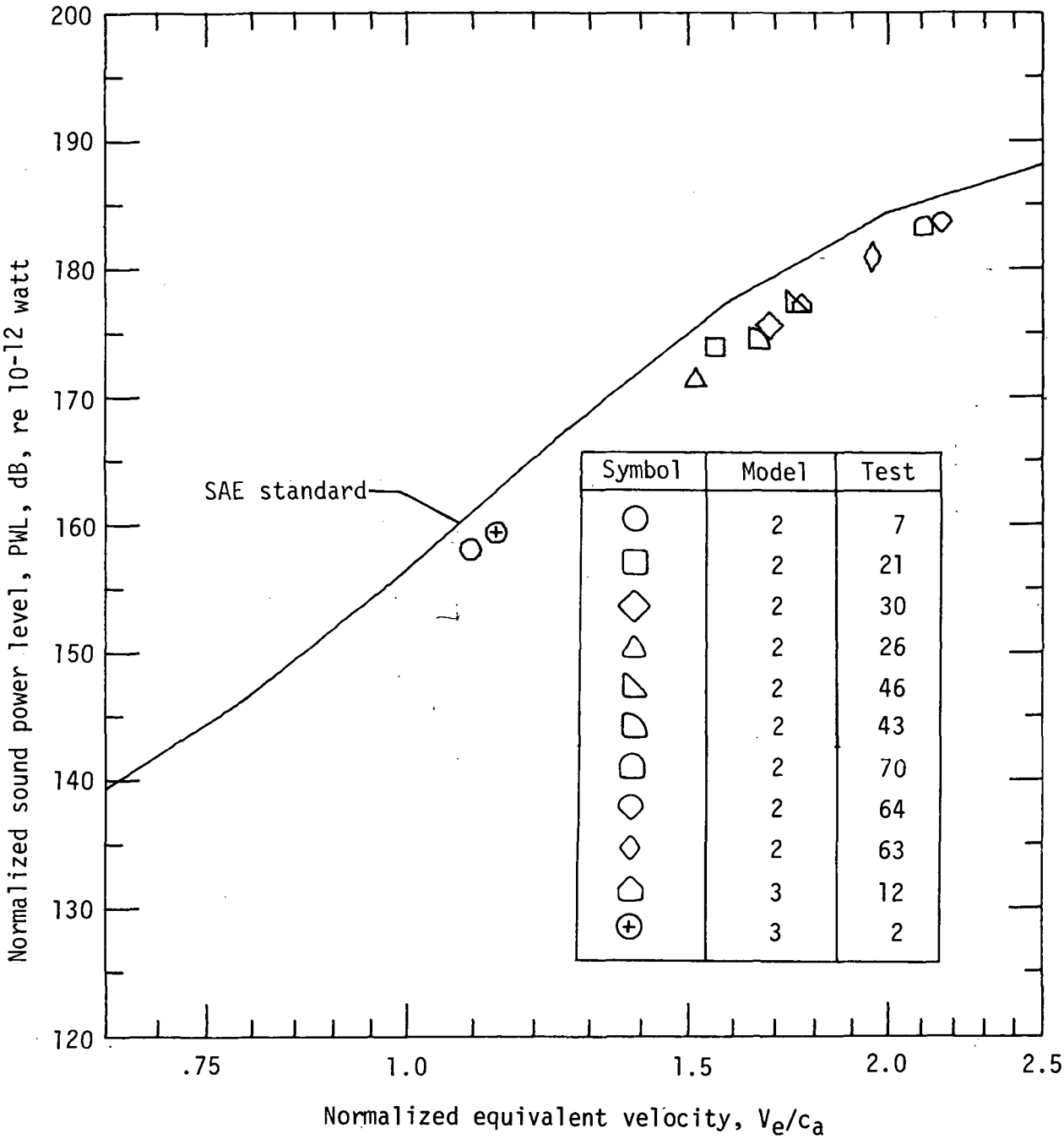

Figure 17.- Models 2 and 3 overall acoustic power levels for velocity ratios near 1.6.

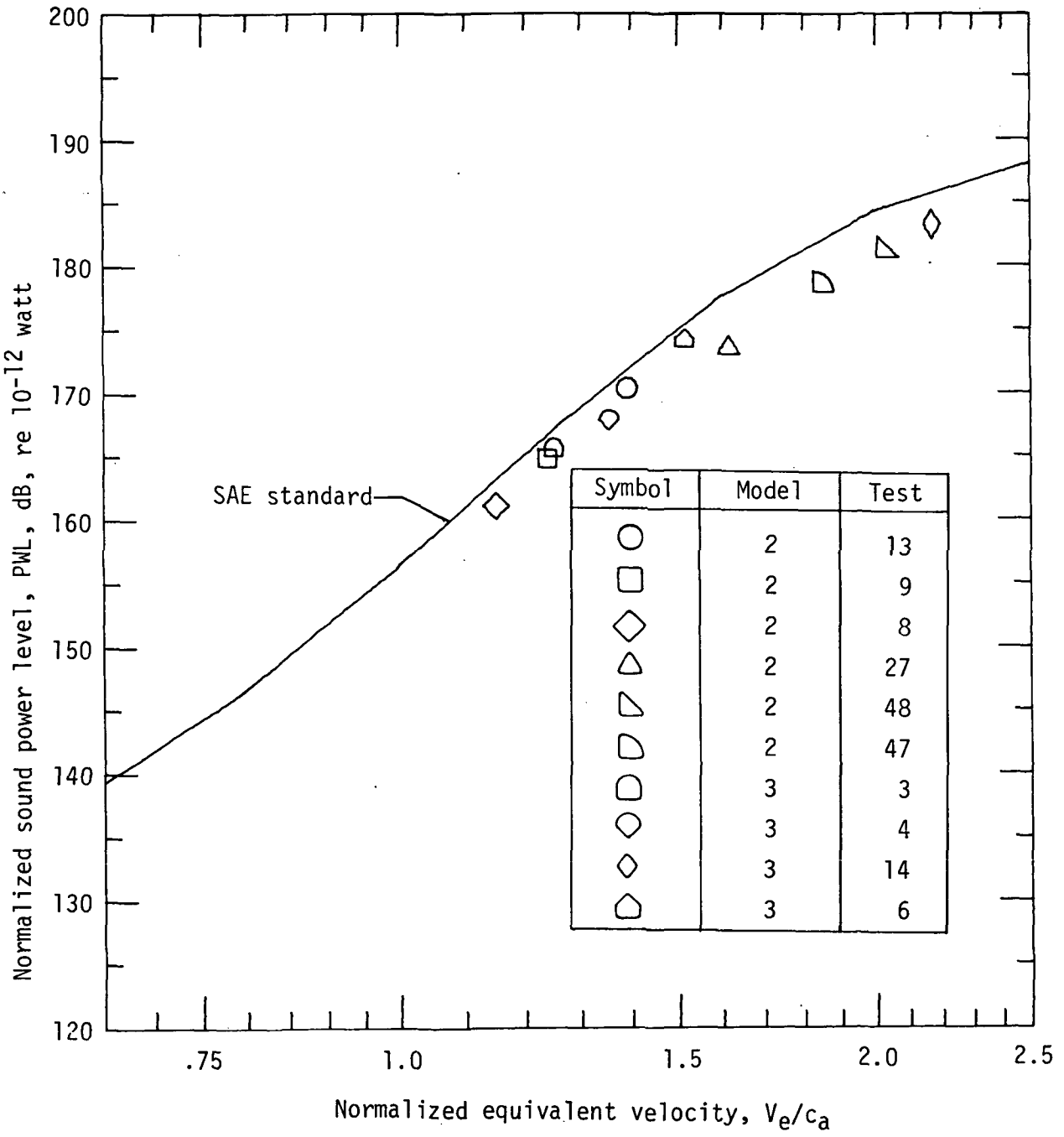

Figure 18.- Models 2 and 3 overall acoustic power levels for velocity ratios near 1.9.

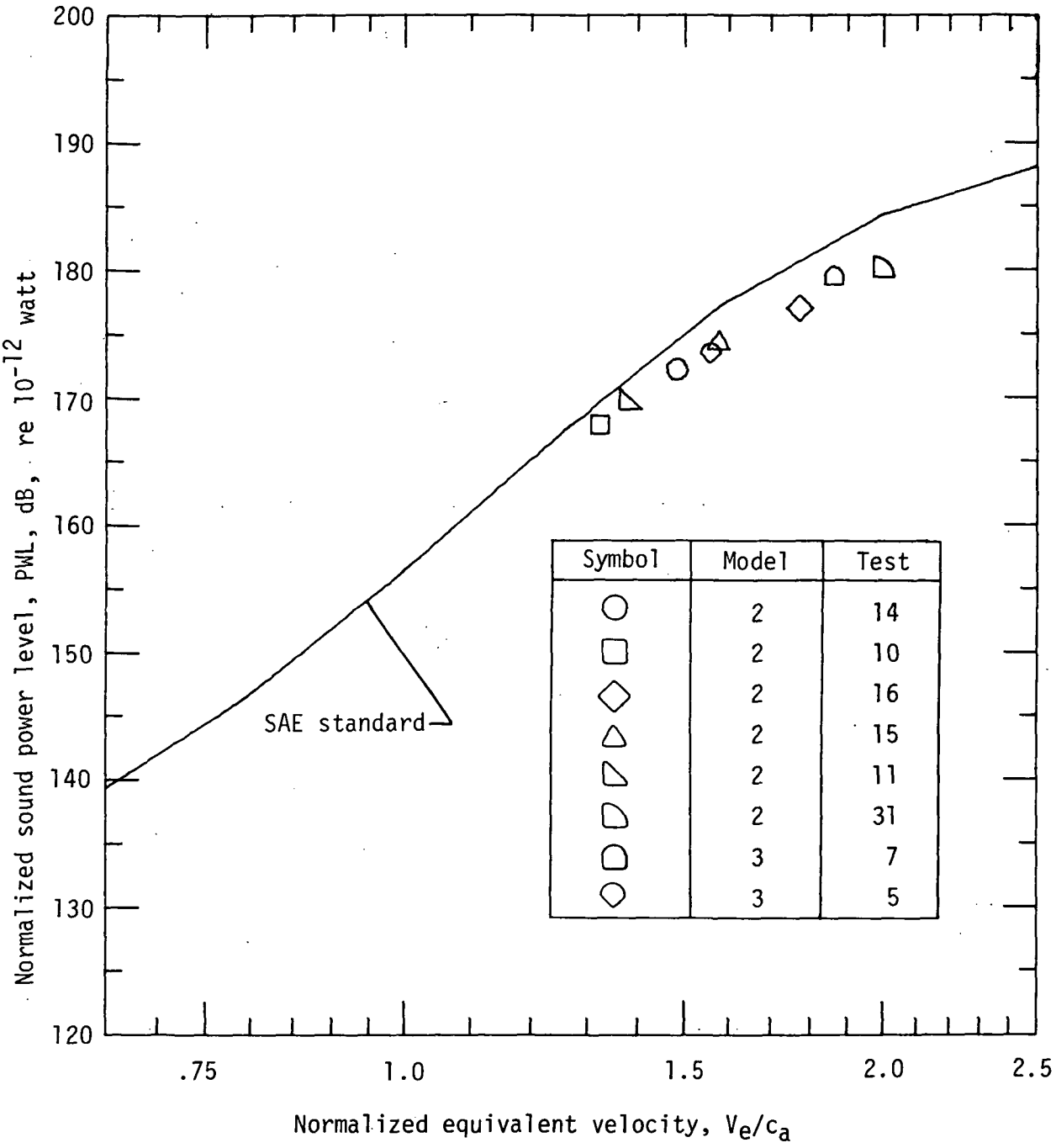

Figure 19.- Models 2 and 3 overall acoustic power levels for velocity ratios near 2.3.

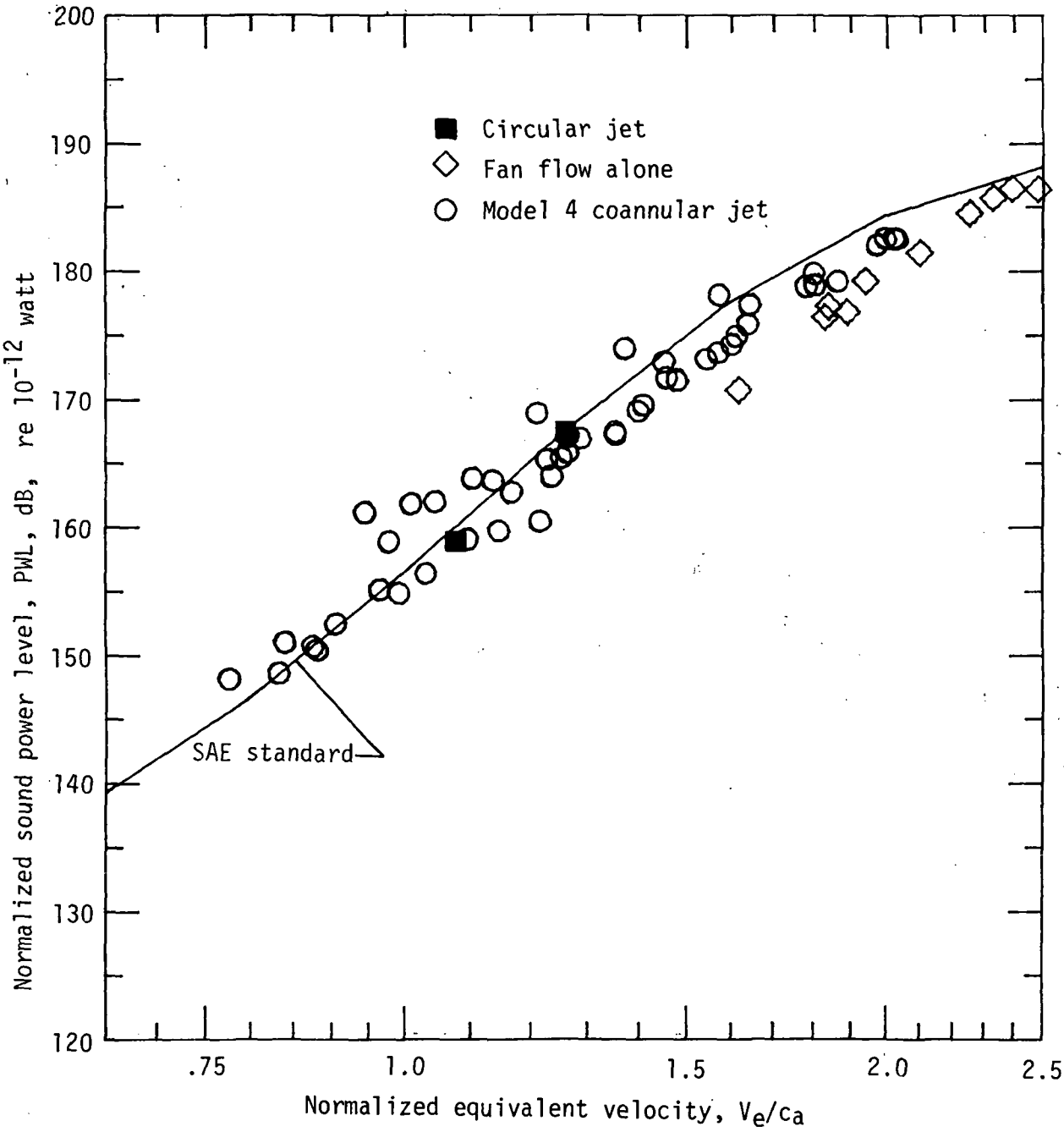

Figure 20.- Model 4 overall acoustic power levels.

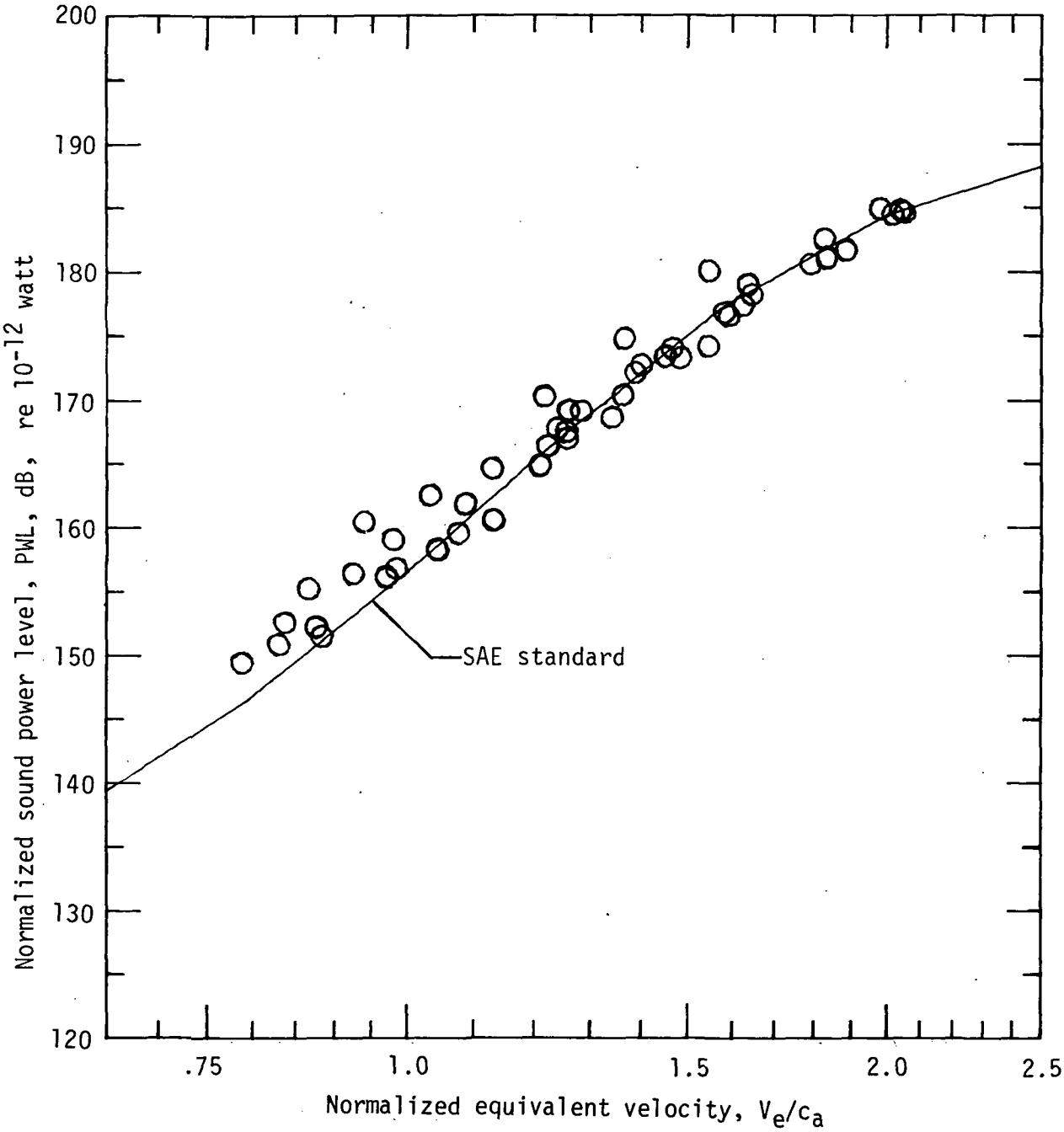

Figure 21.- Model 5 overall acoustic power levels.

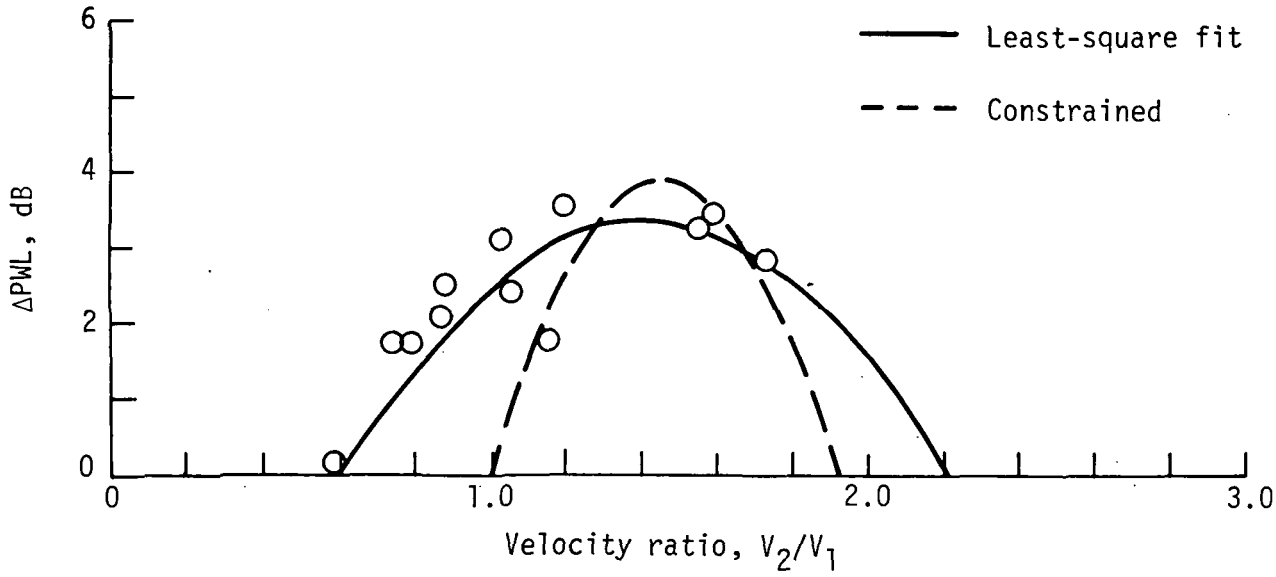

(a) 300 m/s ≦ V_e < 400 m/s.

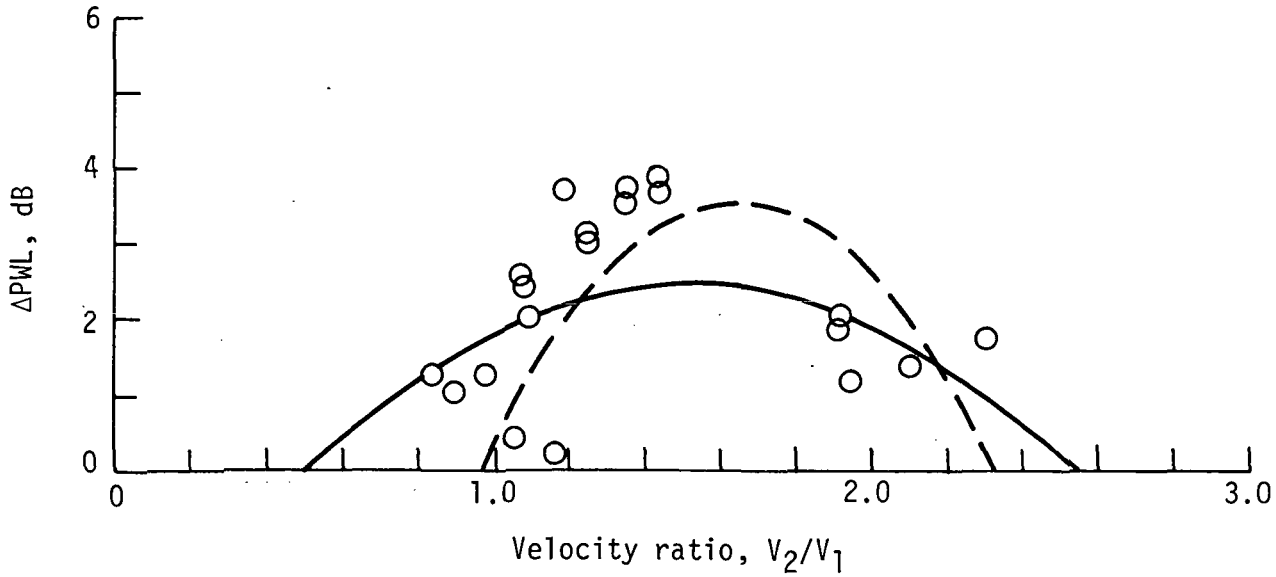

(b) 400 m/s ≦ V_e < 500 m/s.

Figure 22.- Sound power level reduction for models 2 and 3.

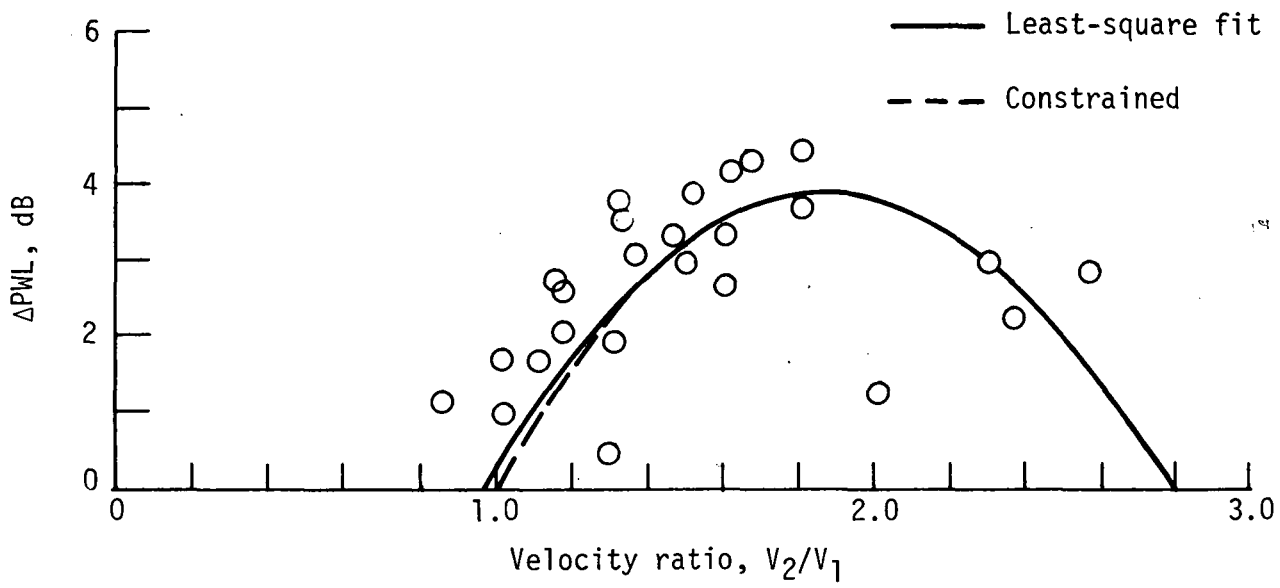

(c) 500 m/s ≦ V_e < 600 m/s.

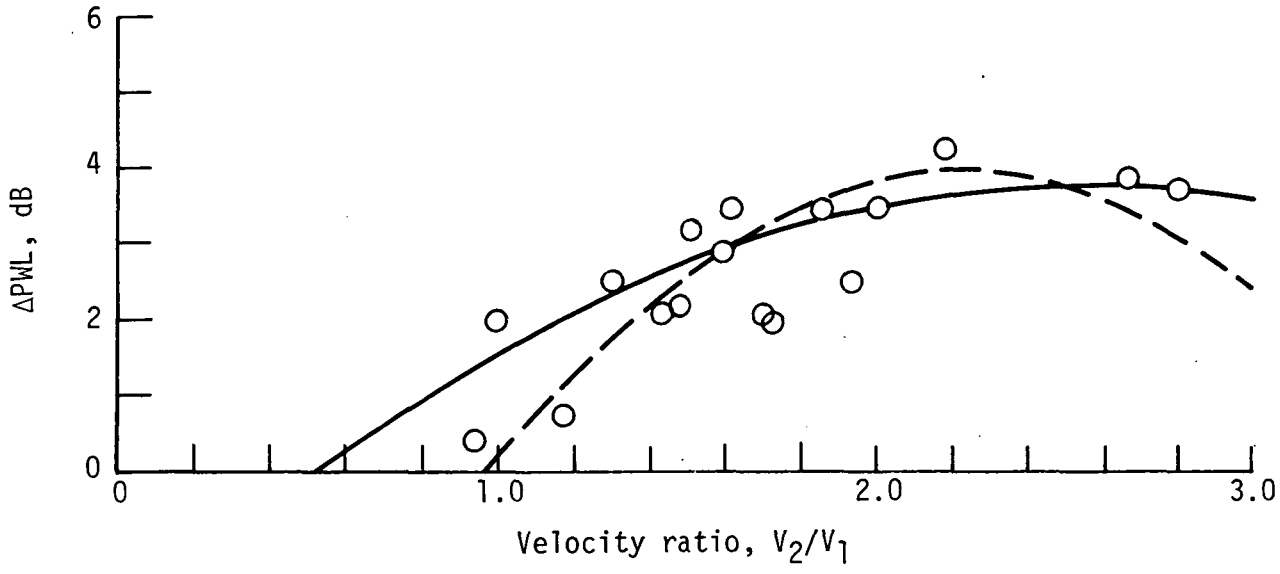

(d) 600 m/s ≦ V_e.

Figure 22.- Concluded.

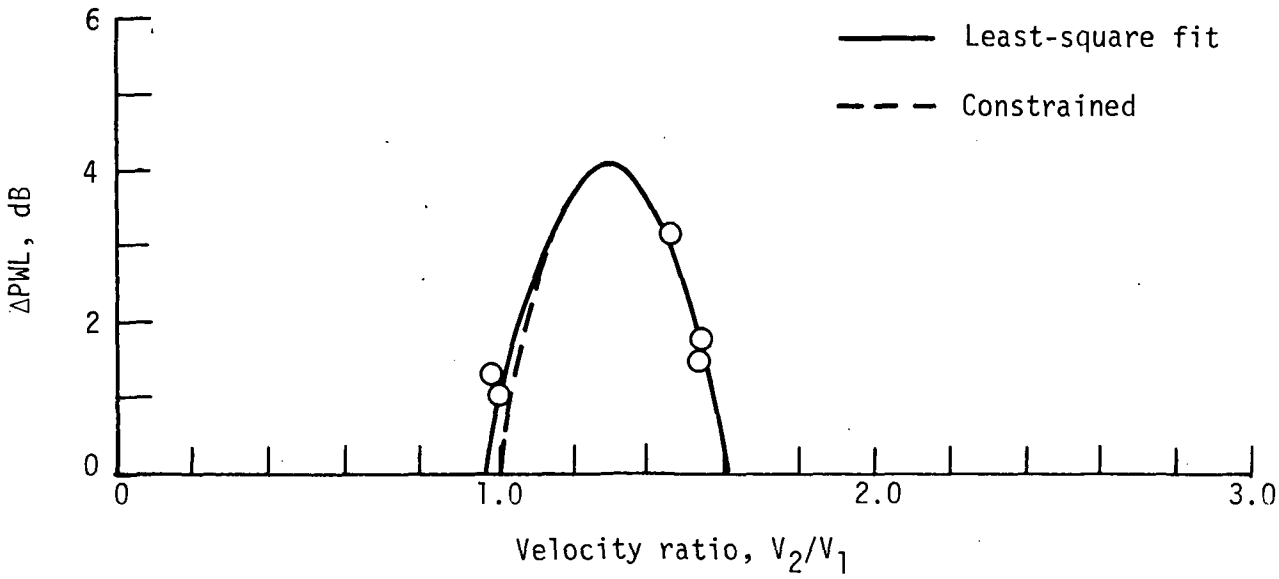

(a) 300 m/s $\leqq V_e <$ 400 m/s.

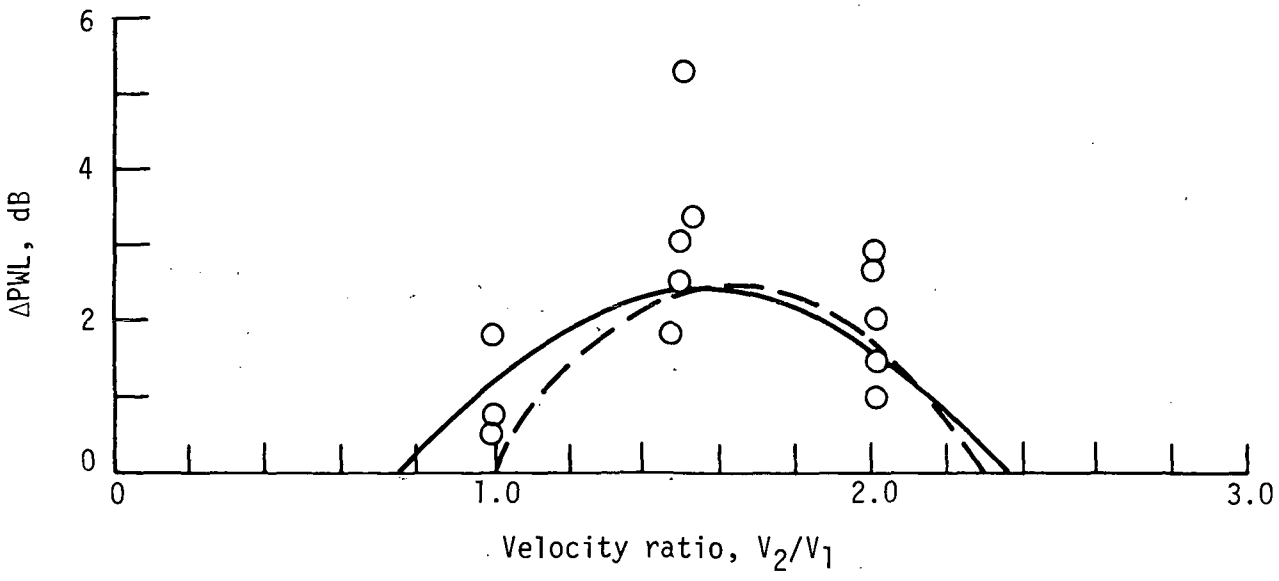

(b) 400 m/s $\leqq V_e <$ 500 m/s.

Figure 23.- Sound power level reduction for model 4.

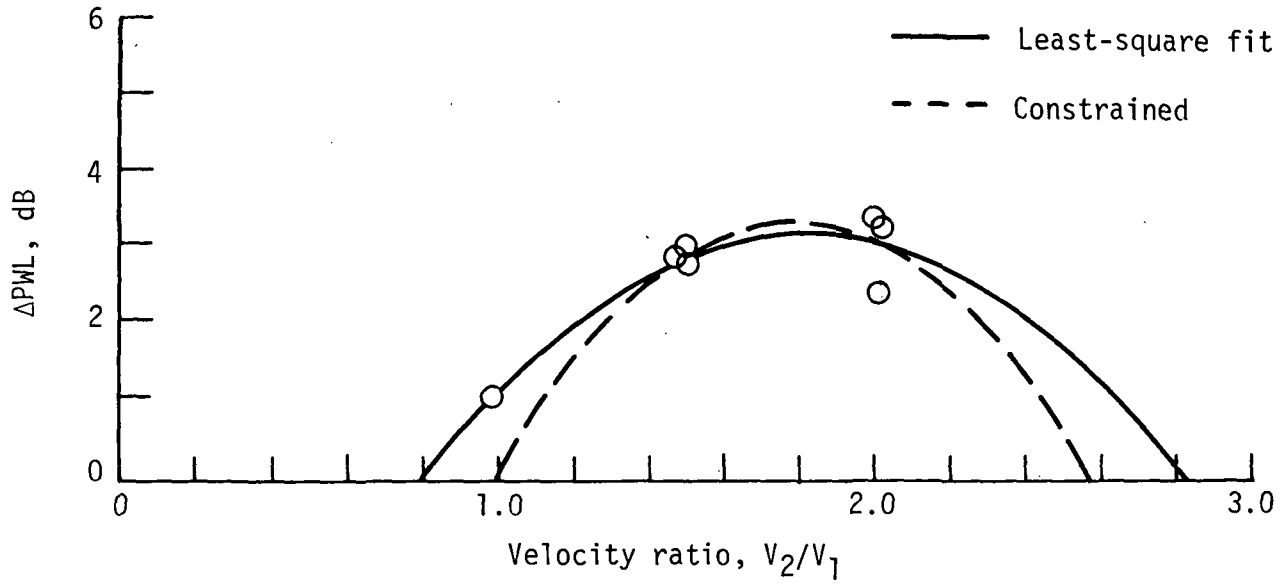

(c) 500 m/s ≦ V_e < 600 m/s.

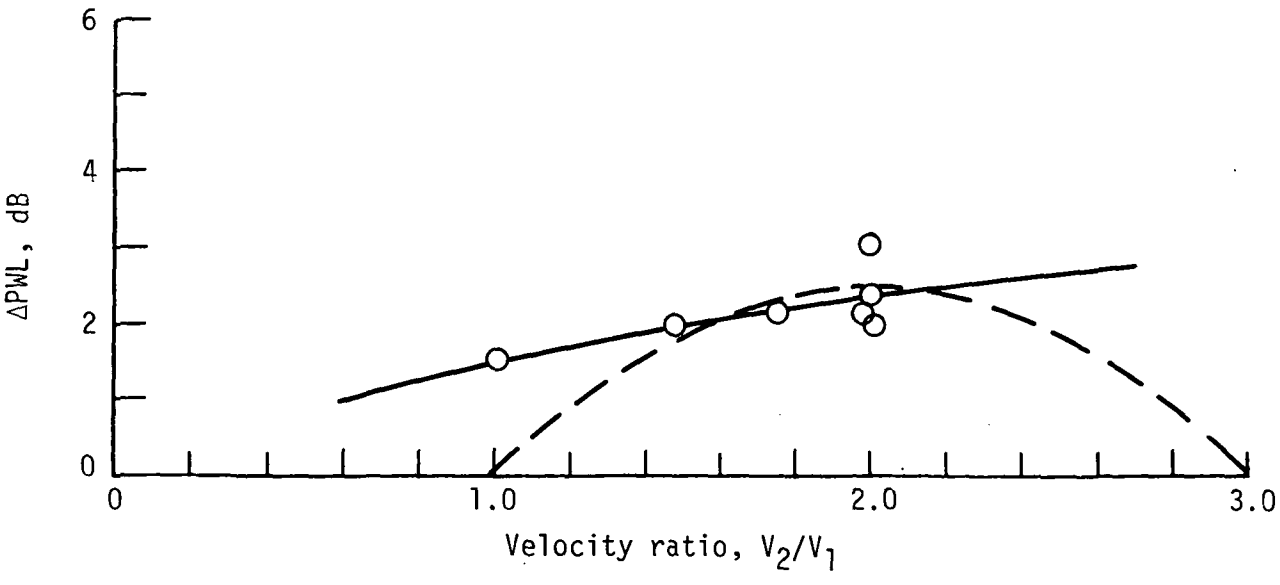

(d) 600 m/s ≦ V_e.

Figure 23.- Concluded.

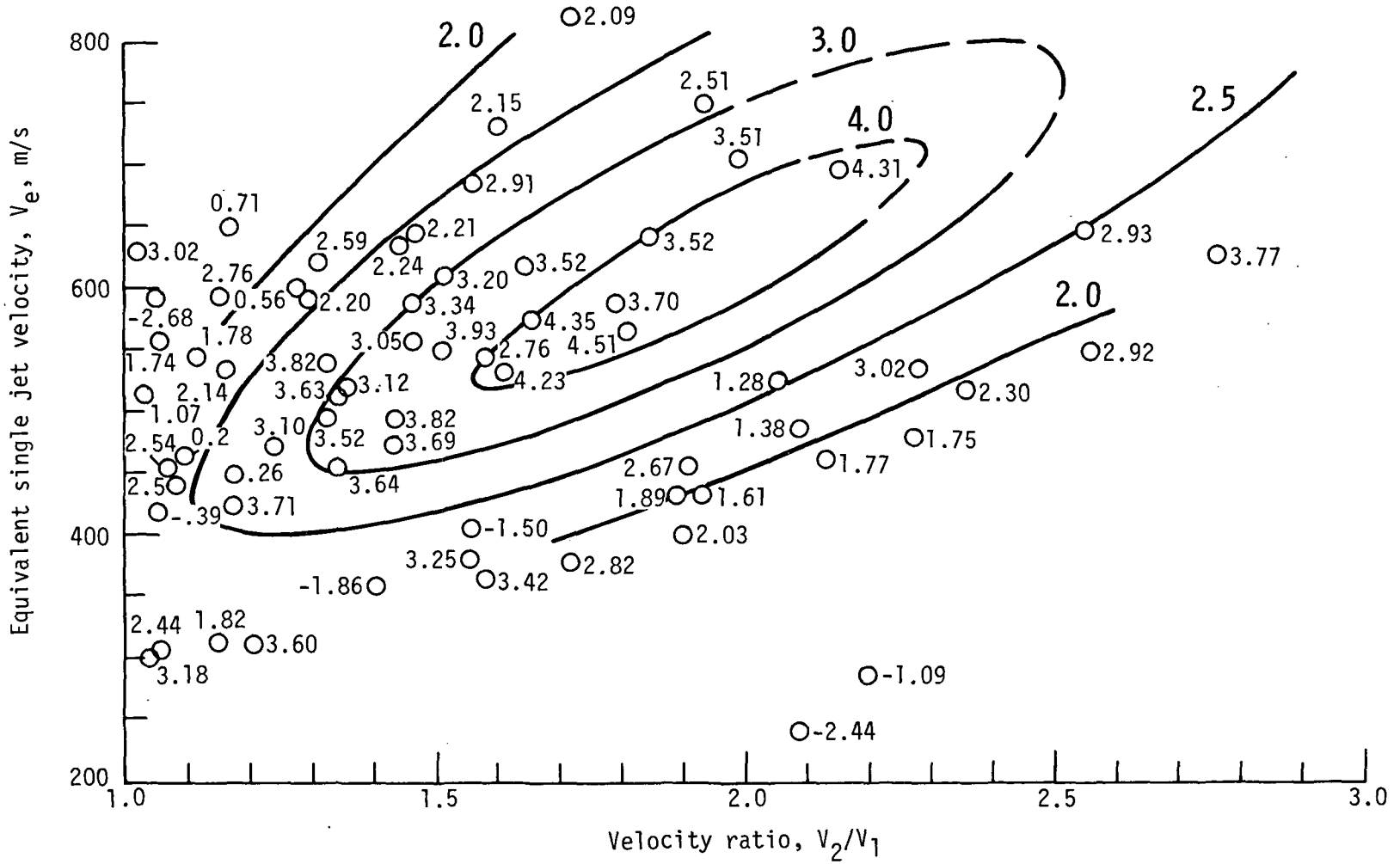

Figure 24.- Sound power level reduction contours for models 2 and 3. Numbers next to data points indicate sound power reduction in dB.

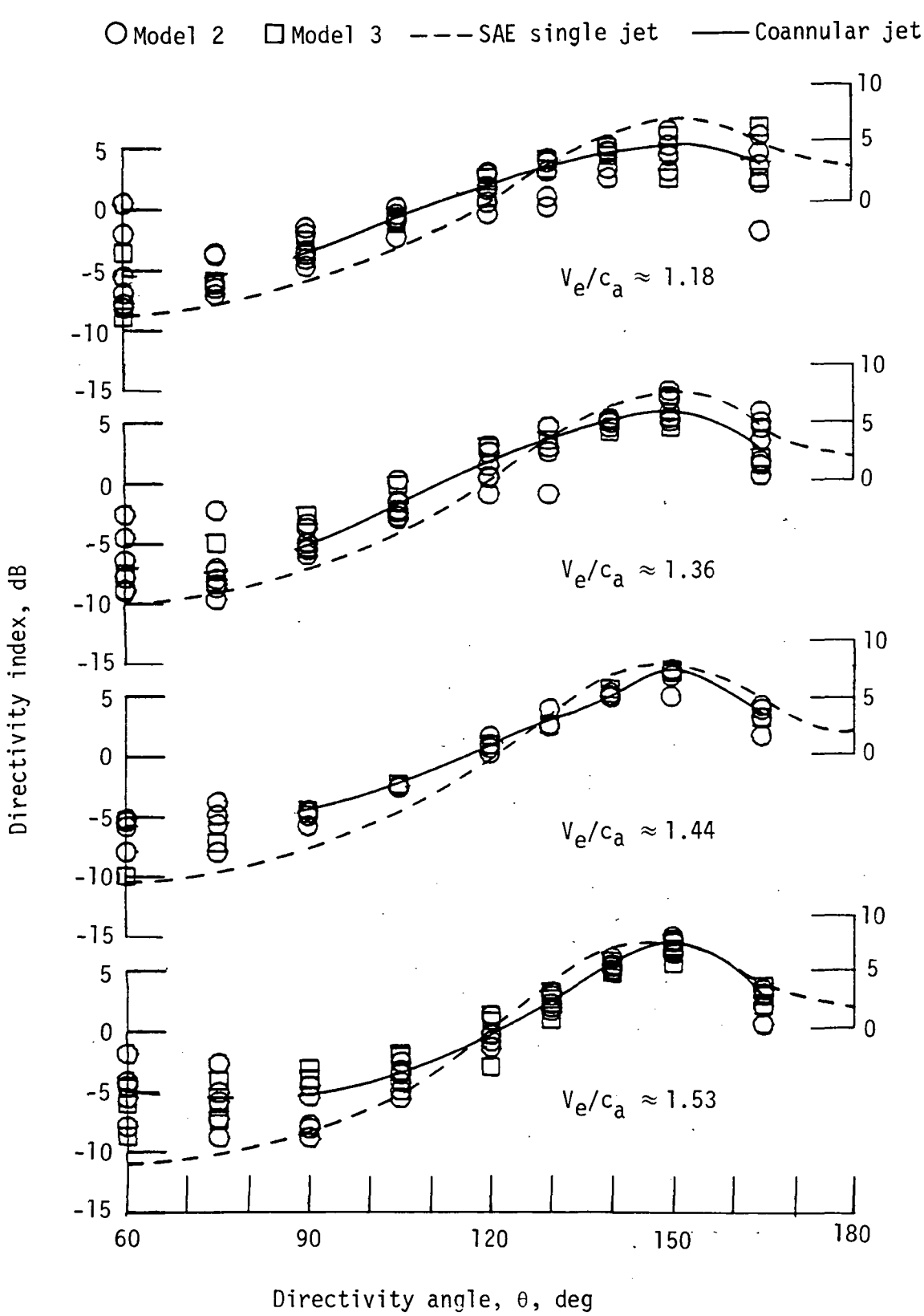

Figure 25.- Directivity index for models 2 and 3.

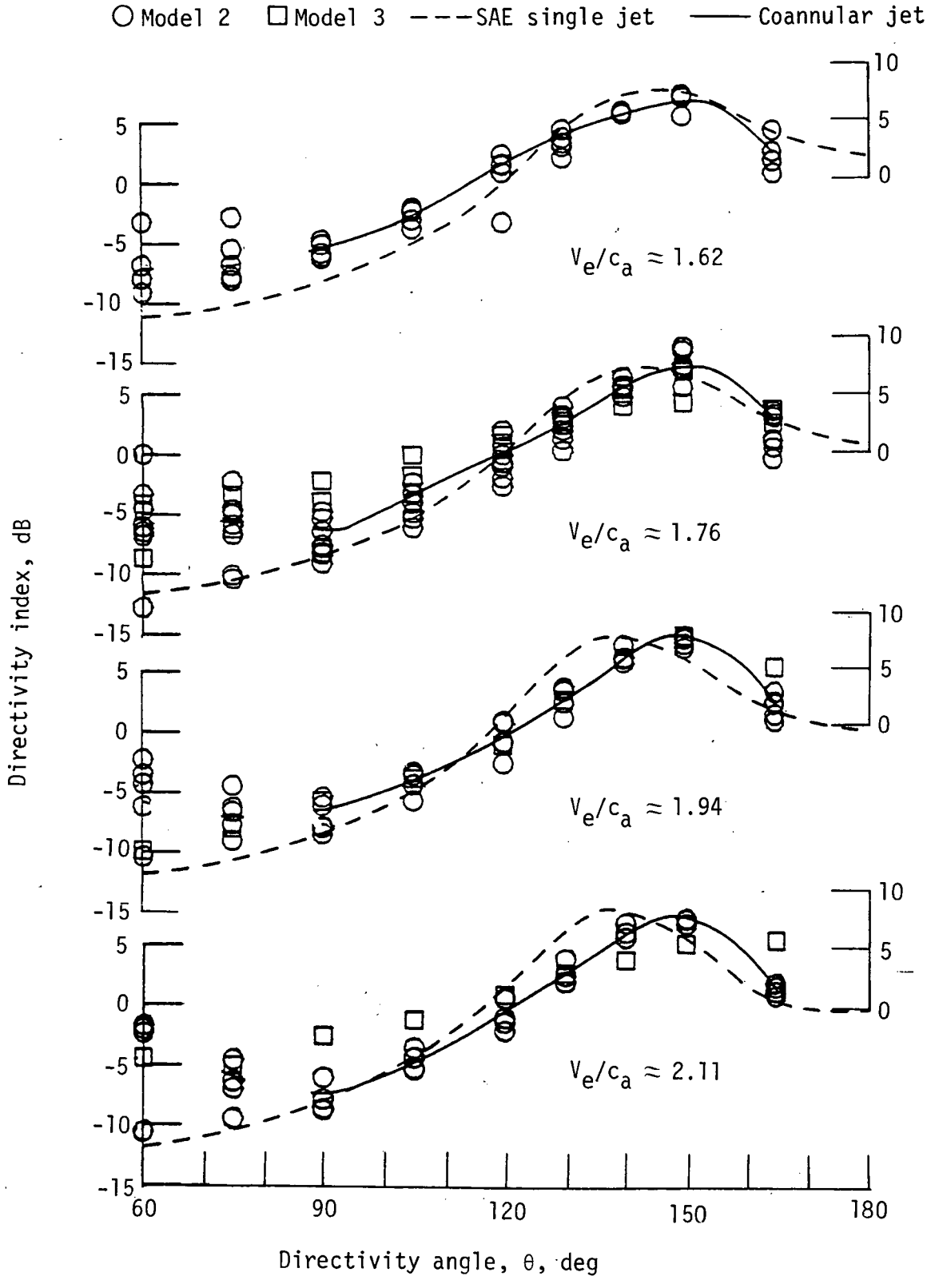

Figure 25.- Concluded.

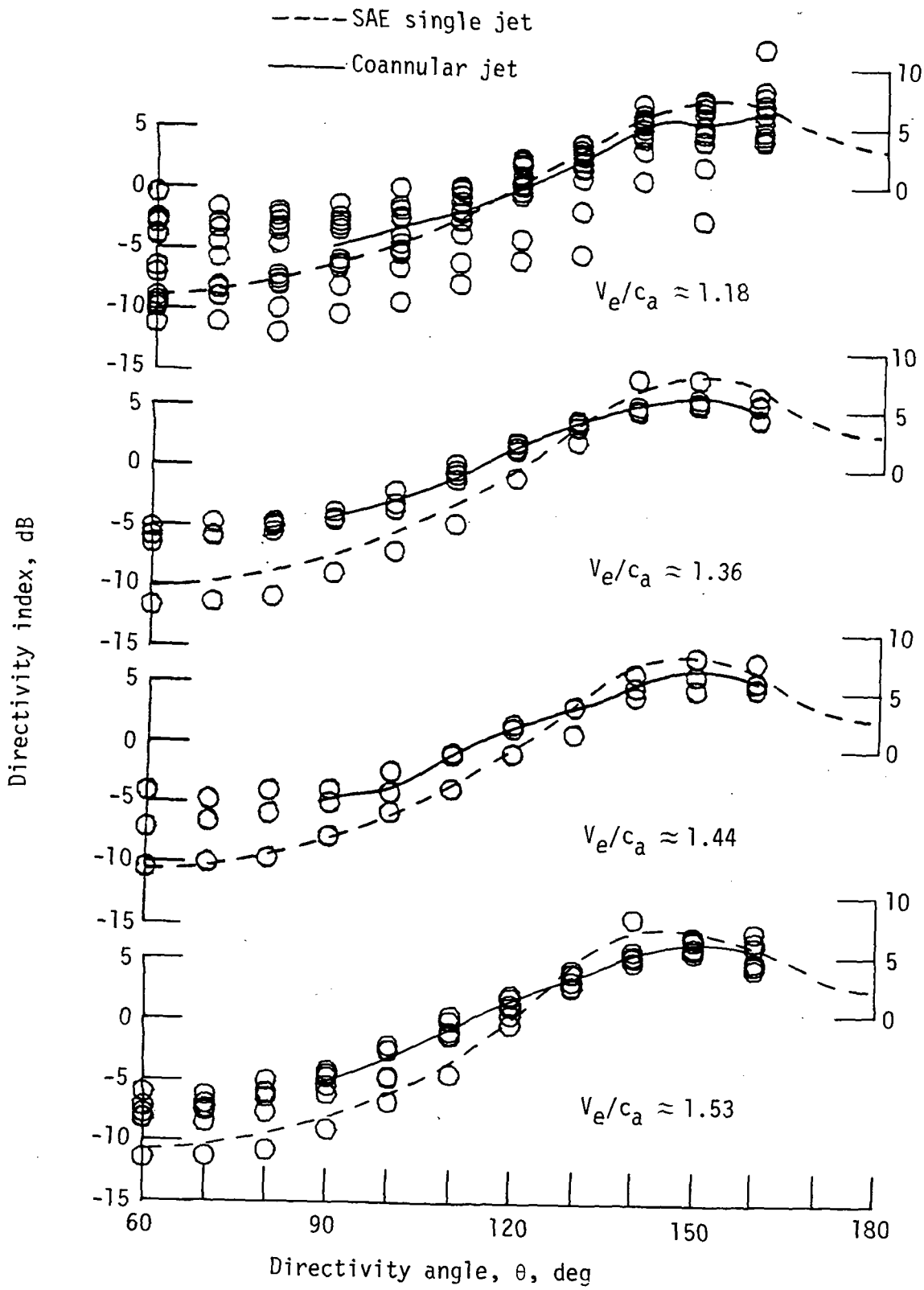

Figure 26.- Directivity index for model 4.

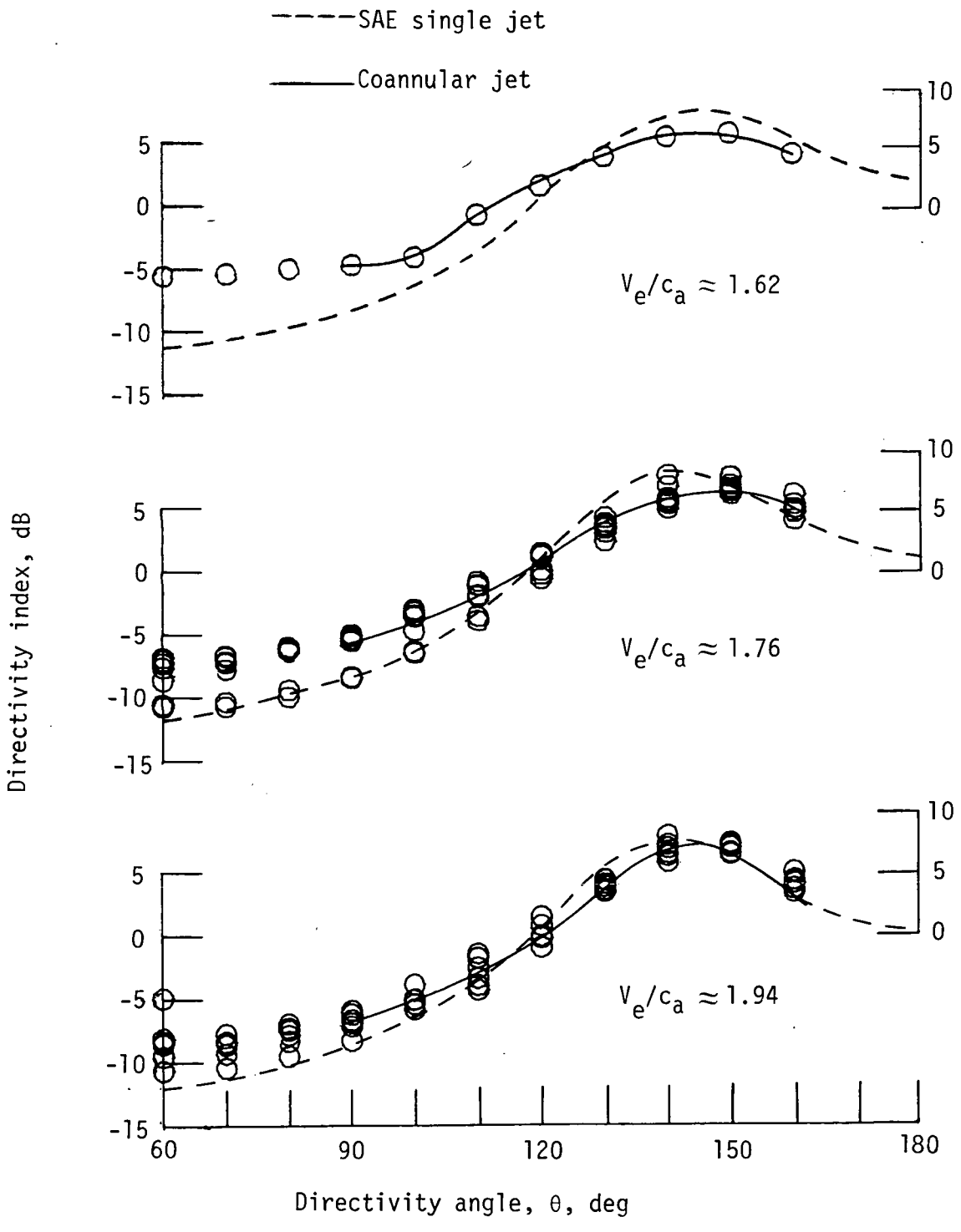

Figure 26.- Concluded.

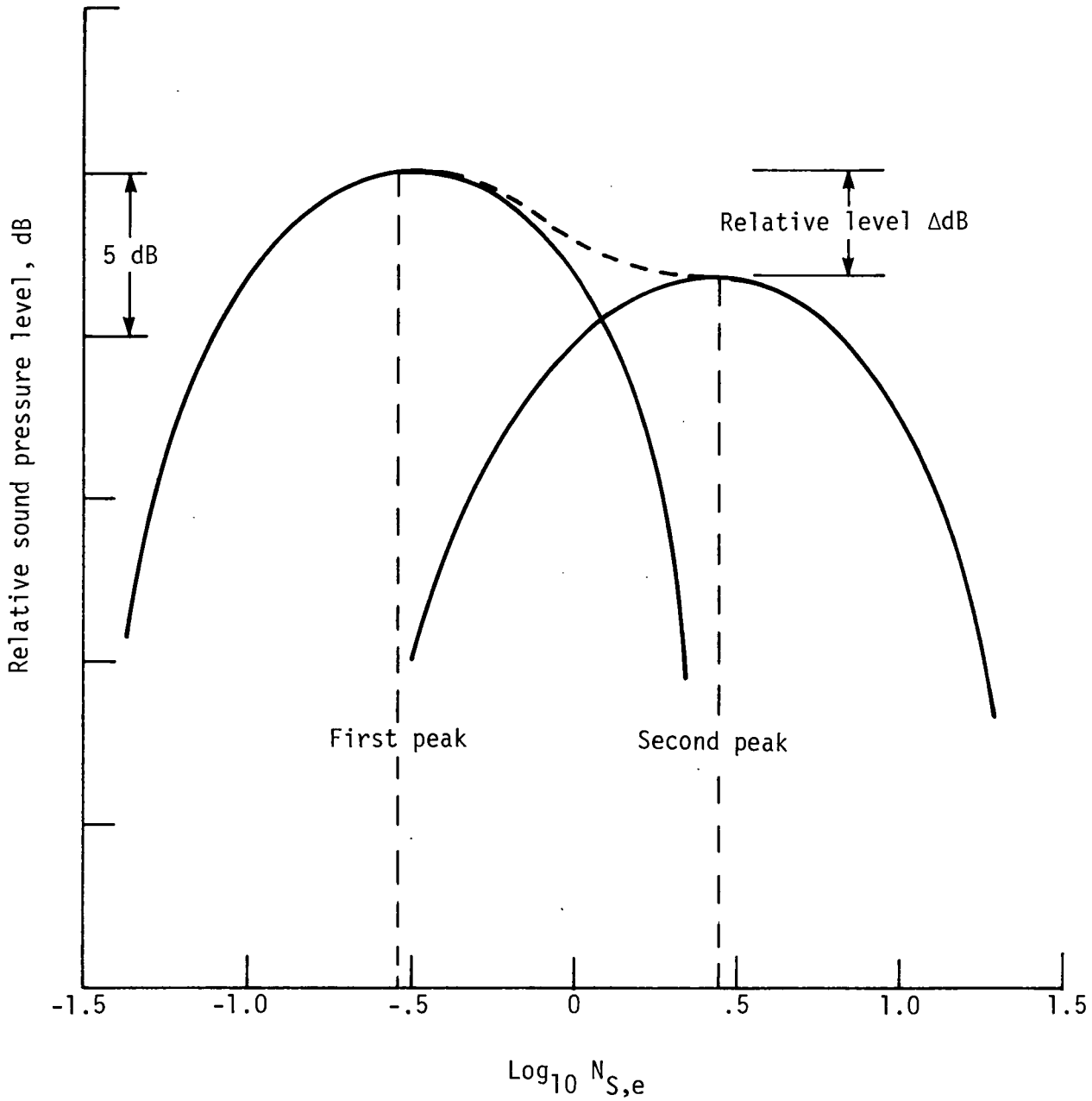

Figure 27.- Typical spectrum for coannular jet.

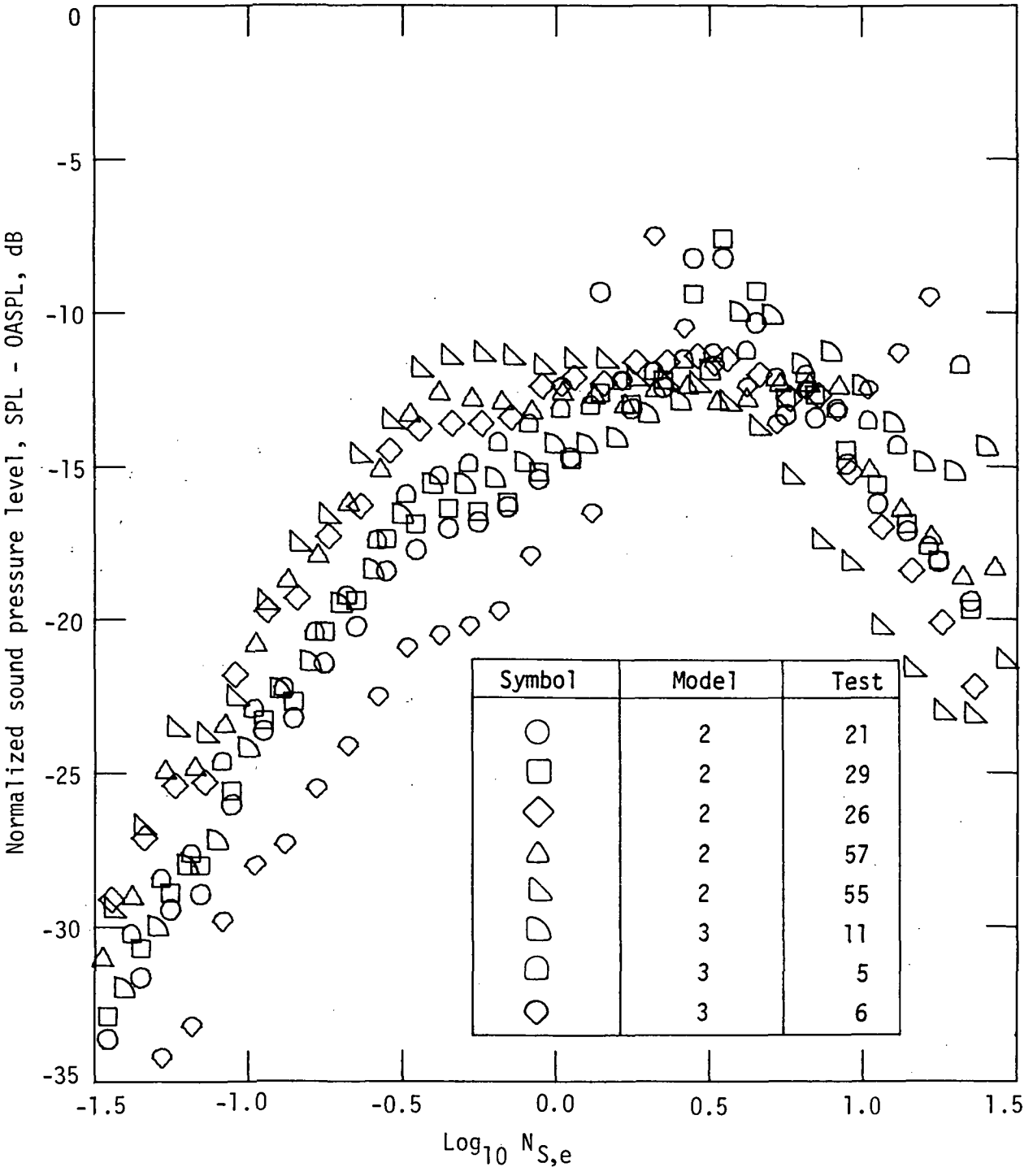

(a) Directivity angle, 90°.

Figure 28.- One-third-octave band spectrum for models 2 and 3 with V_e/c_a near 1.55.

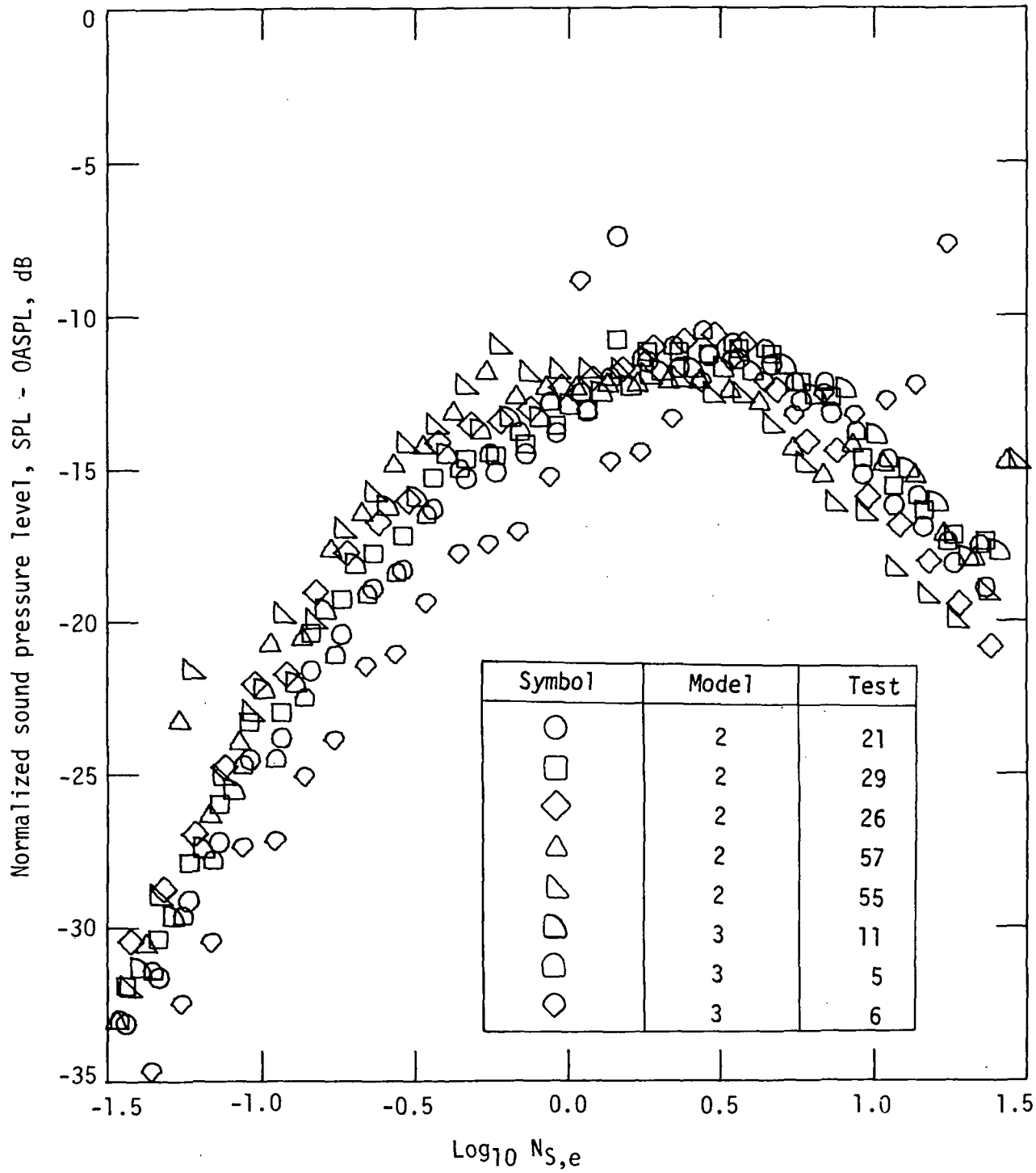

(b) Directivity angle, 105°.

Figure 28.- Continued.

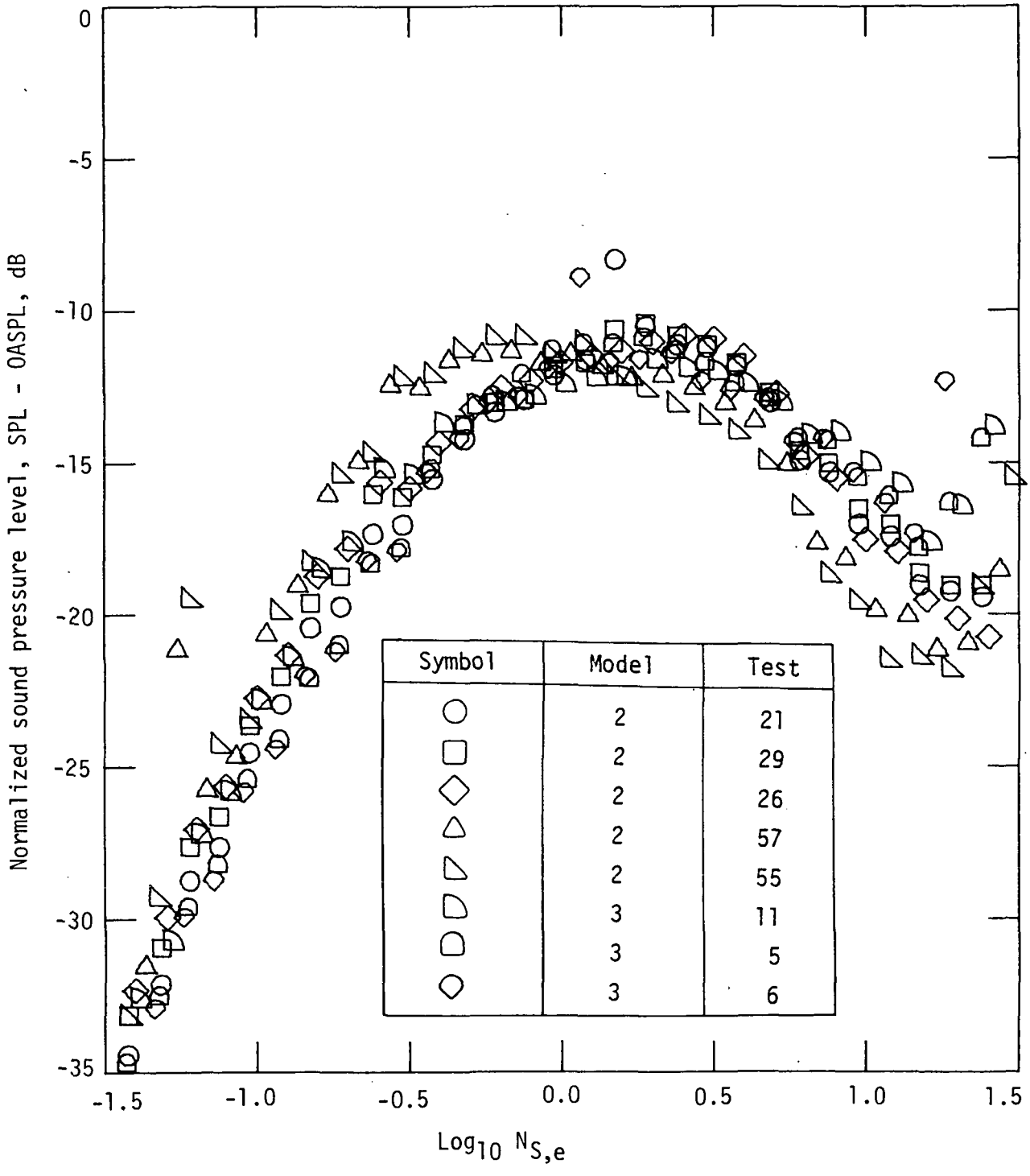

(c) Directivity angle, 120°.

Figure 28.- Continued.

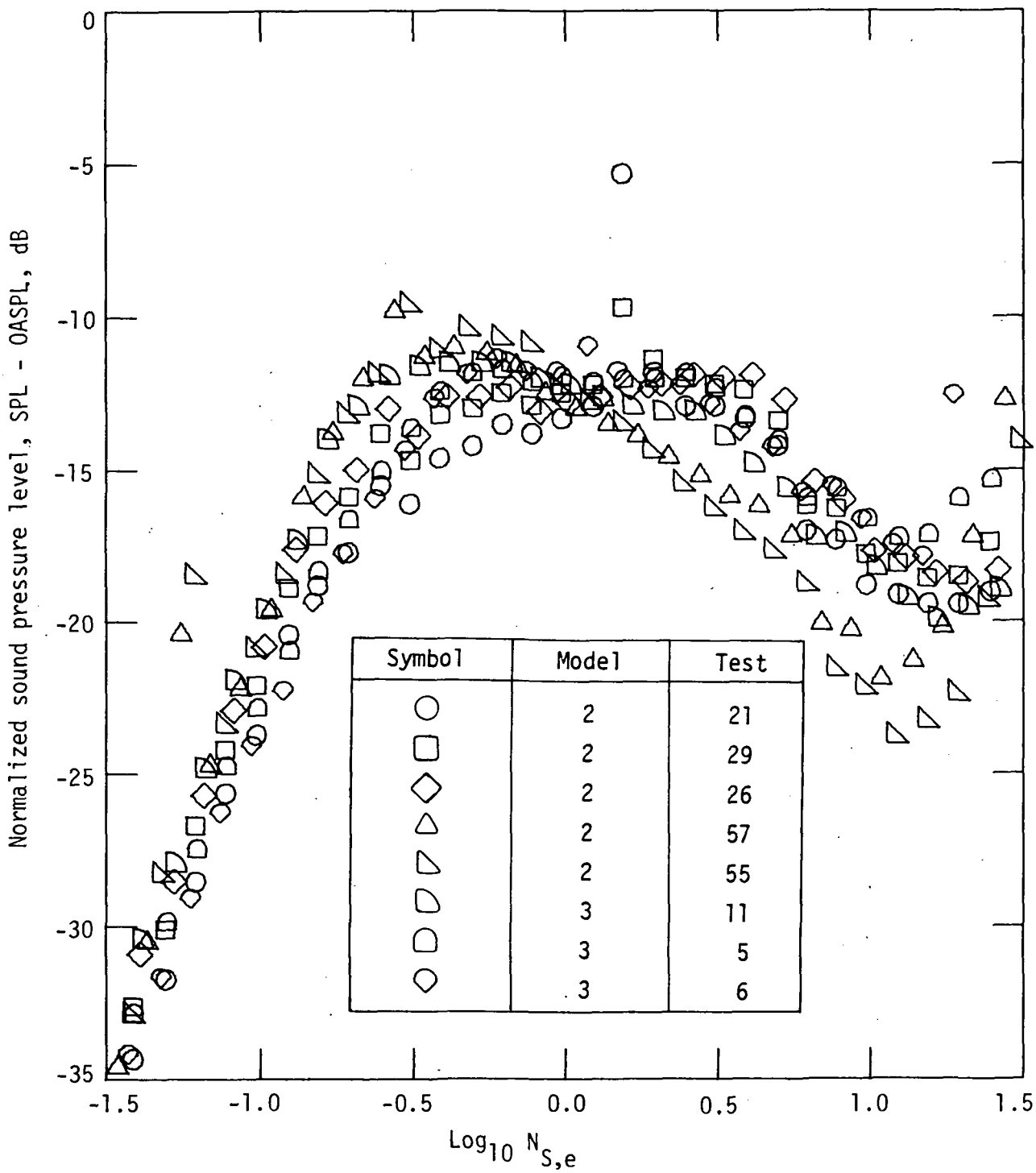

(d) Directivity angle, 130°.

Figure 28.- Continued.

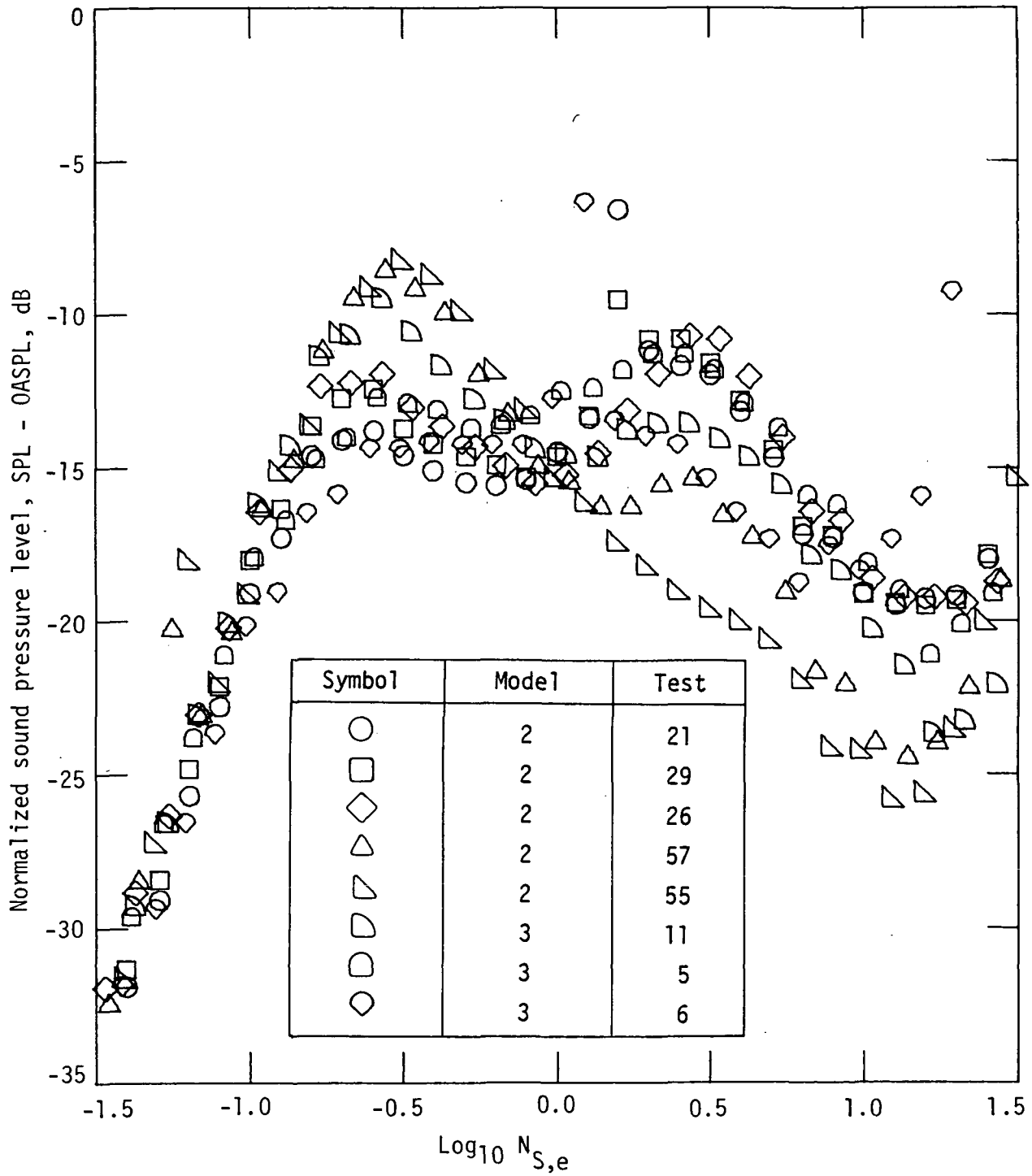

(e) Directivity angle, 140°.

Figure 28.- Continued.

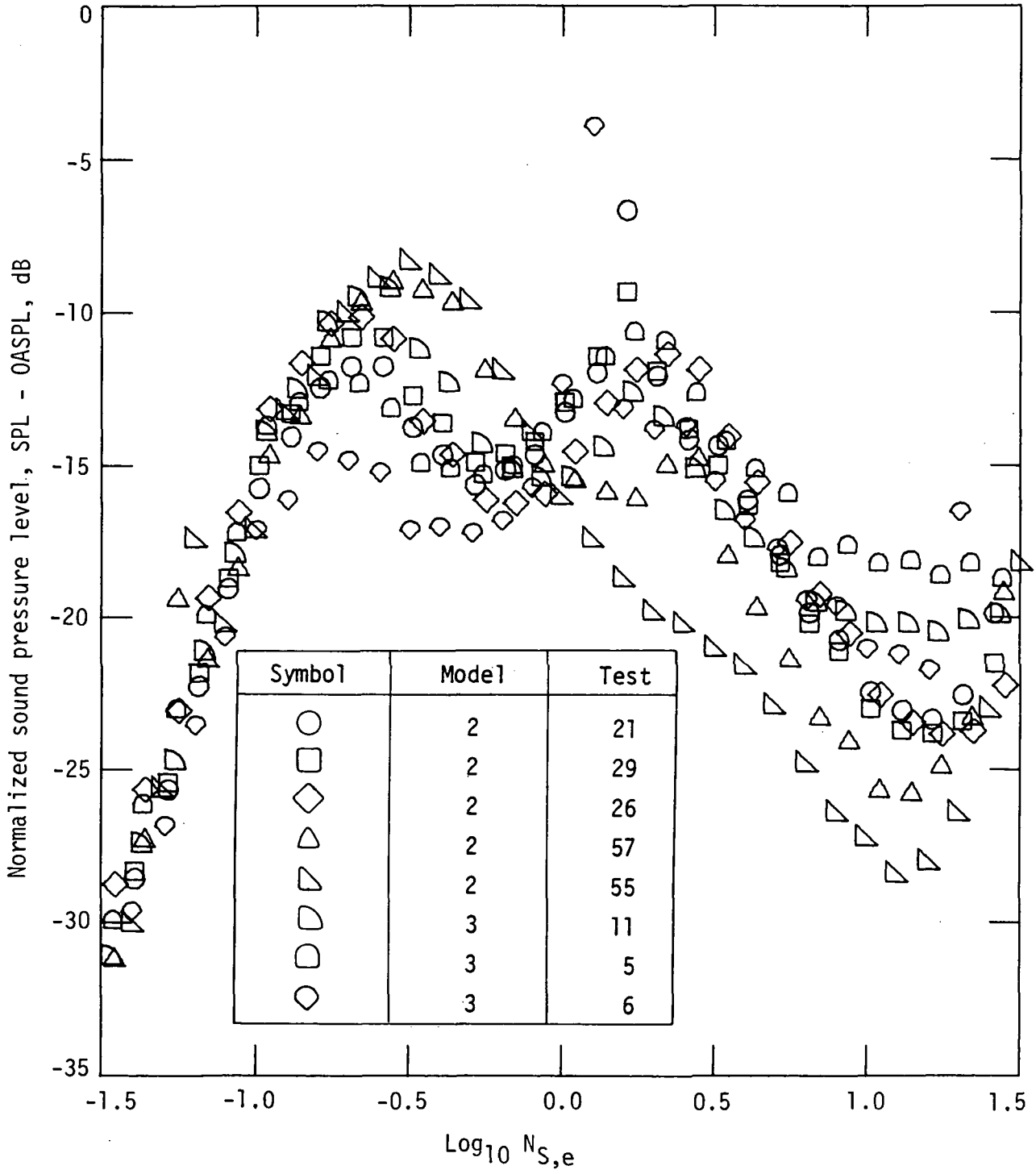

(f) Directivity angle, 150°.

Figure 28.- Continued.

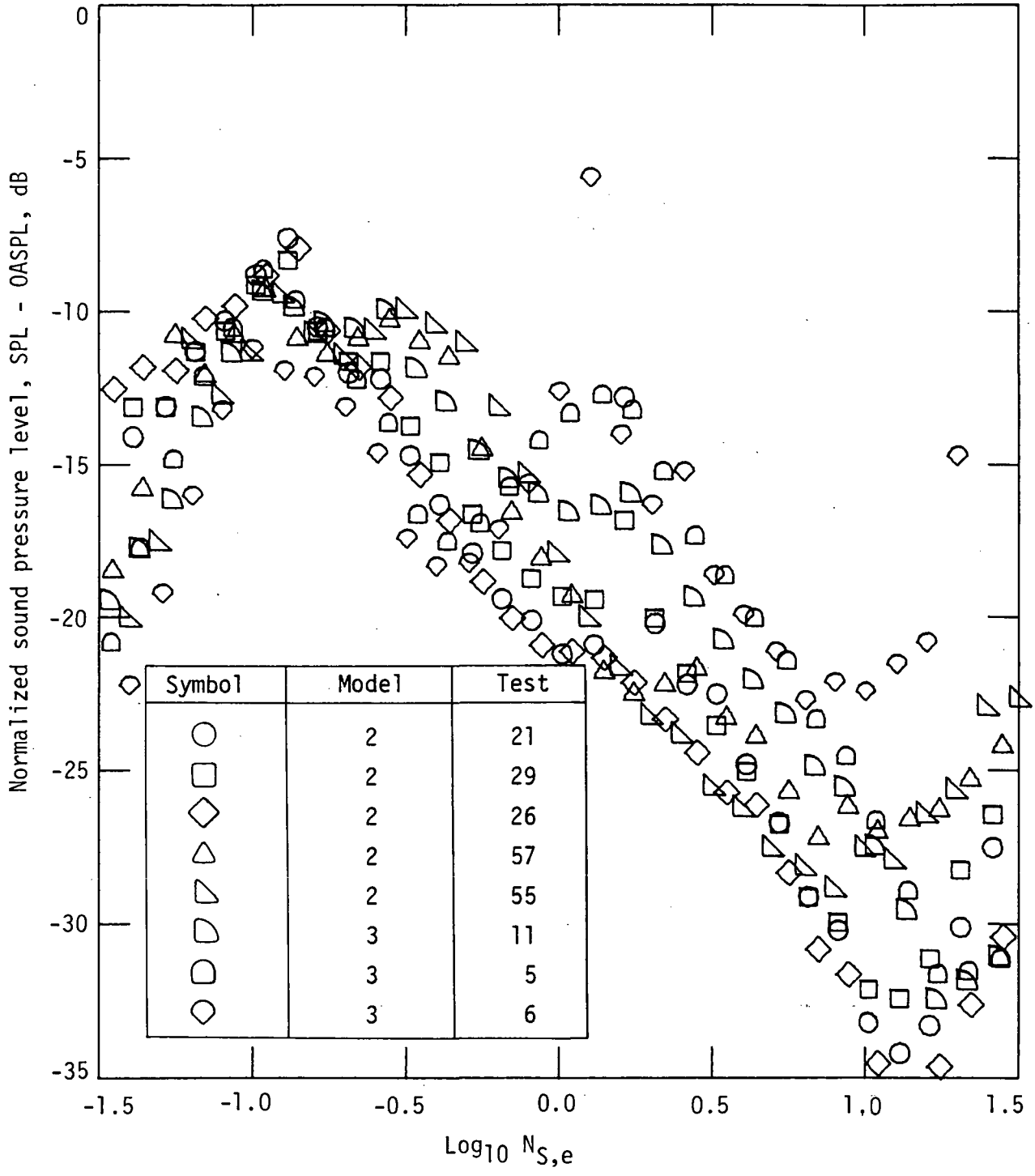

(g) Directivity angle, 165°.

Figure 28.- Concluded.

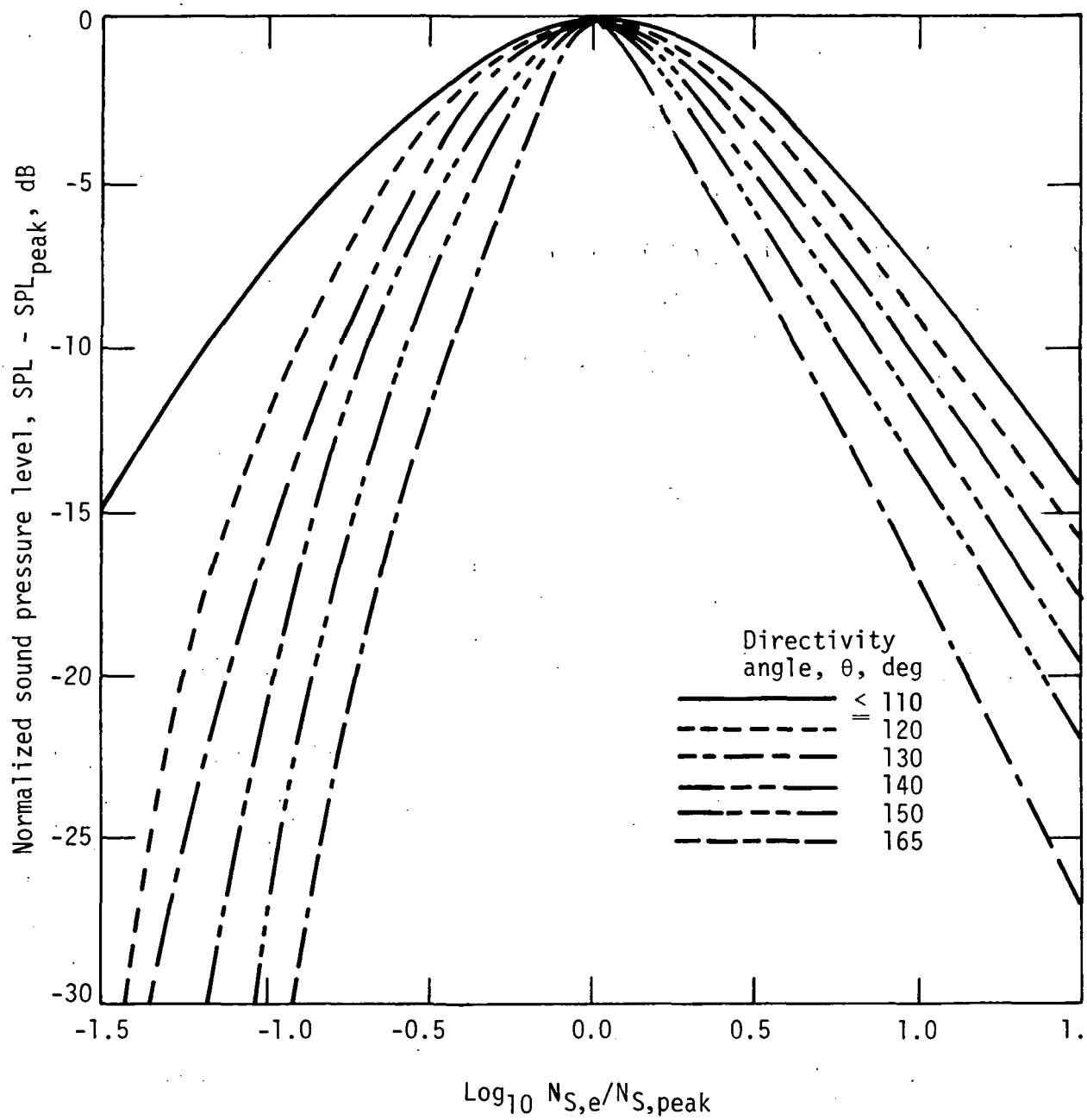

Figure 29.- Variation of spectral shape with directivity angle for models 2 and 3.

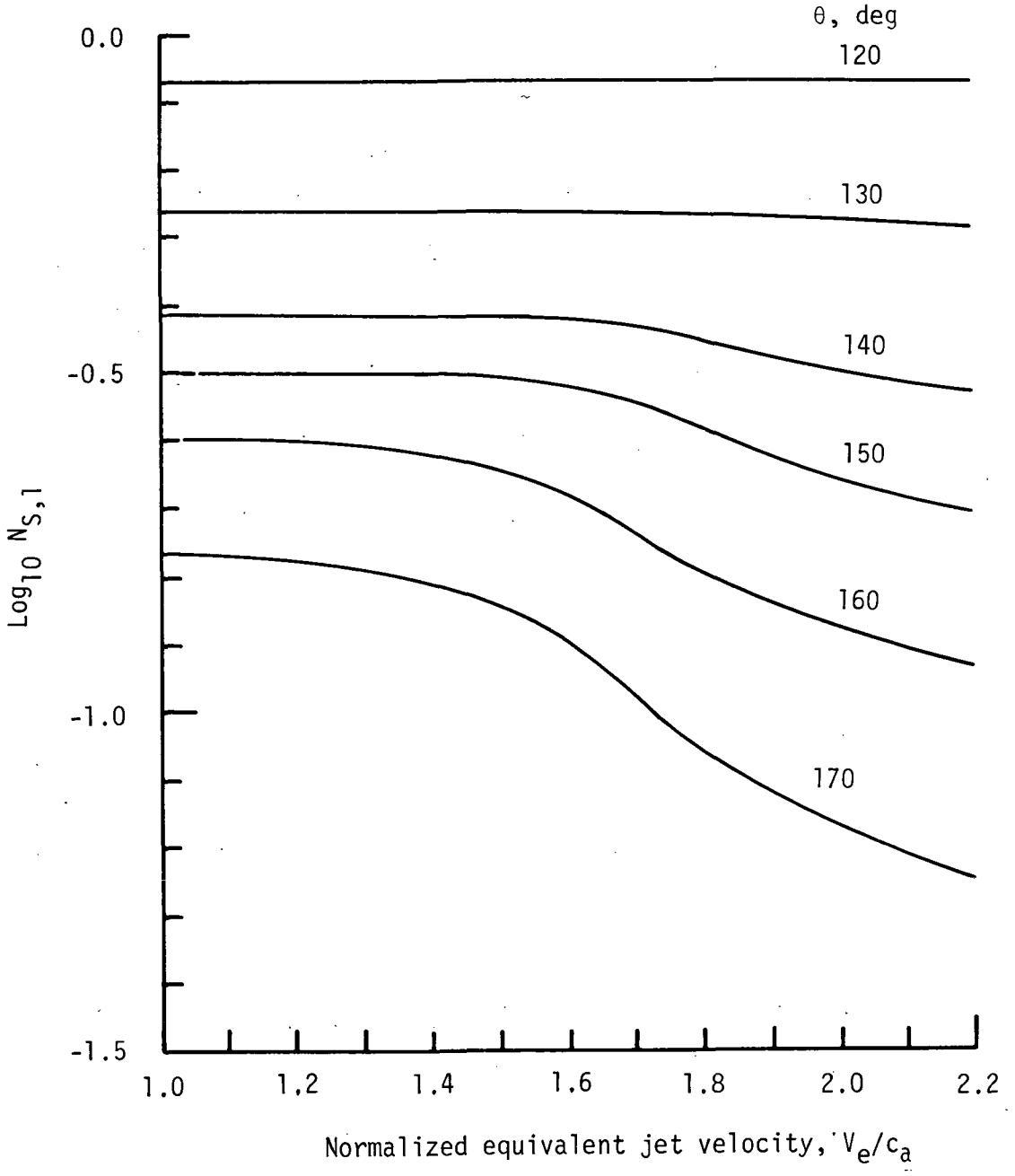

Figure 30.- Peak Strouhal number of first spectral component for models 2 and 3.

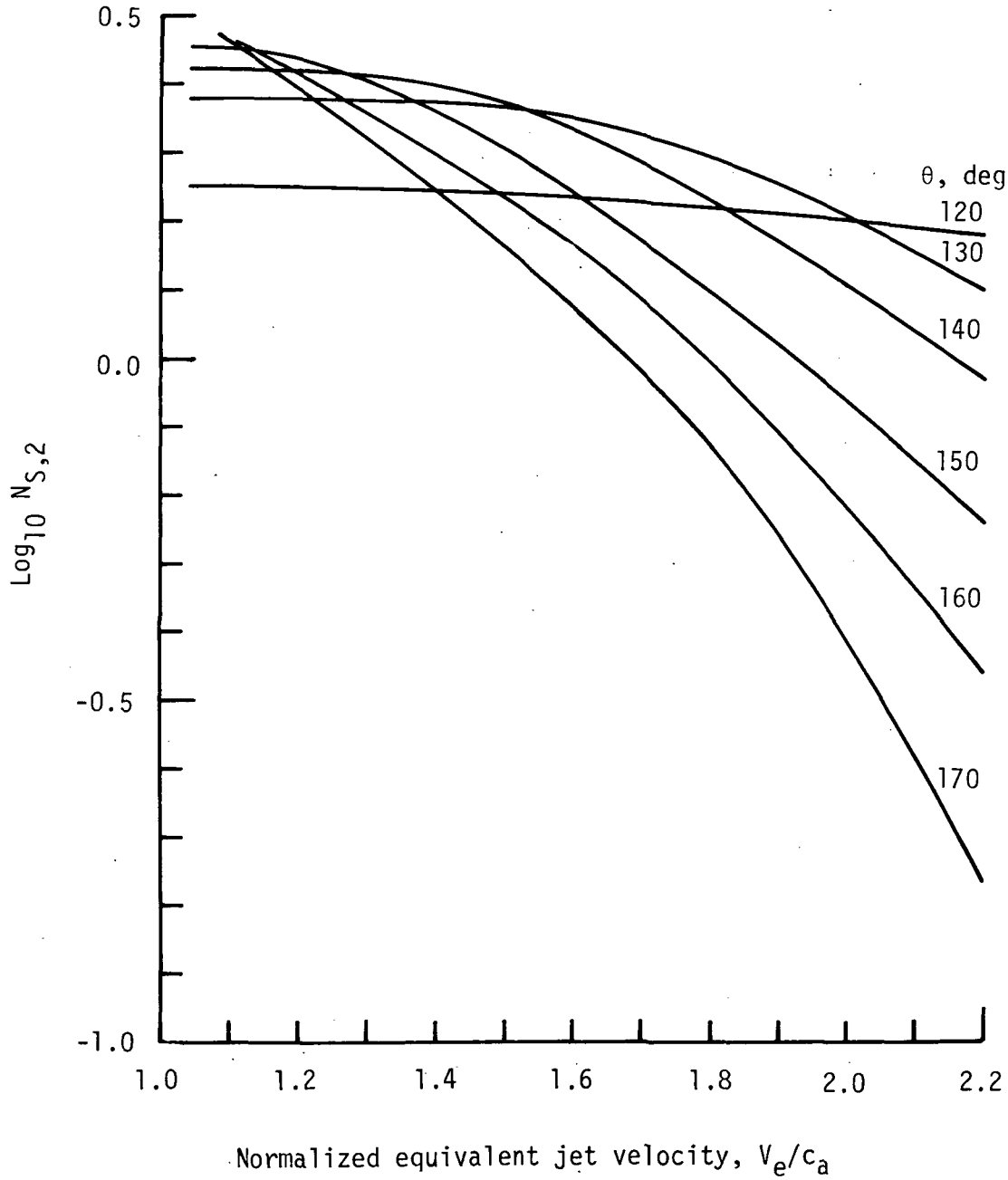

Figure 31.- Peak Strouhal number of second spectral component for models 2 and 3.

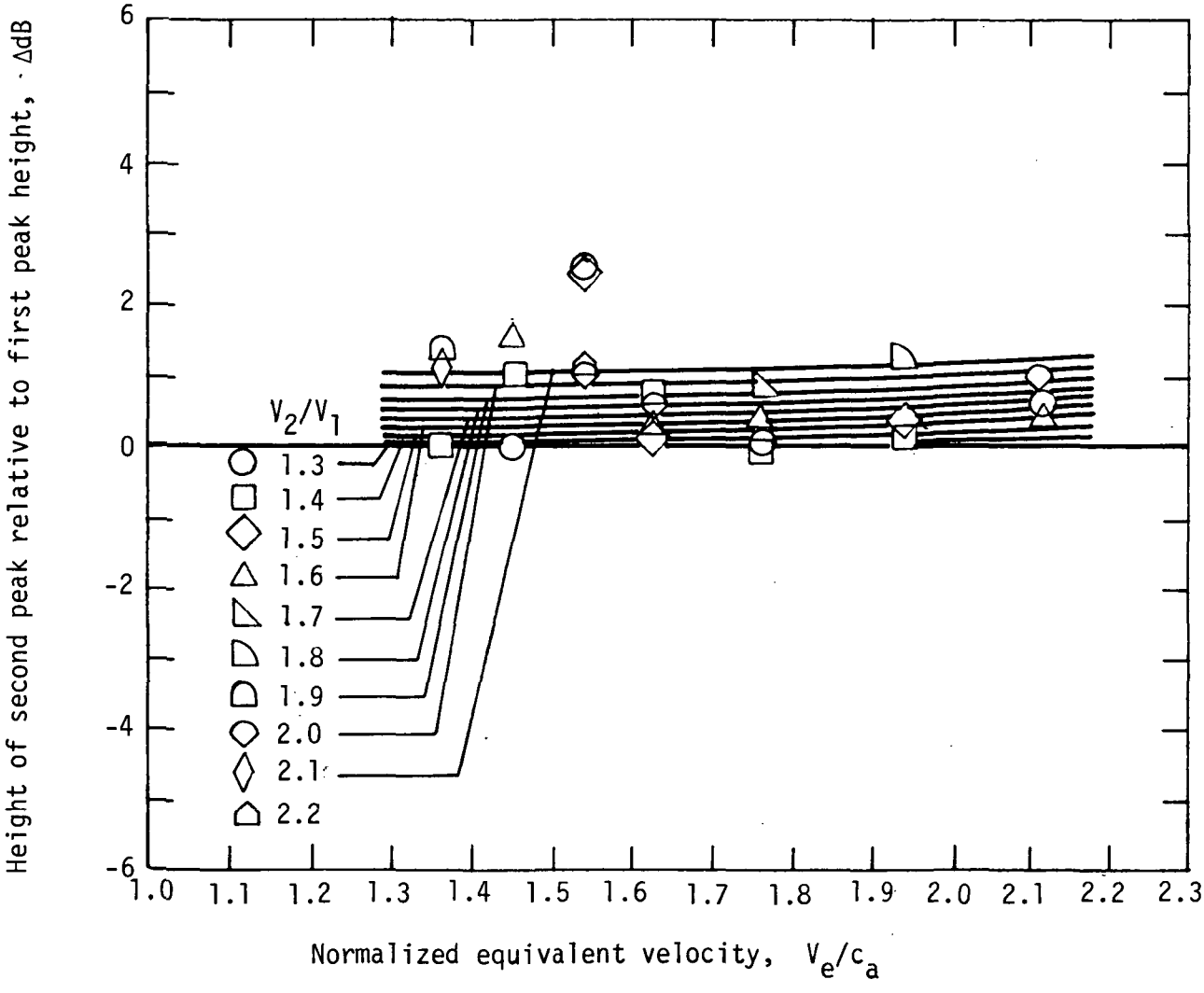

(a) Directivity angle, 120°.

Figure 32.- Relative levels of spectral peaks for models 2 and 3.

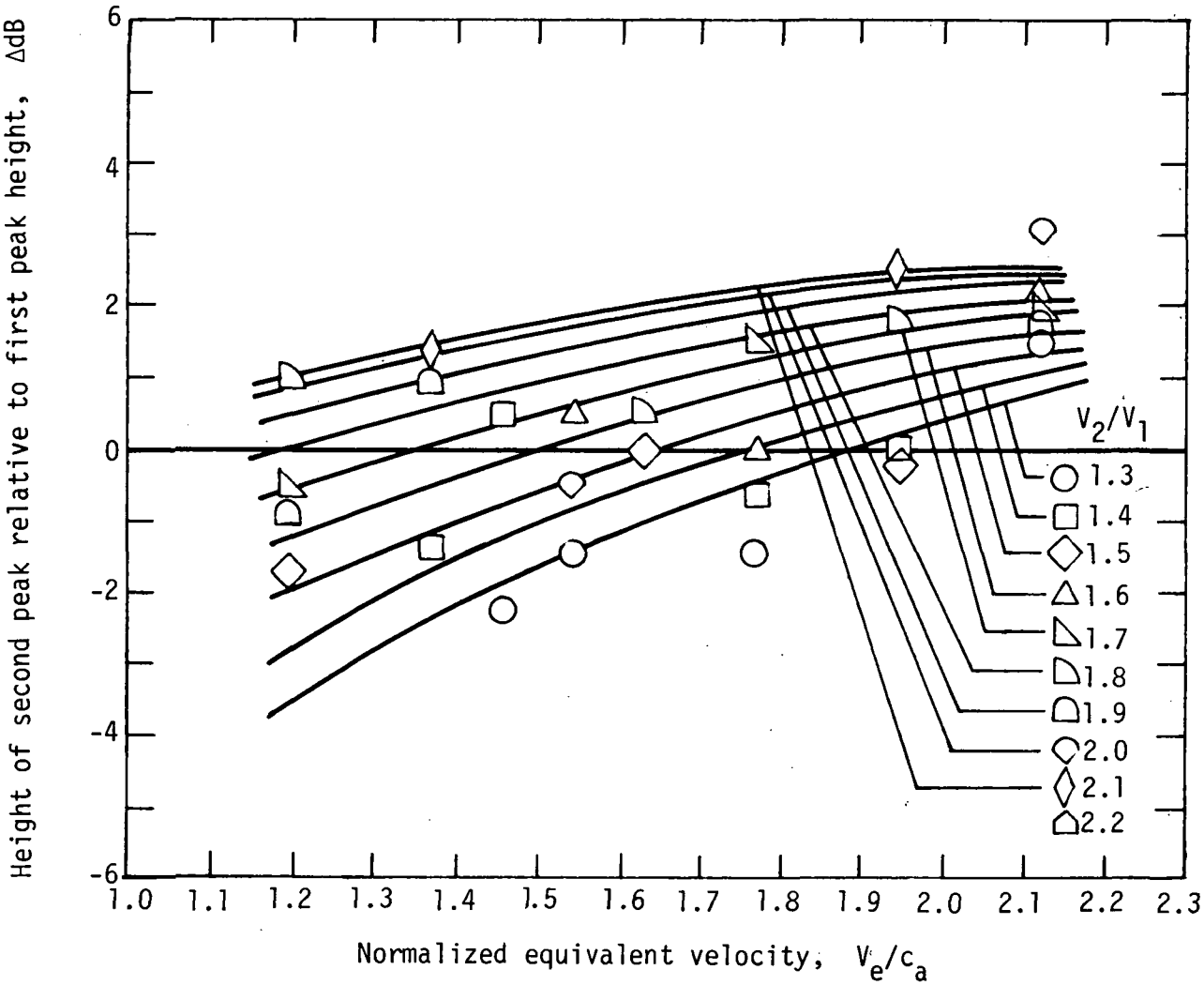

(b) Directivity angle, 130°.

Figure 32.- Continued.

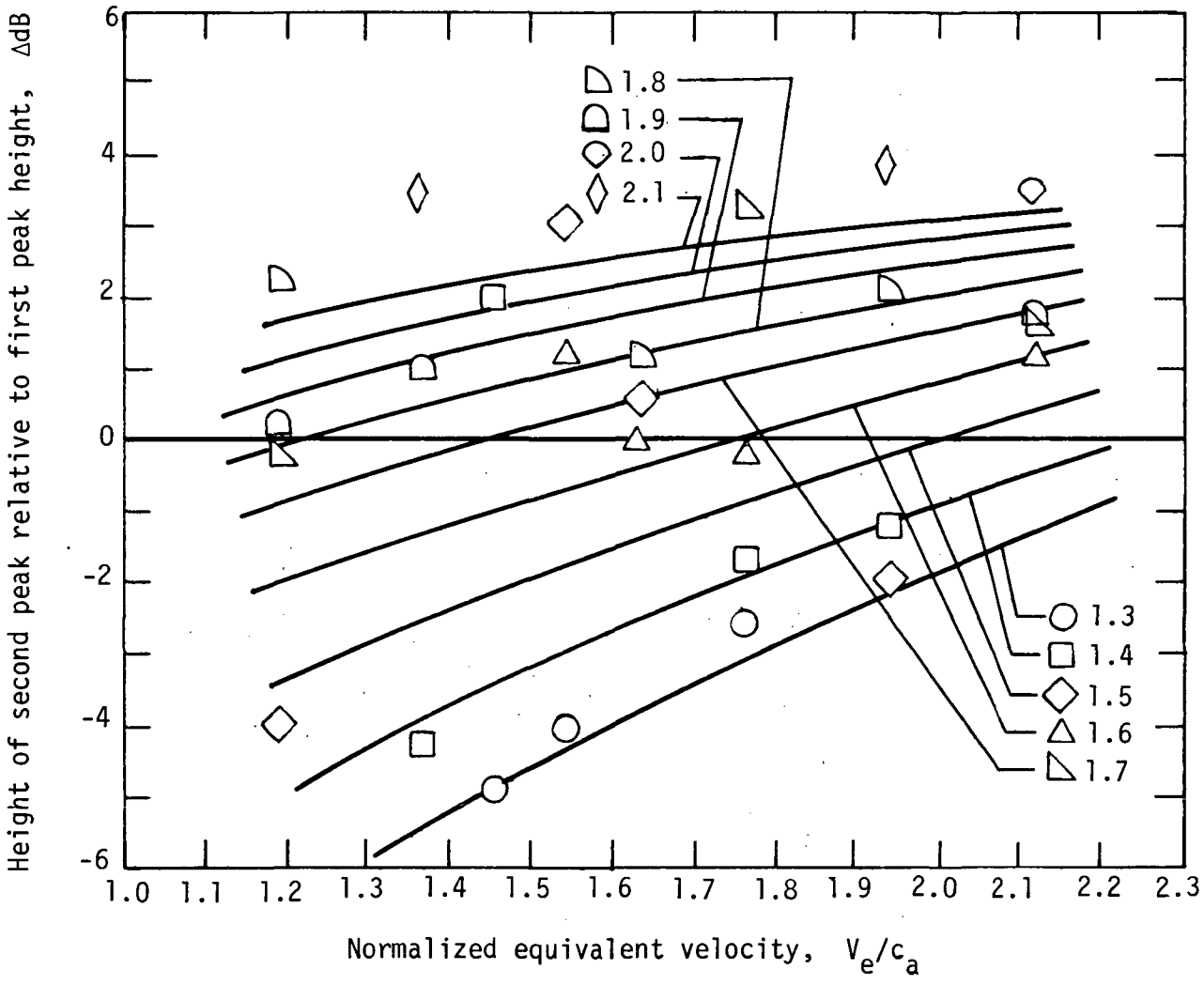

(c) Directivity angle, 140°.

Figure 32.- Continued.

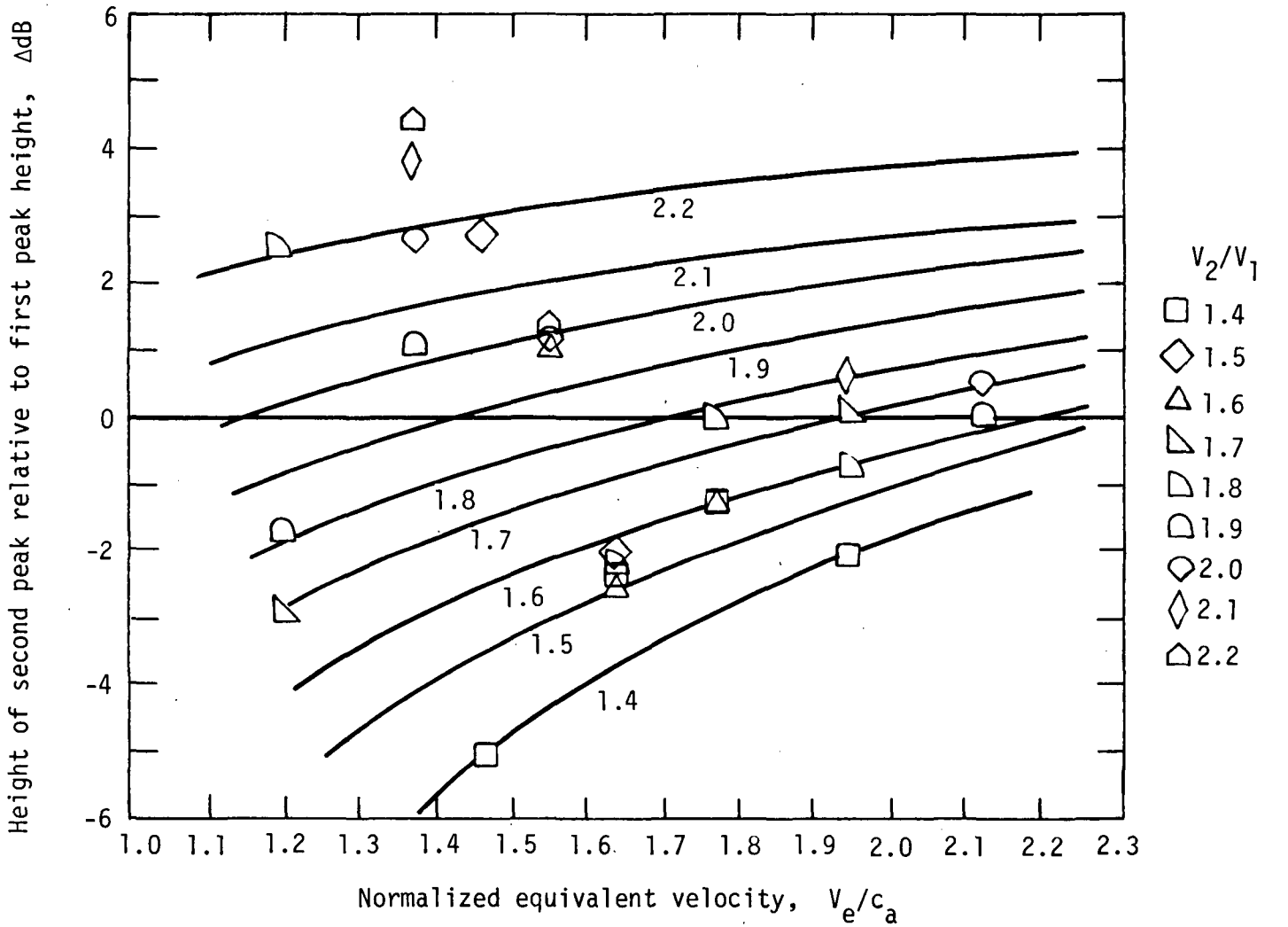

(d) Directivity angle, 150°.

Figure 32.- Continued.

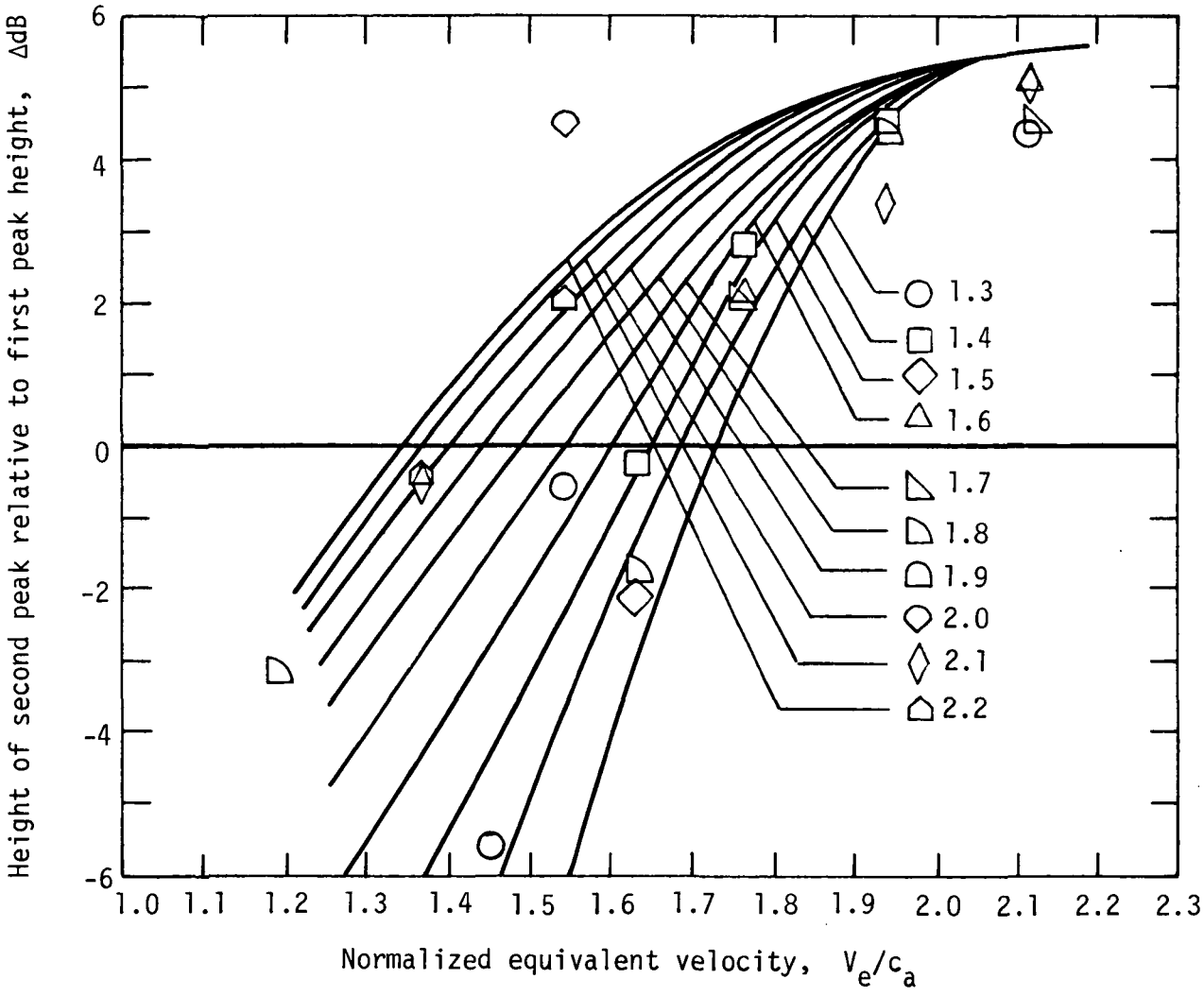

(e) Directivity angle, 165°.

Figure 32.- Concluded.

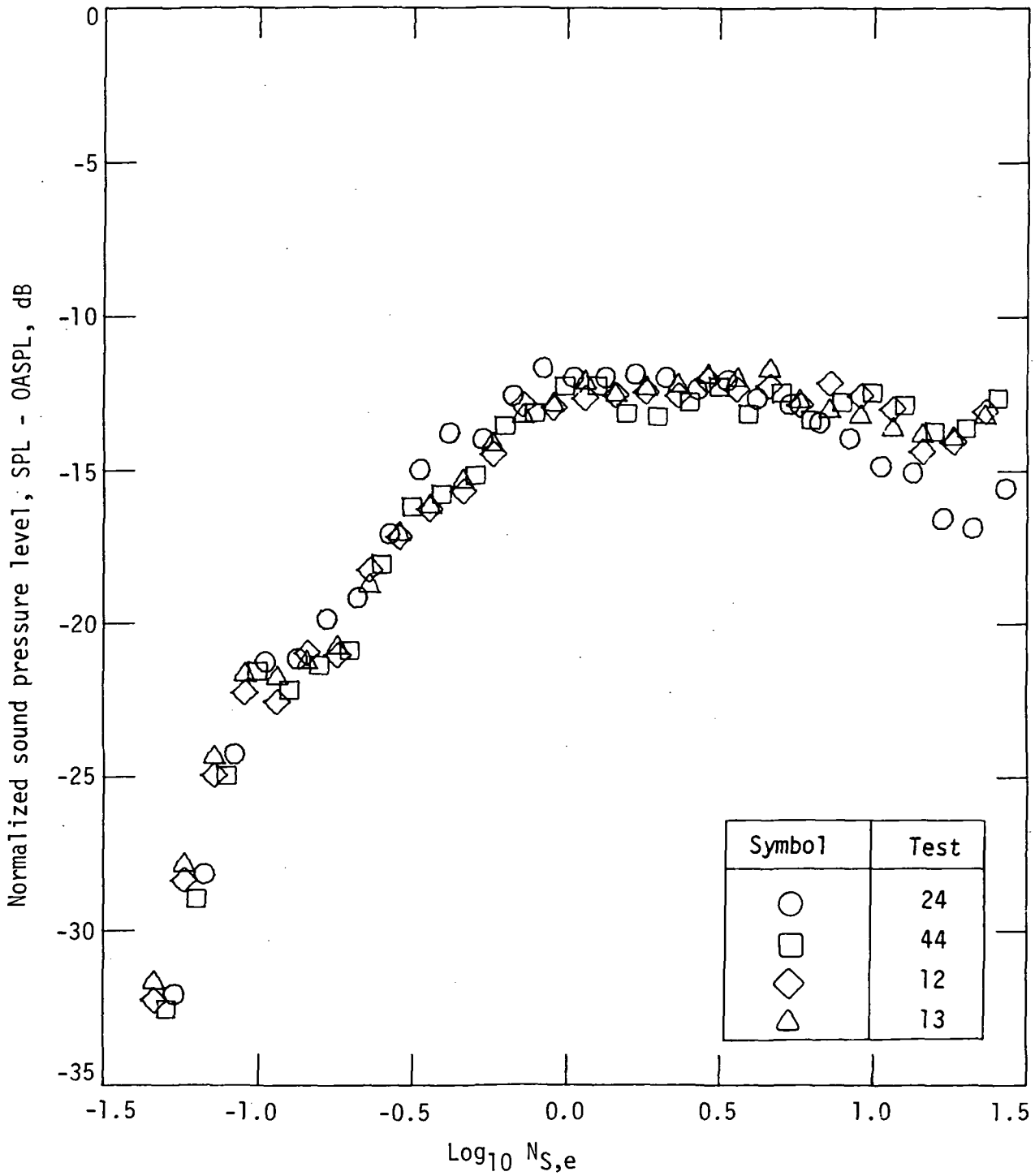

(a) Directivity angle, 90°.

Figure 33.- One-third-octave band spectrum for model 4 with V_e/c_a near 1.55.

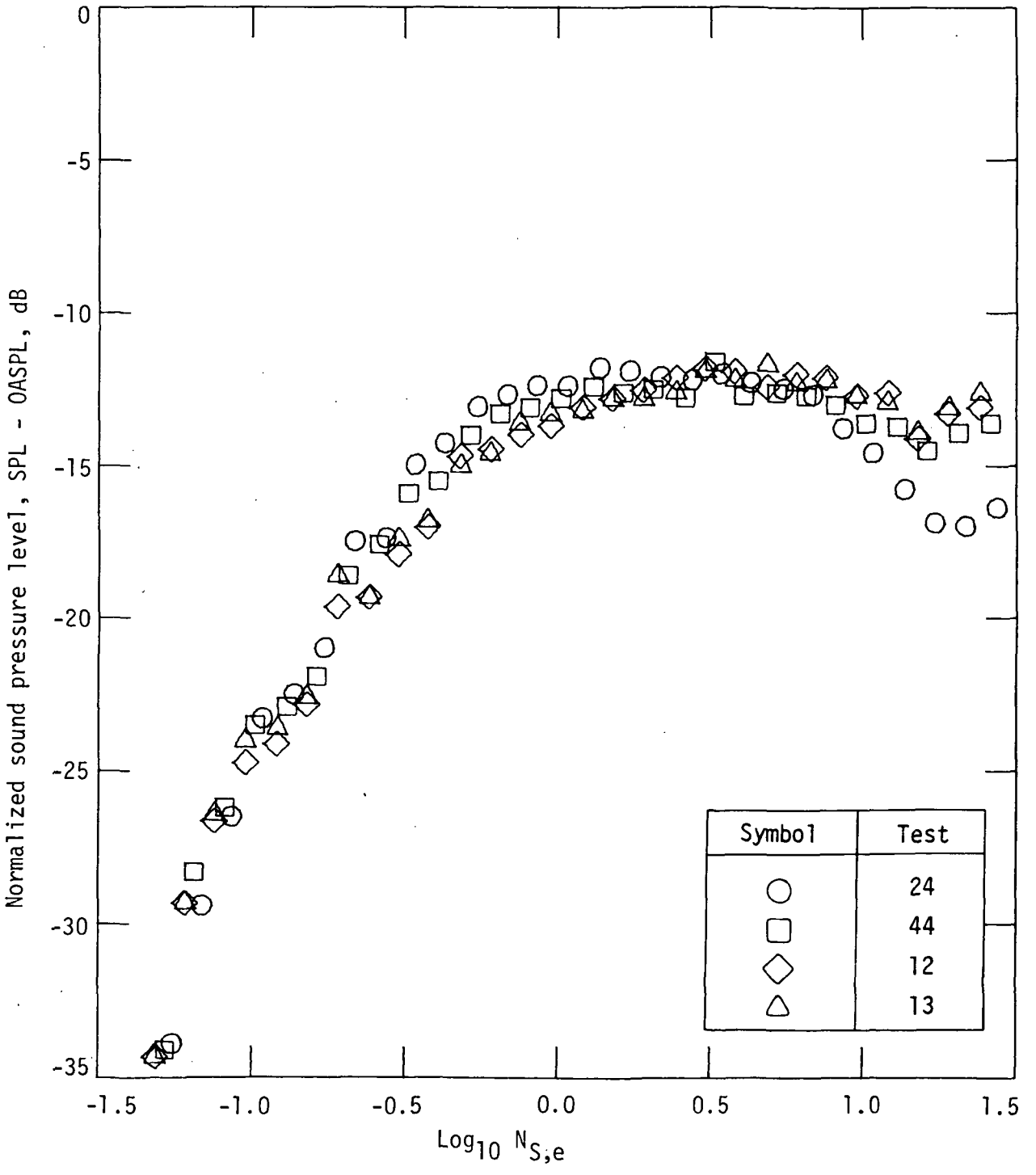

(b) Directivity angle, 100°.

Figure 33.- Continued.

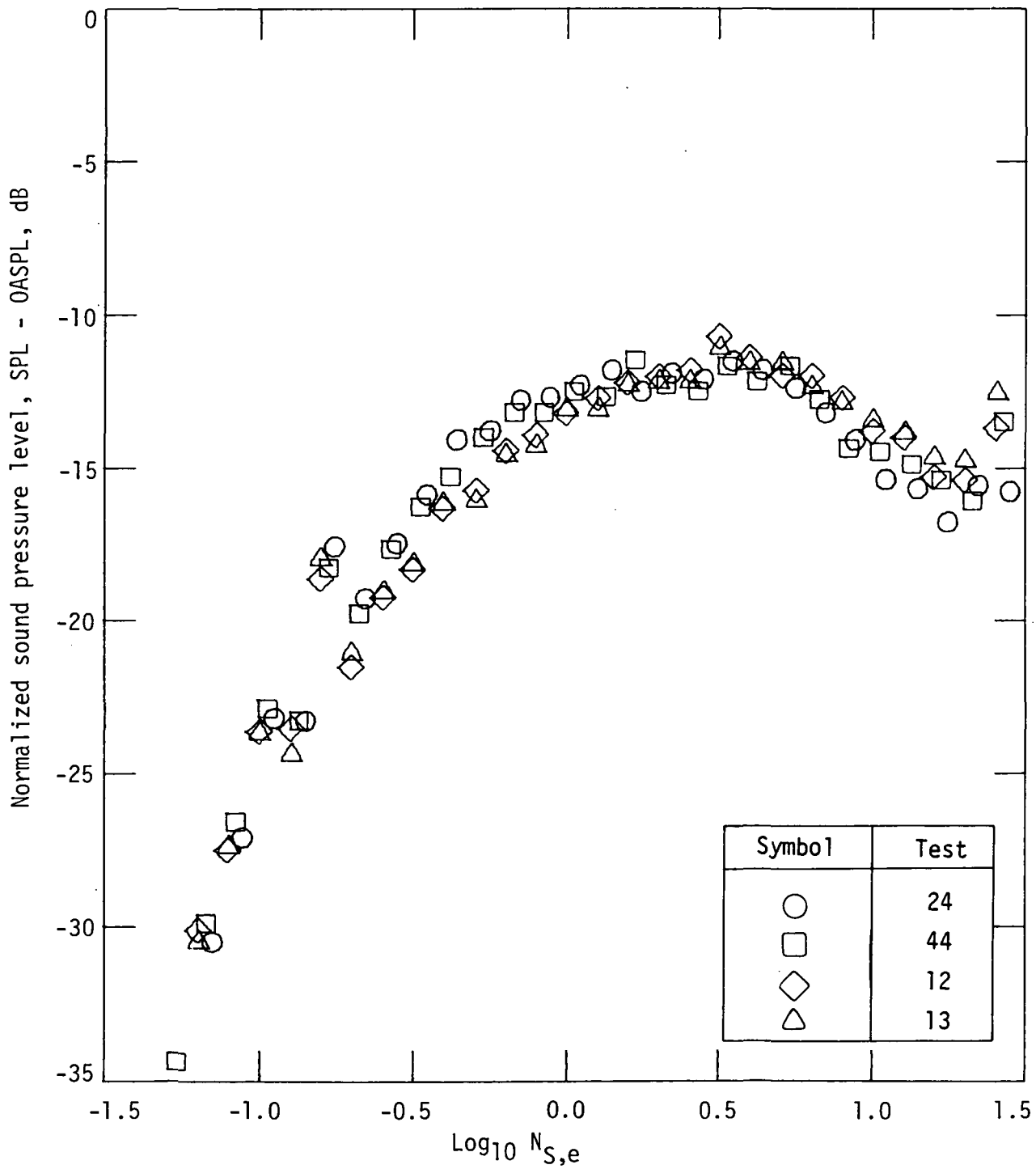

(c) Directivity angle, 110°.

Figure 33.- Continued.

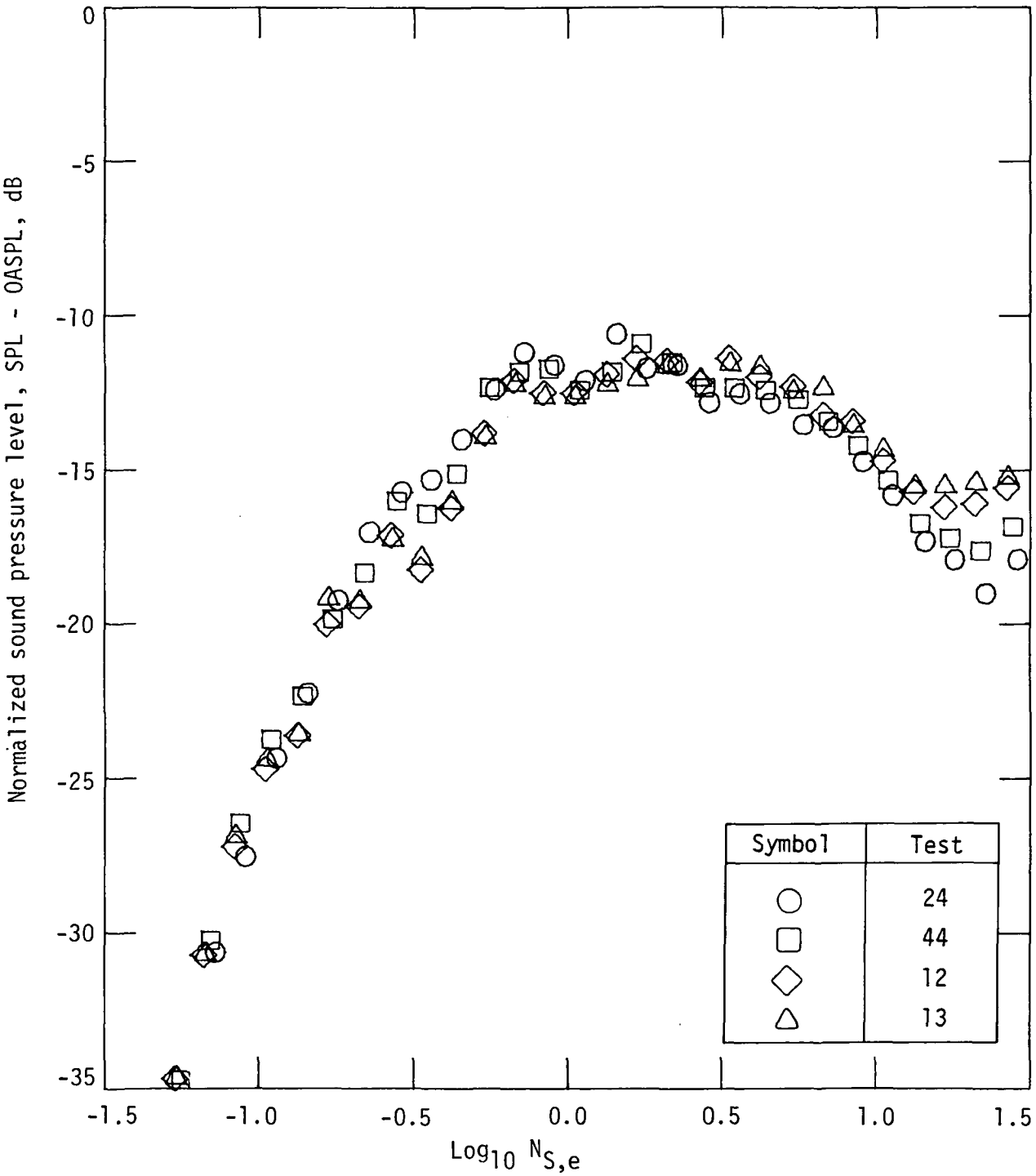

(d) Directivity angle, 120°.

Figure 33.- Continued.

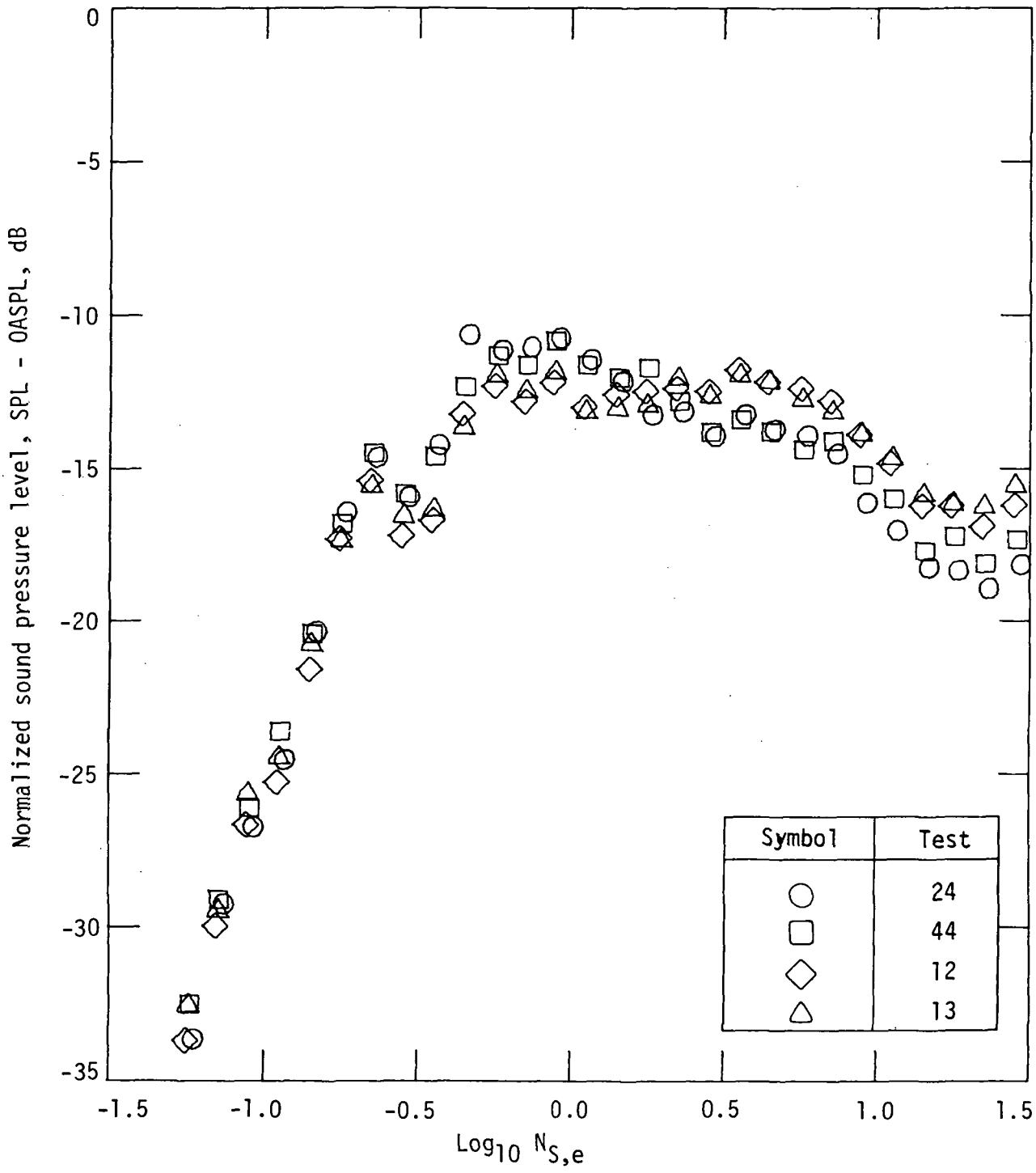

(e) Directivity angle, 130°.

Figure 33.- Continued.

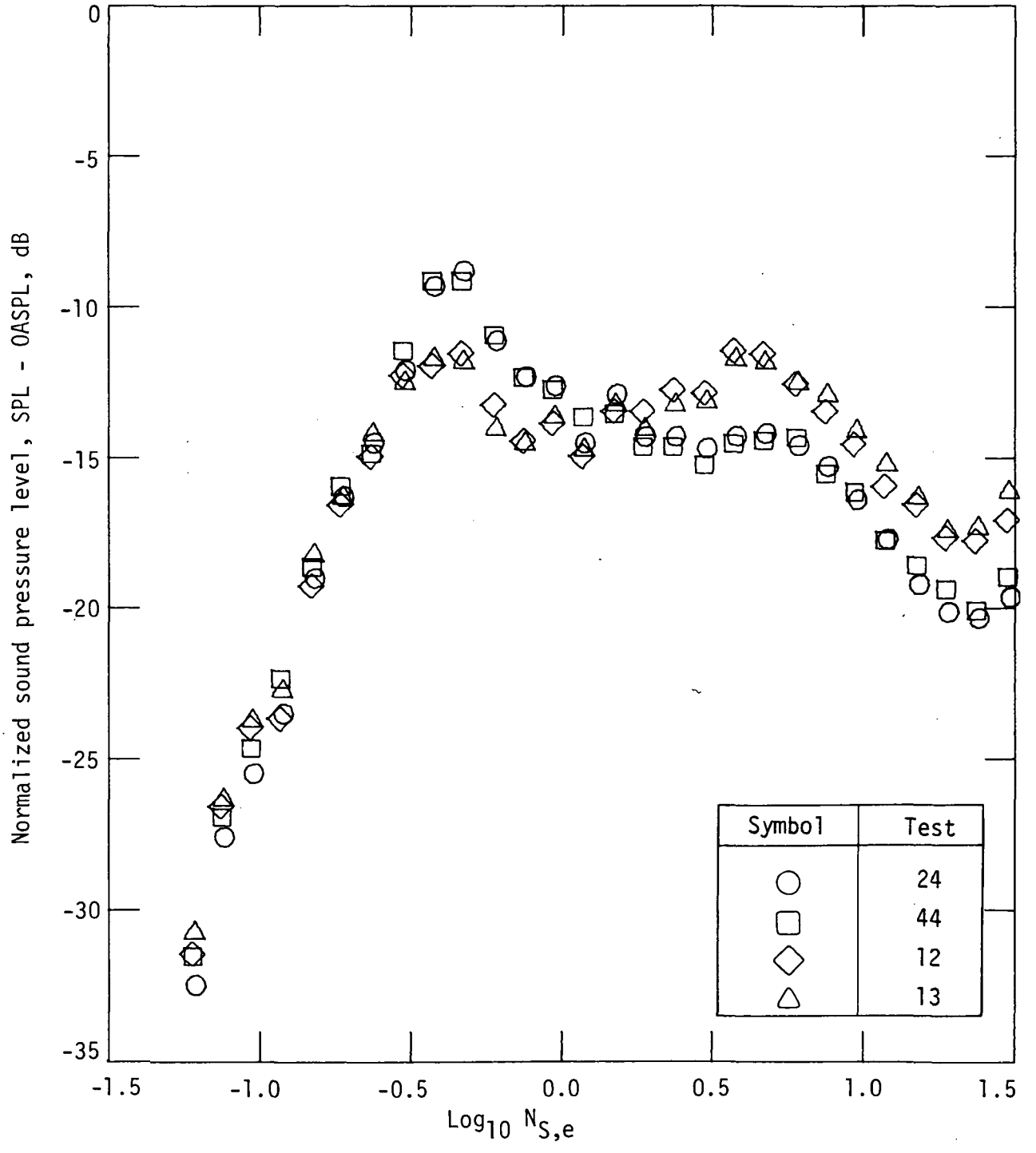

(f) Directivity angle, 140°.

Figure 33.- Continued.

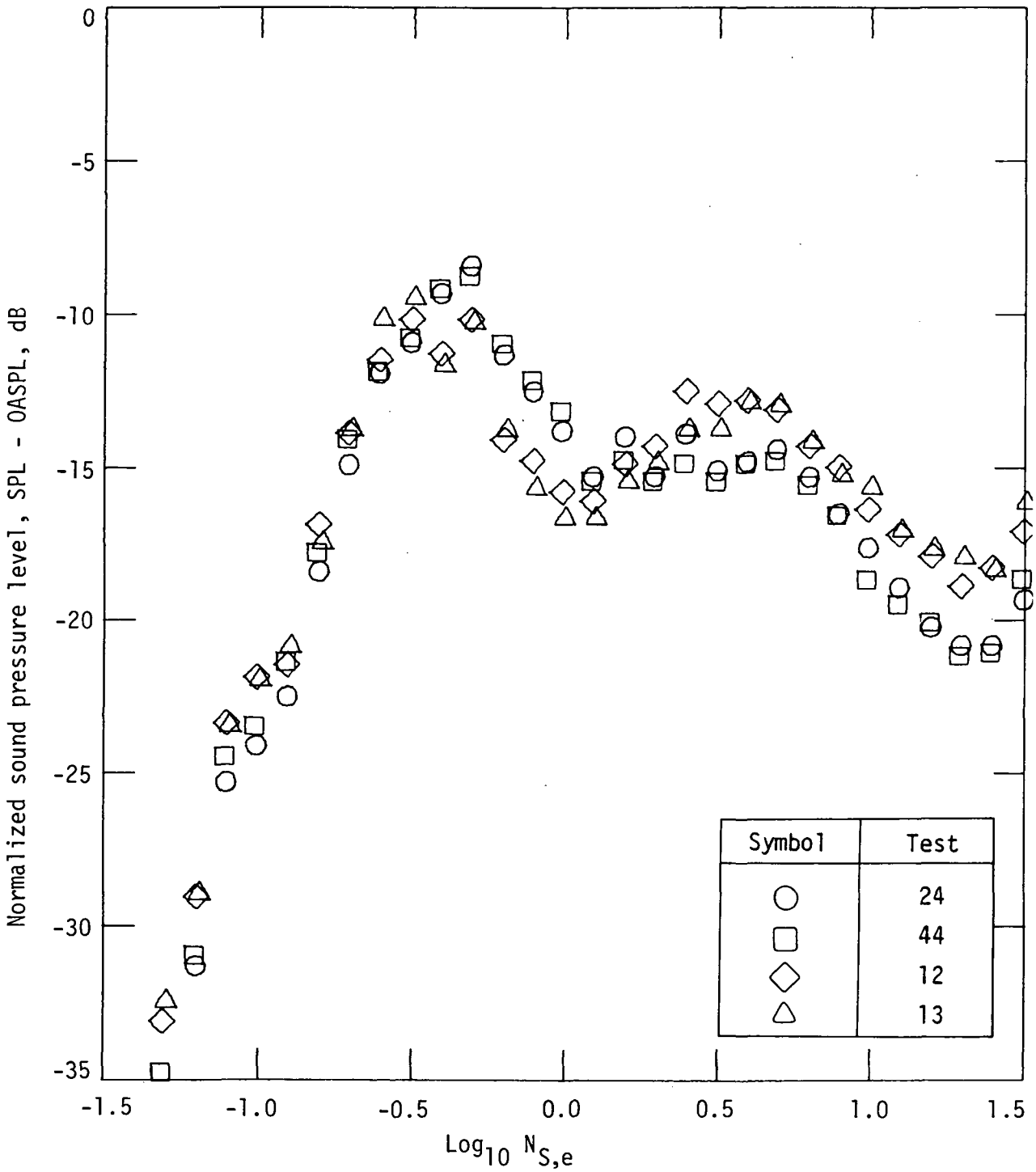

(g) Directivity angle, 150°.

Figure 33.- Continued.

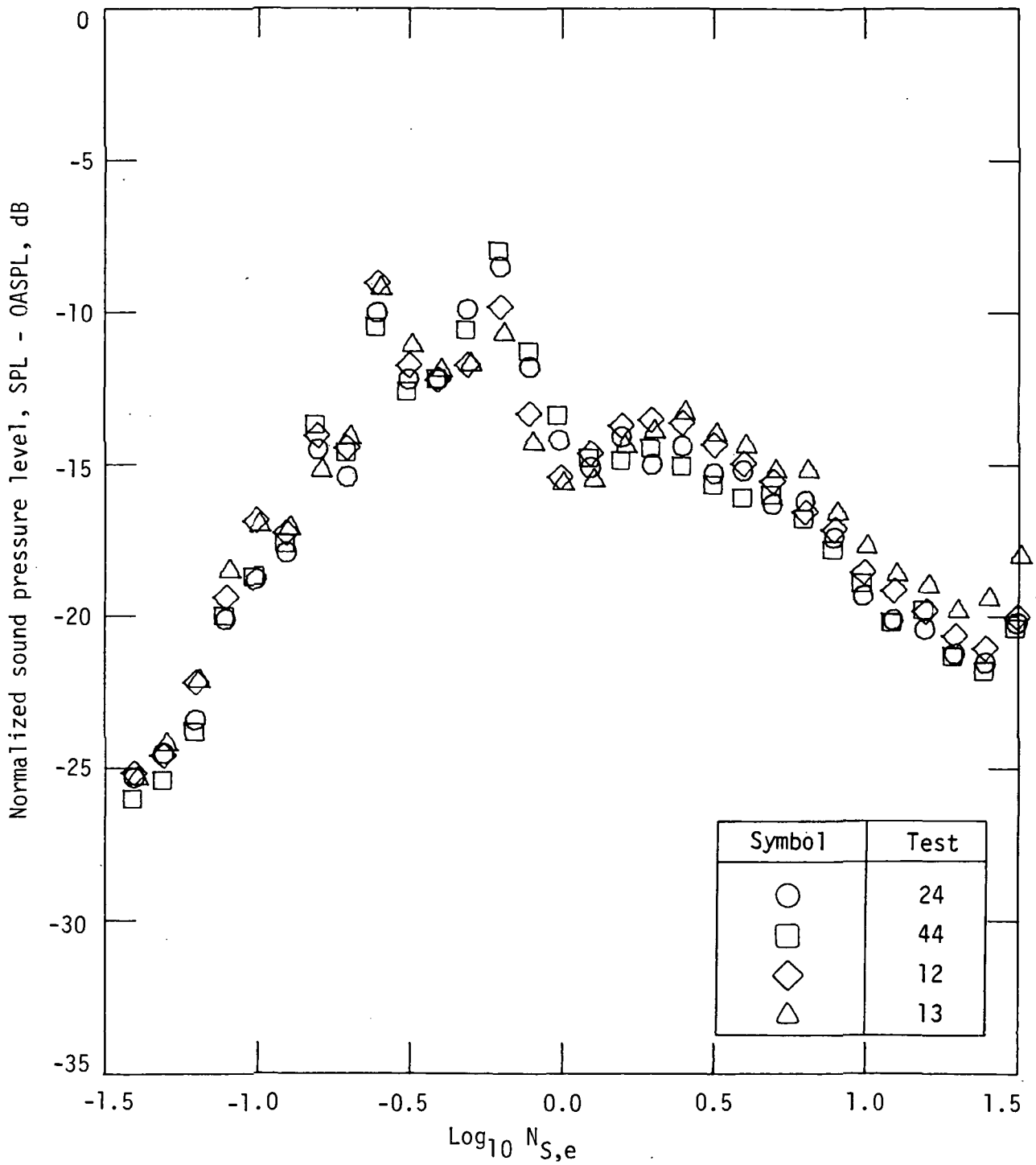

(h) Directivity angle, 160°.

Figure 33.- Concluded.

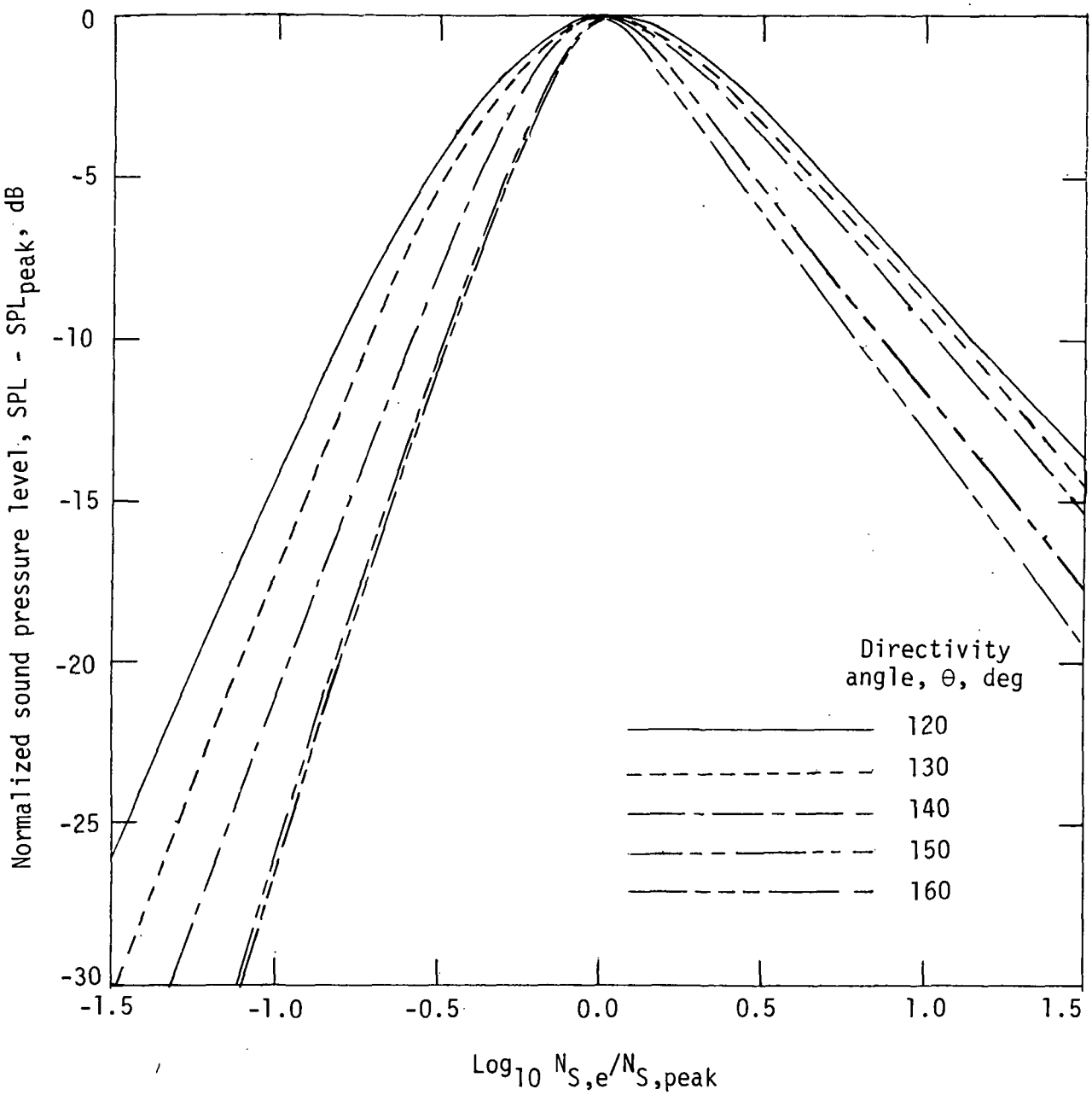

Figure 34.- Variation of spectral shape with directivity angle for model 4.

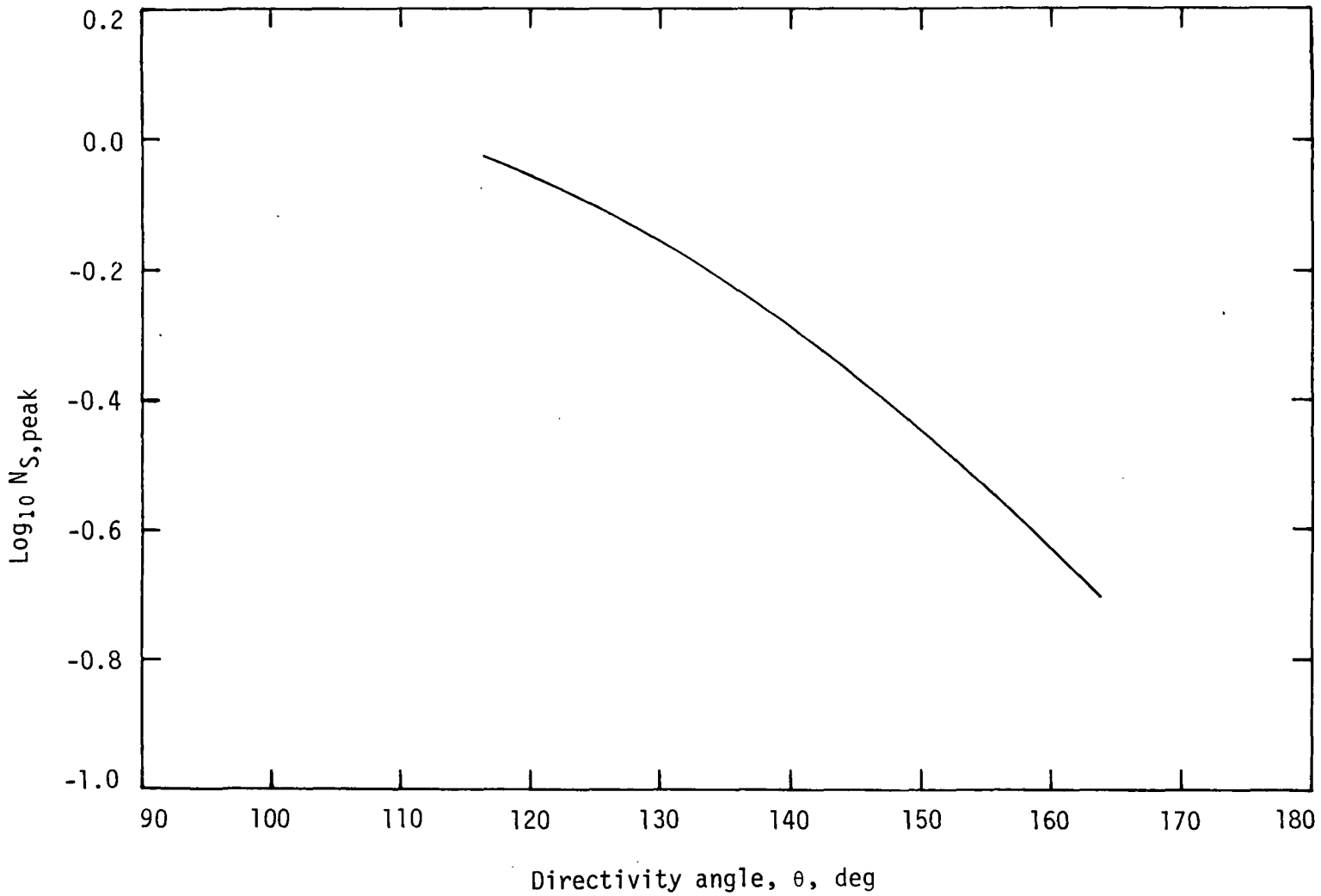

Figure 35.- Strouhal number for first spectral peak for model 4.

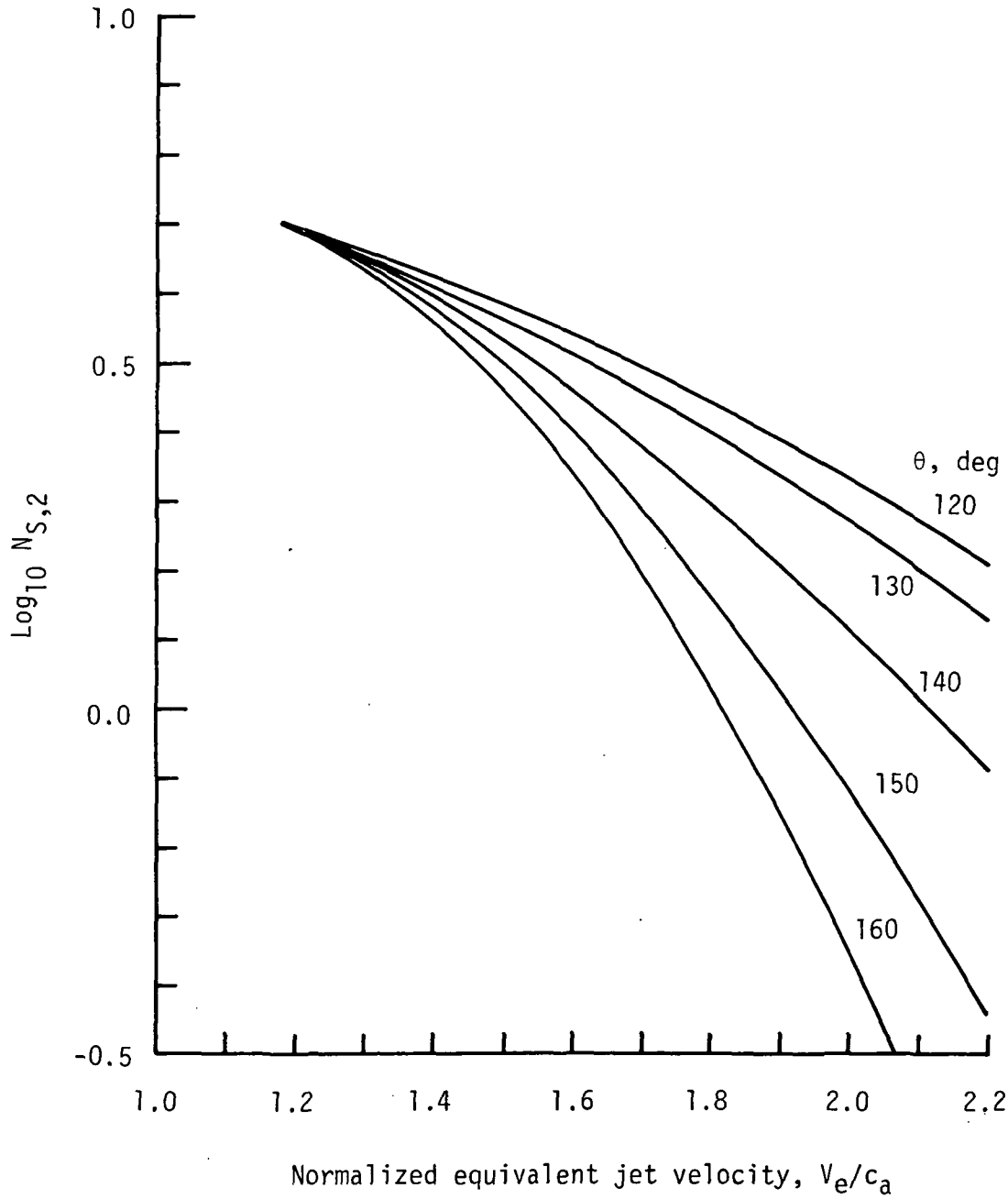

Figure 36.- Peak Strouhal number of second spectral component for model 4.

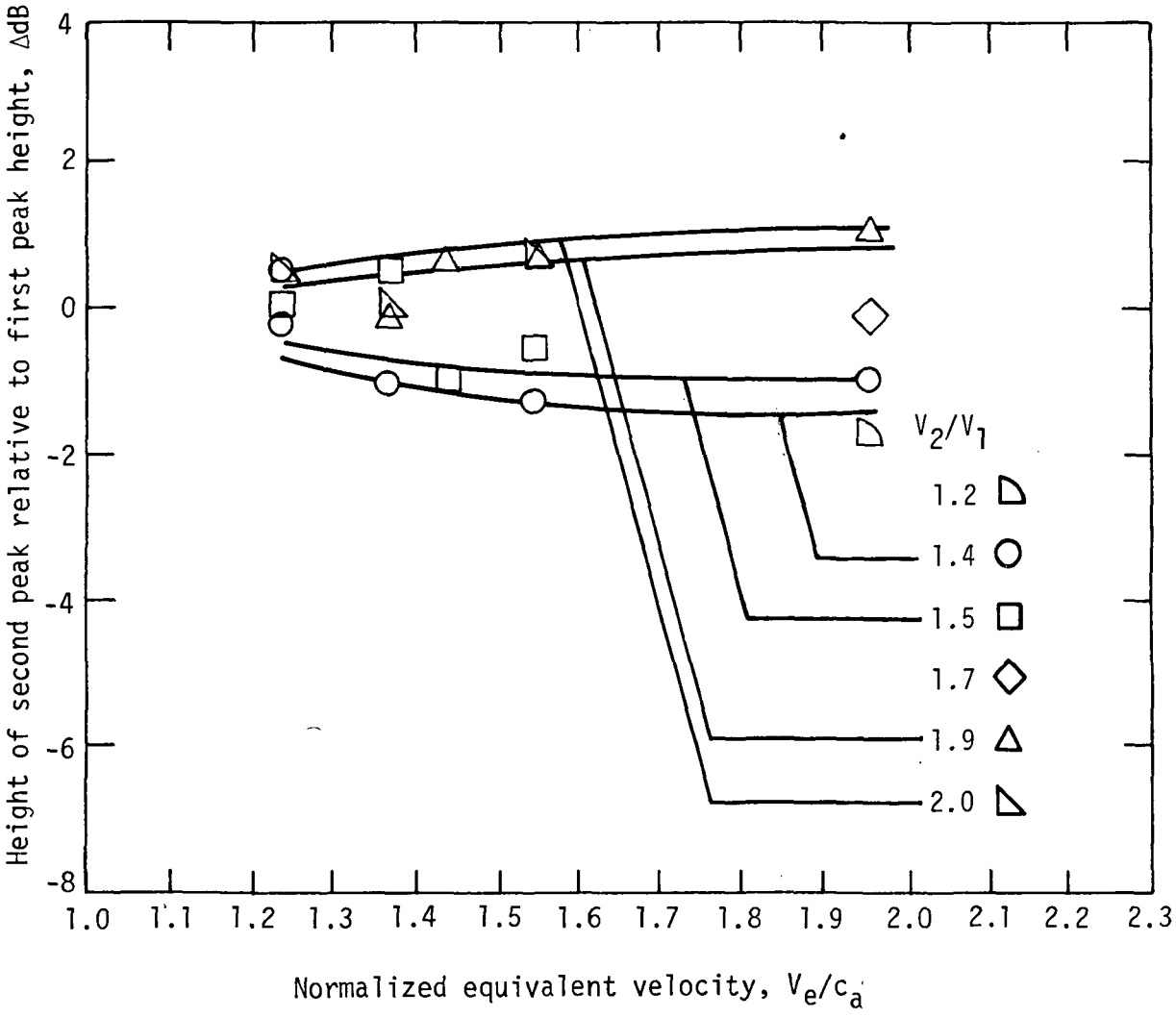

(a) Directivity angle, 120°.

Figure 37.- Relative levels of spectral peaks for model 4.

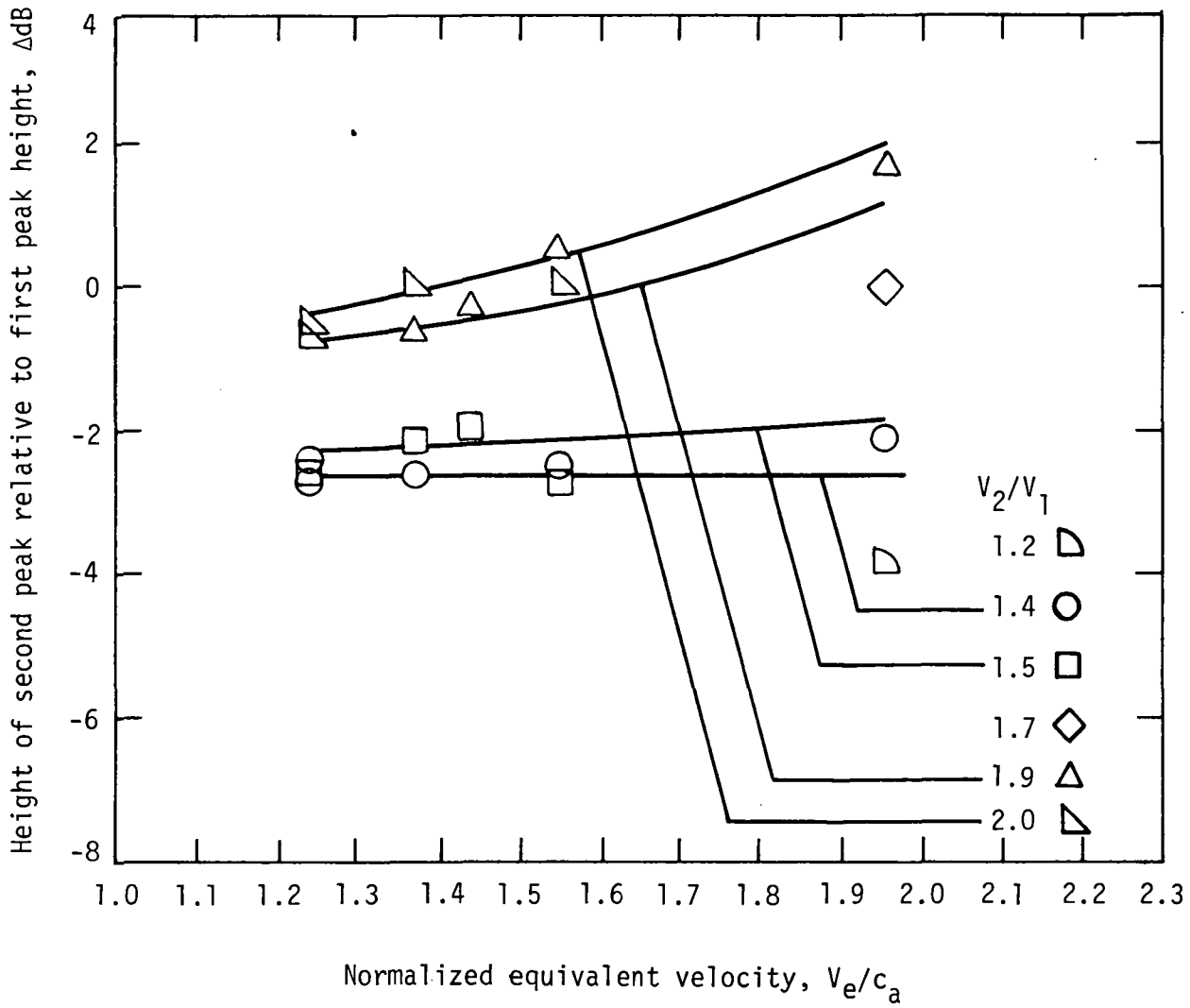

(b) Directivity angle, 130°.

Figure 37.- Continued.

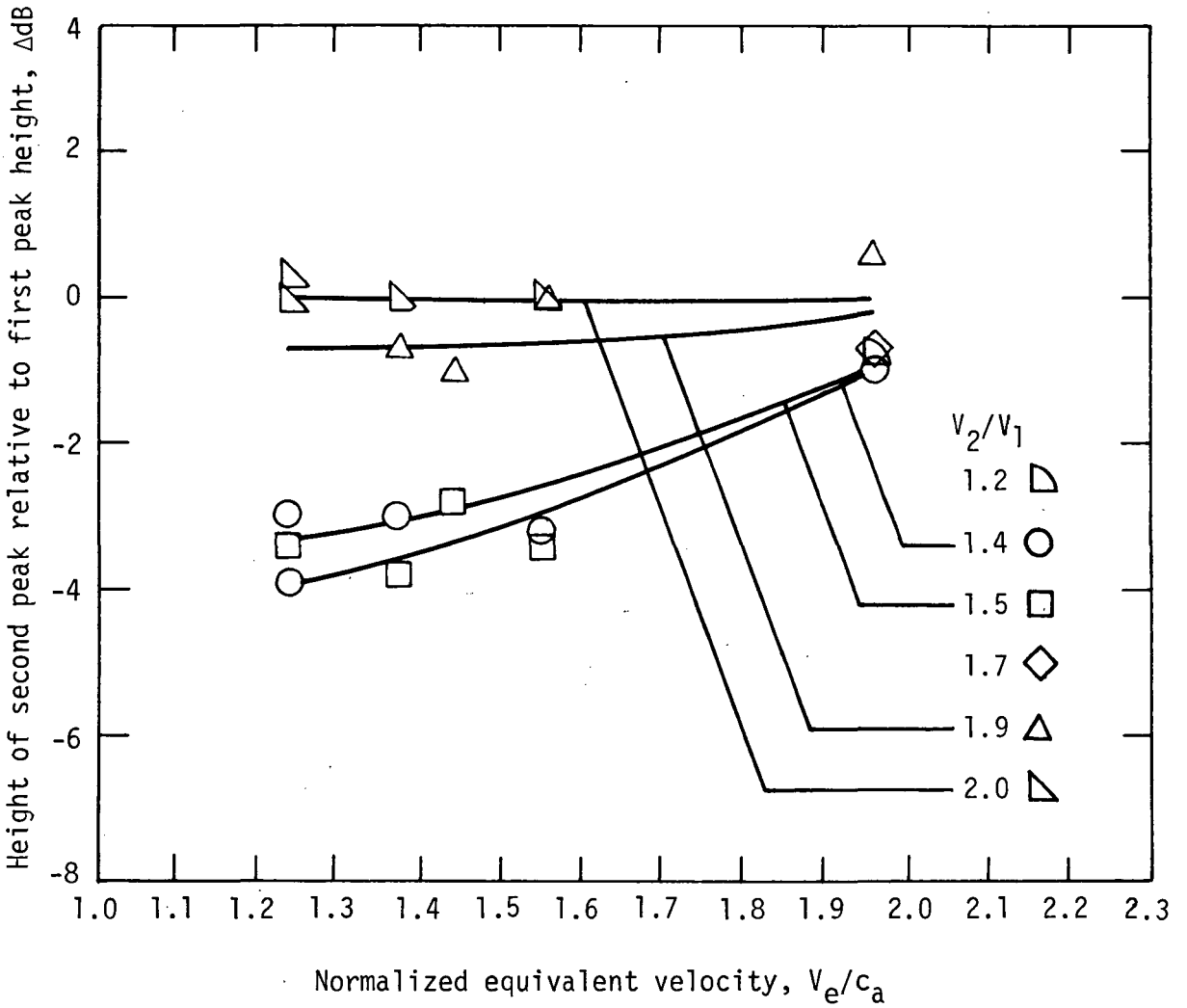

(c) Directivity angle, 140°.

Figure 37.- Continued.

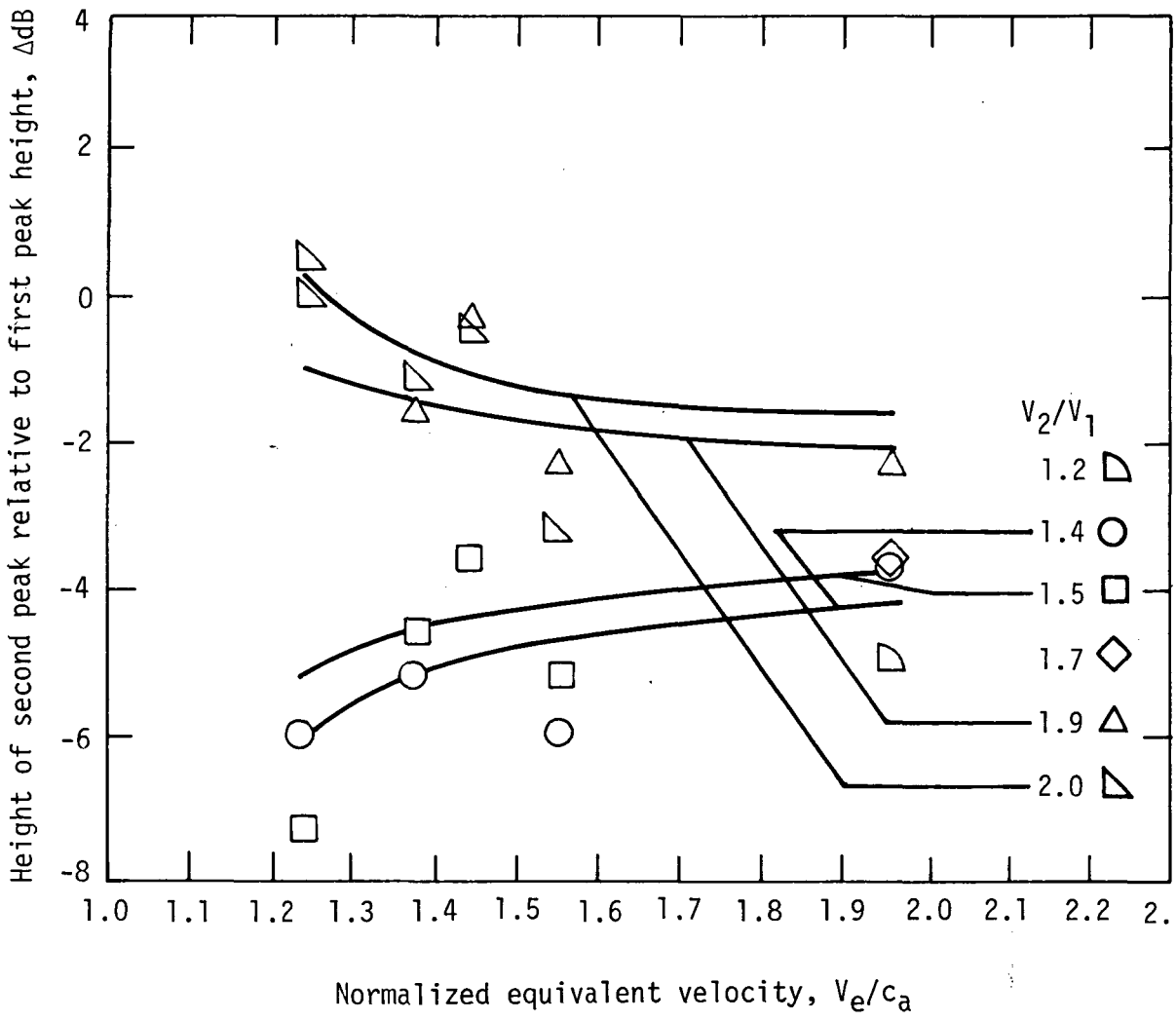

(d) Directivity angle, 150°.

Figure 37.- Continued.

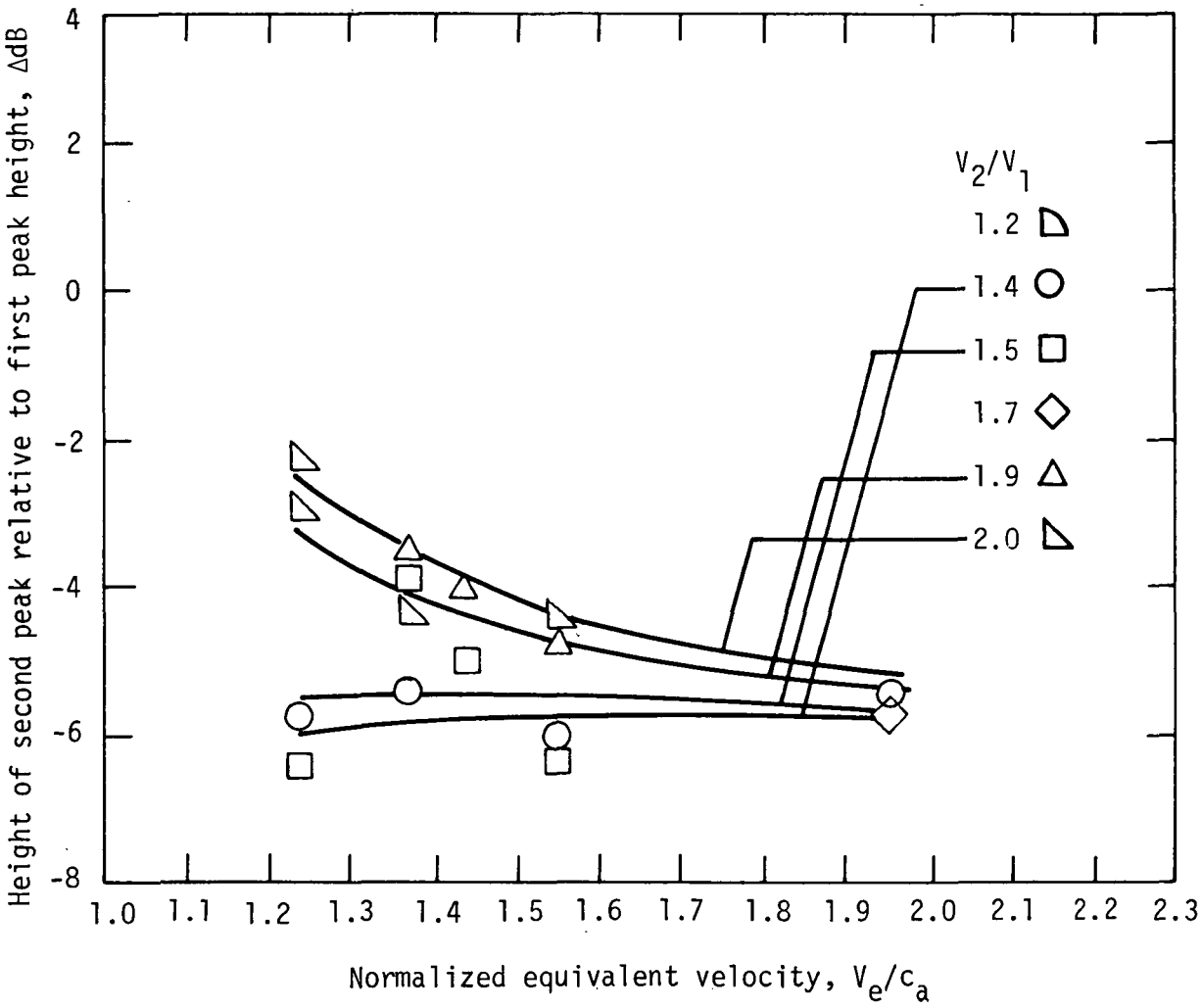

(e) Directivity angle, 160°.

Figure 37.- Concluded.

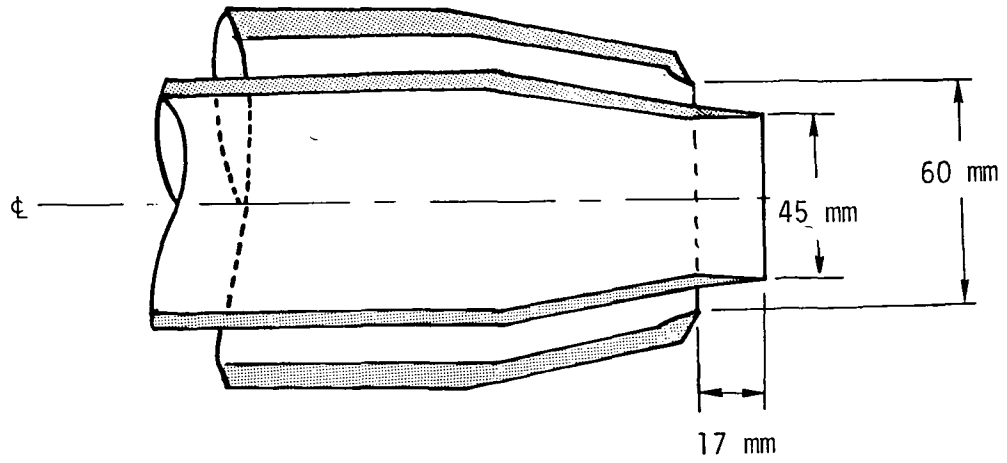

Figure 38.- Model 6, 0.75-area-ratio wind-tunnel coannular nozzle.

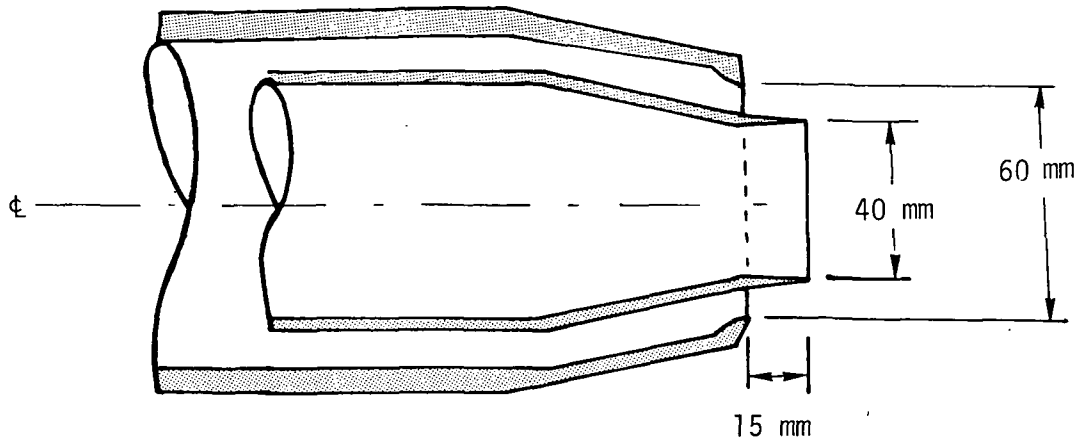

Figure 39.- Model 7, 1.2-area-ratio wind-tunnel coannular nozzle.

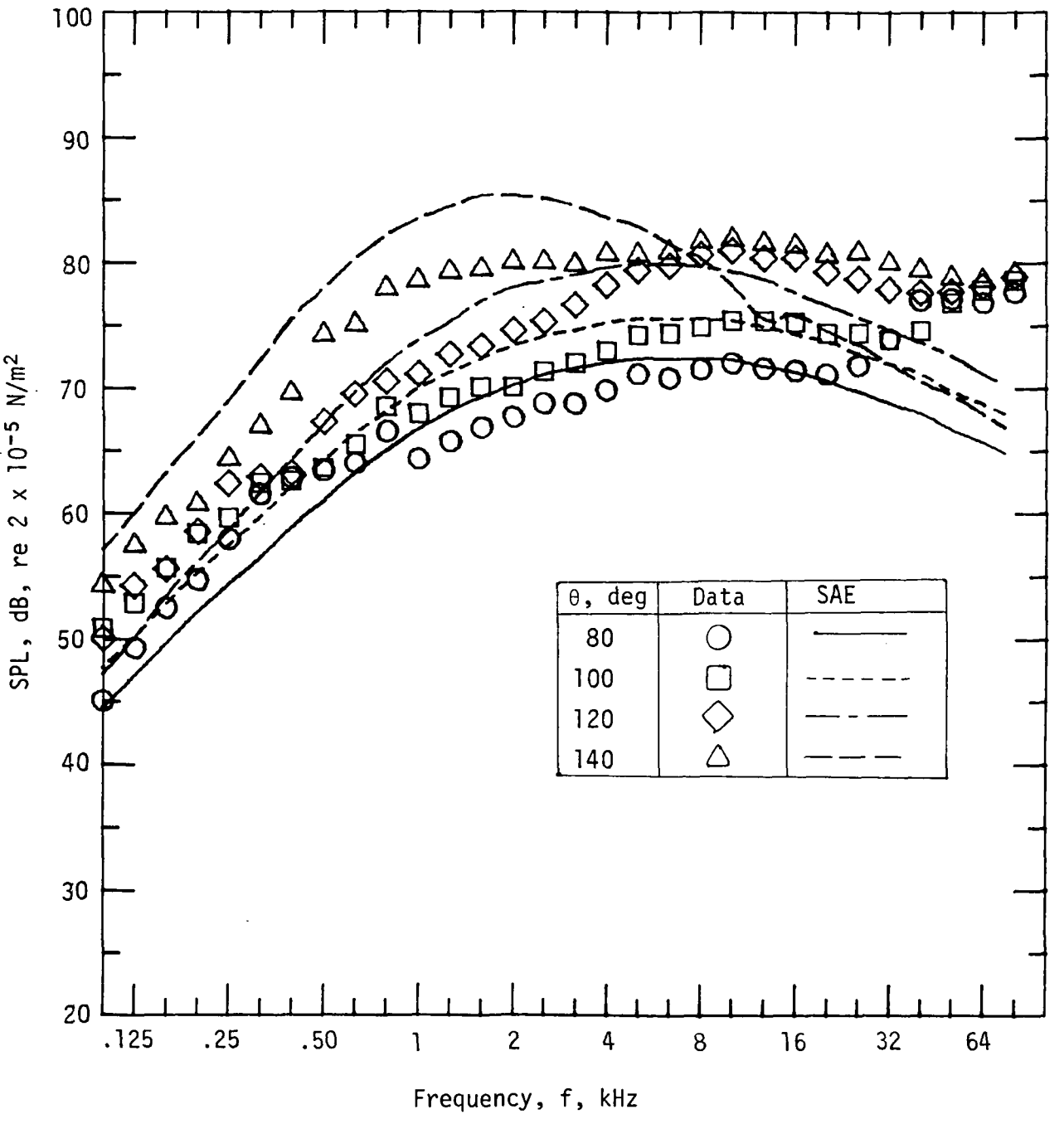

Figure 40.- Typical model 6 spectral data scaled to 45.7-m radius with forward velocity near 7 m/s (test 39, table VIII).

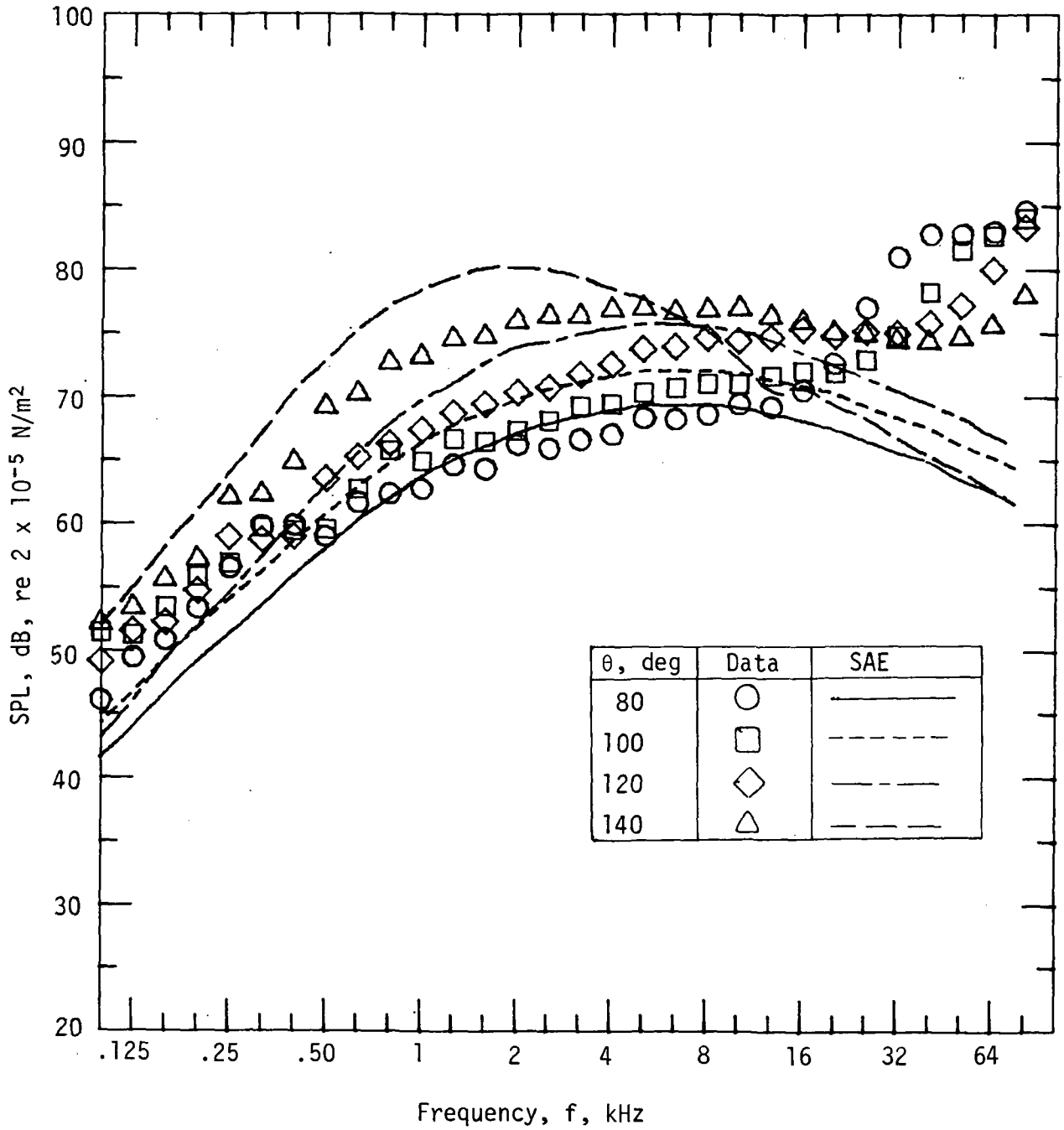

Figure 41.- Typical model 6 spectral data scaled to 45.7-m radius with forward velocity near 30 m/s (test 34, table VIII).

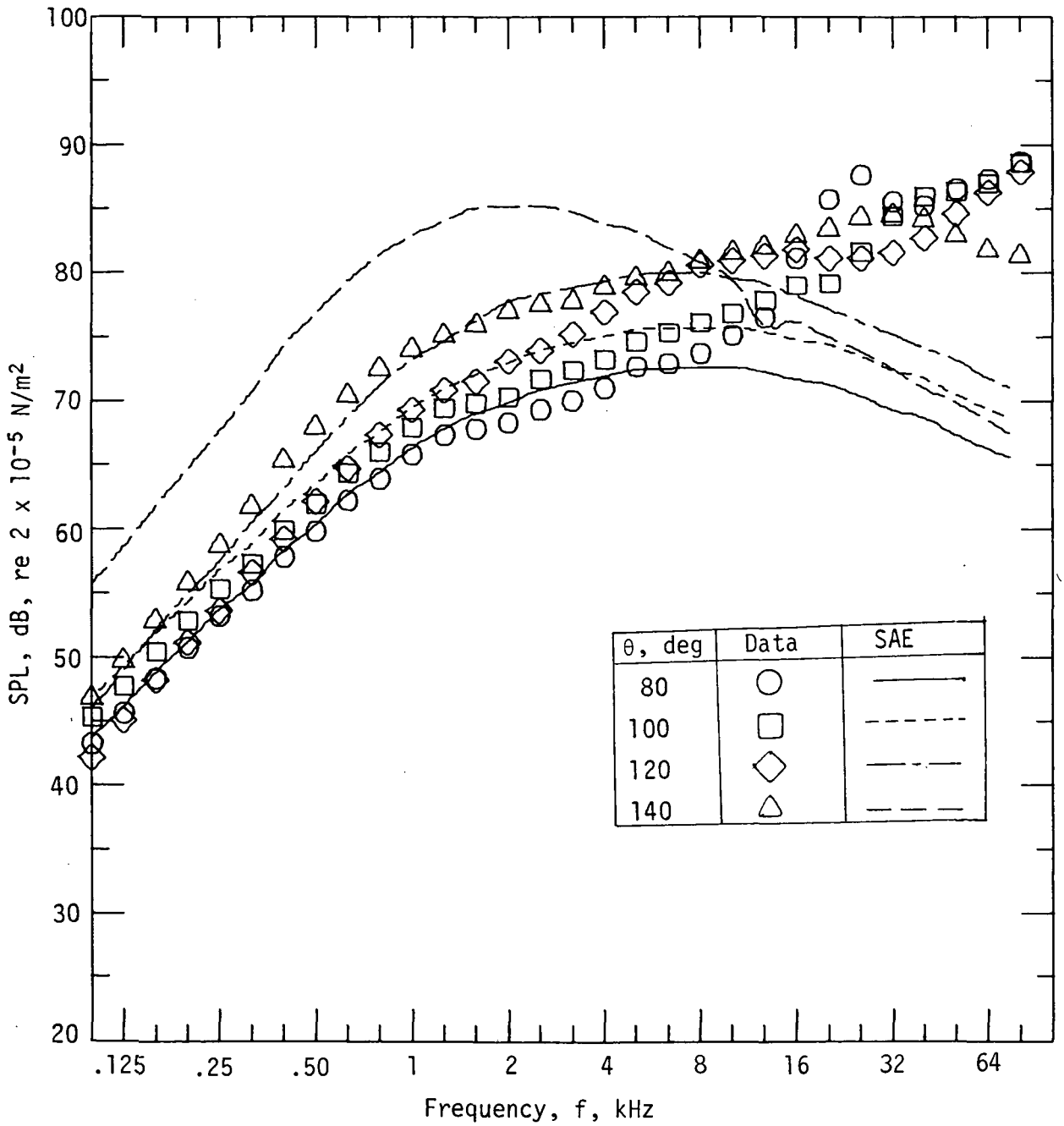

Figure 42.- Typical model 6 spectral data scaled to 45.7-m radius with forward velocity near 61 m/s (test 47, table VIII).

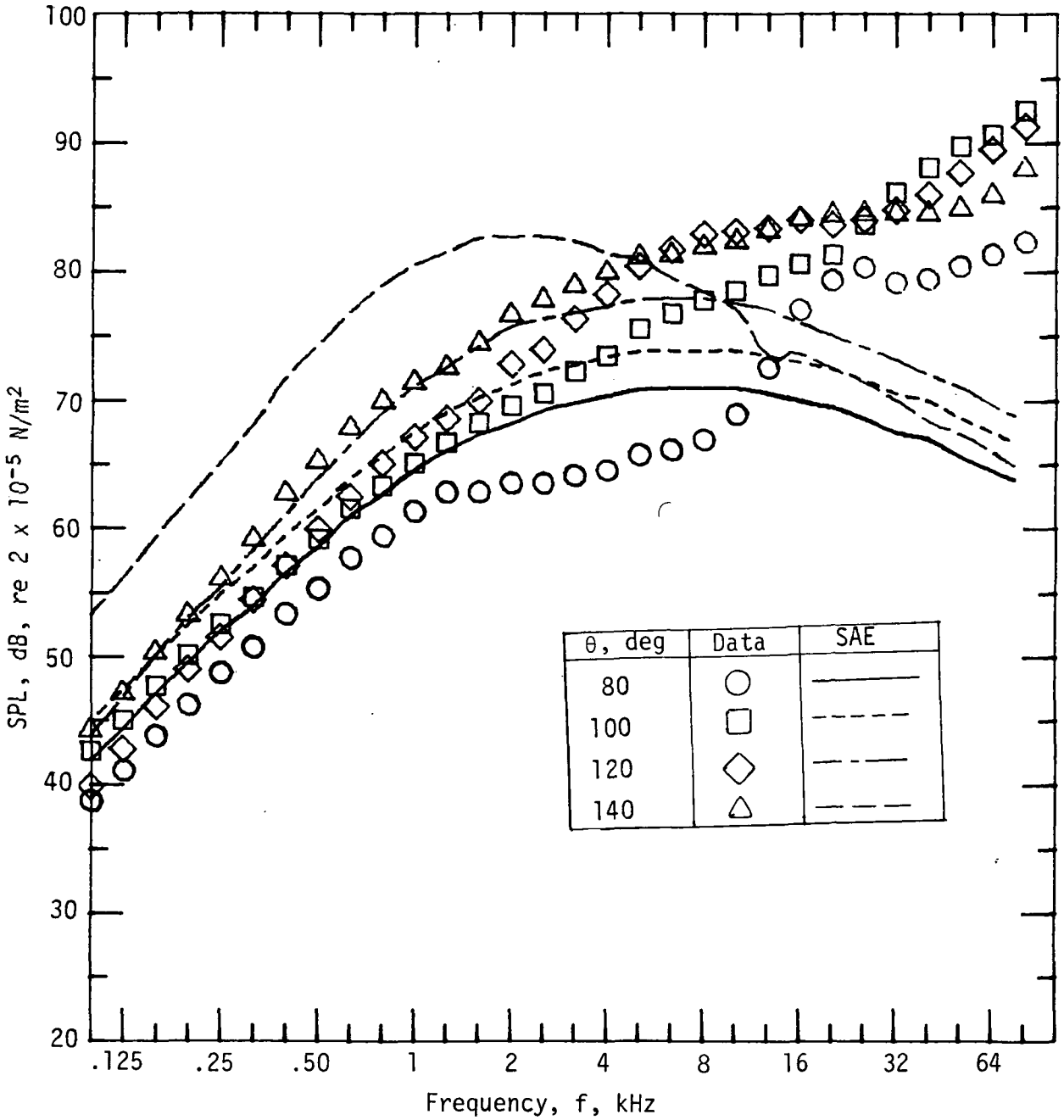

Figure 43.- Typical model 6 spectral data scaled to 45.7-m radius with forward velocity near 103 m/s (test 42, table VIII).

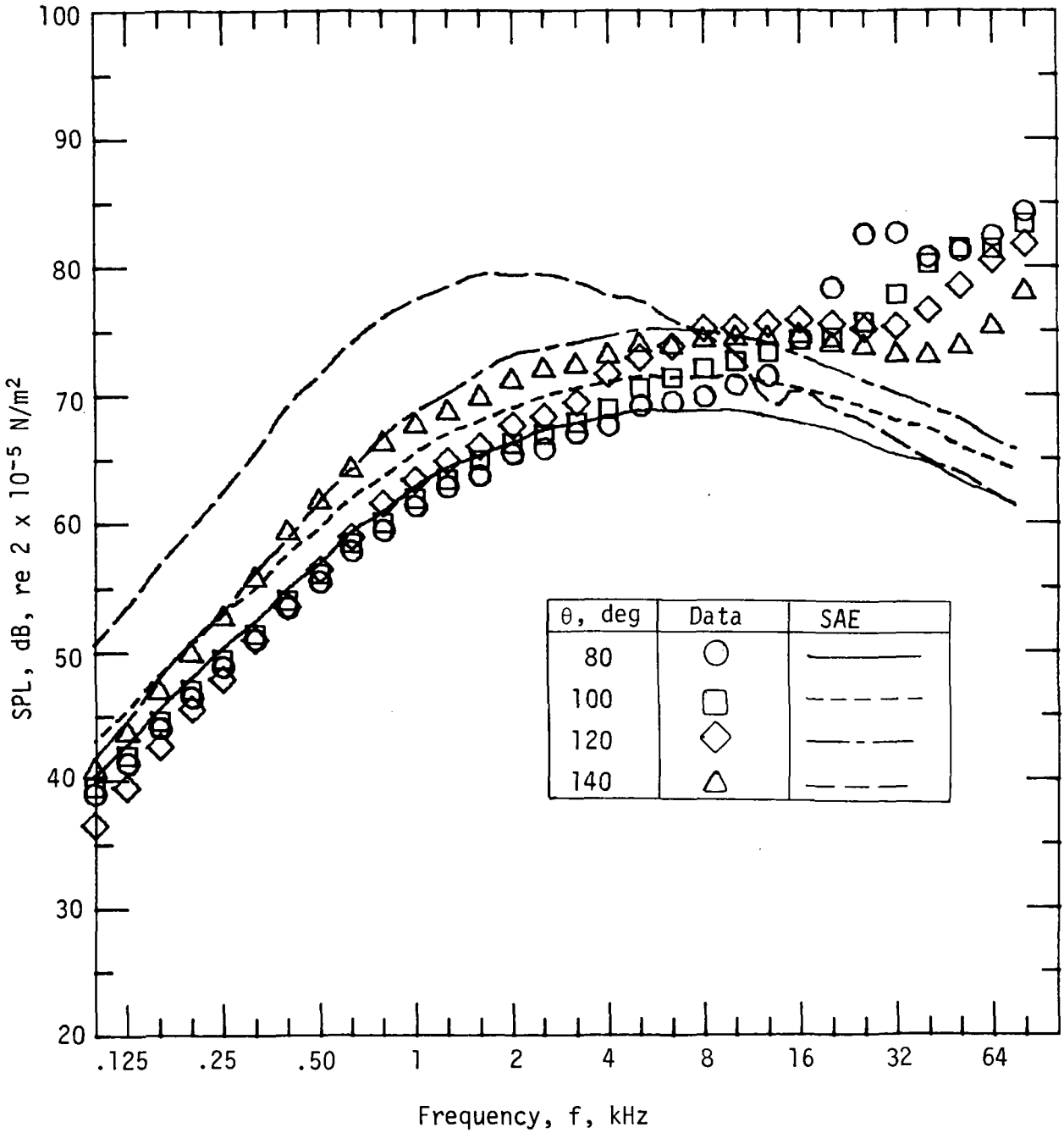

Figure 44.- Typical model 7 spectral data scaled to 45.7-m radius with forward velocity near 105 m/s (test 41, table IX).

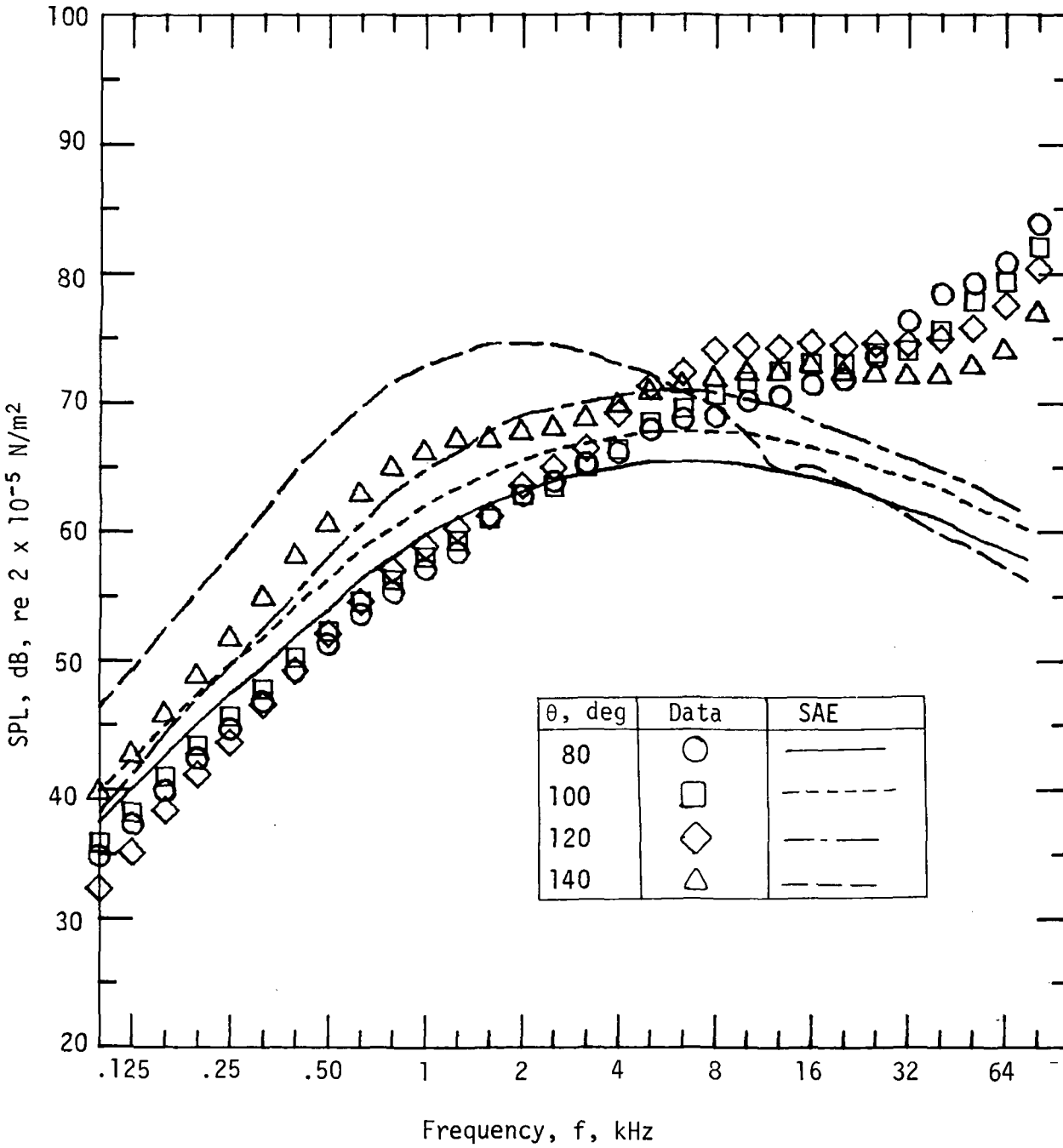

Figure 45.- Typical model 6 spectral data scaled to 45.7-m radius with forward velocity near 128 m/s (test 30, table VIII).

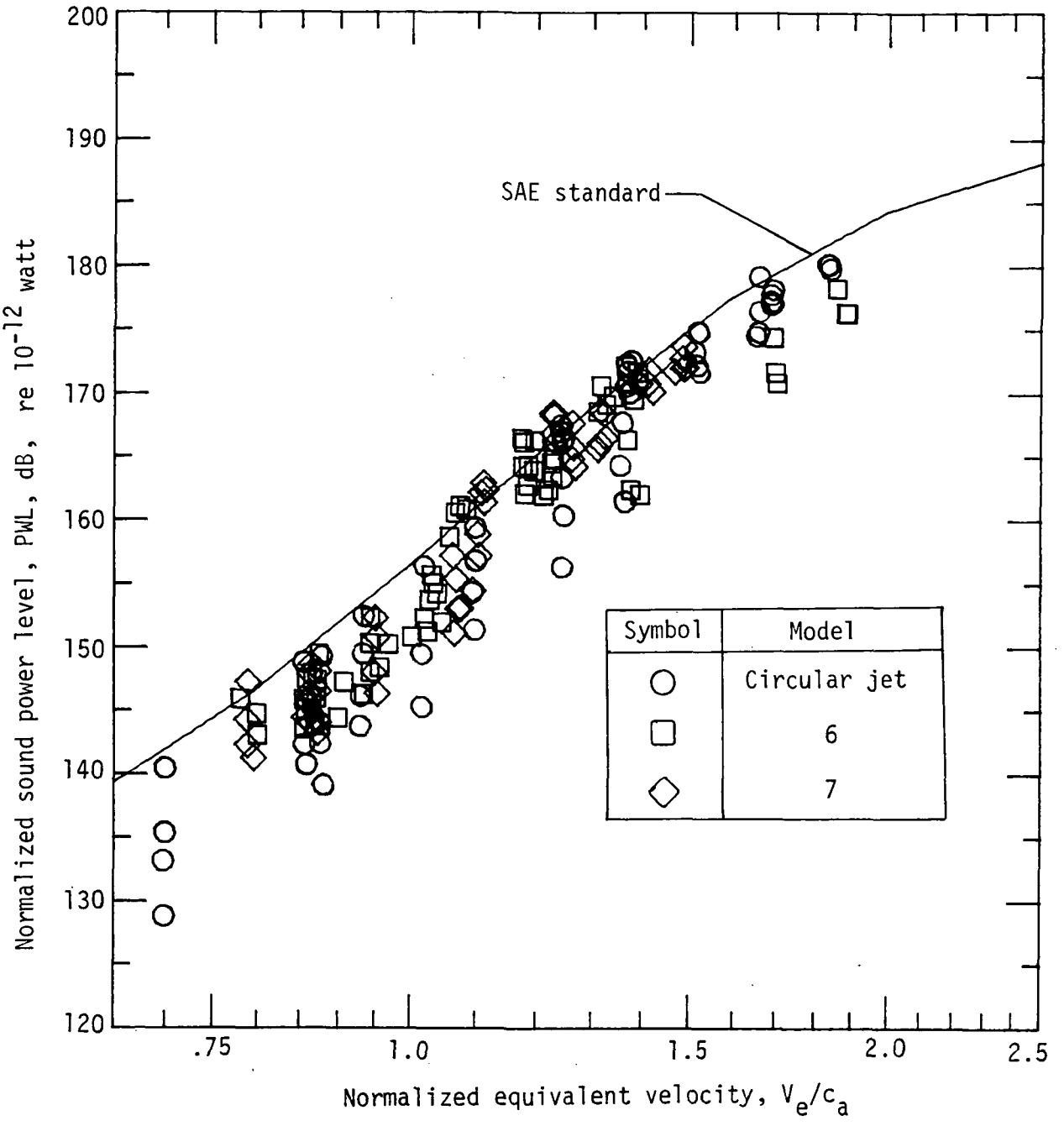

Figure 46.- Models 6 and 7 overall acoustic power levels with no forward velocity corrections.

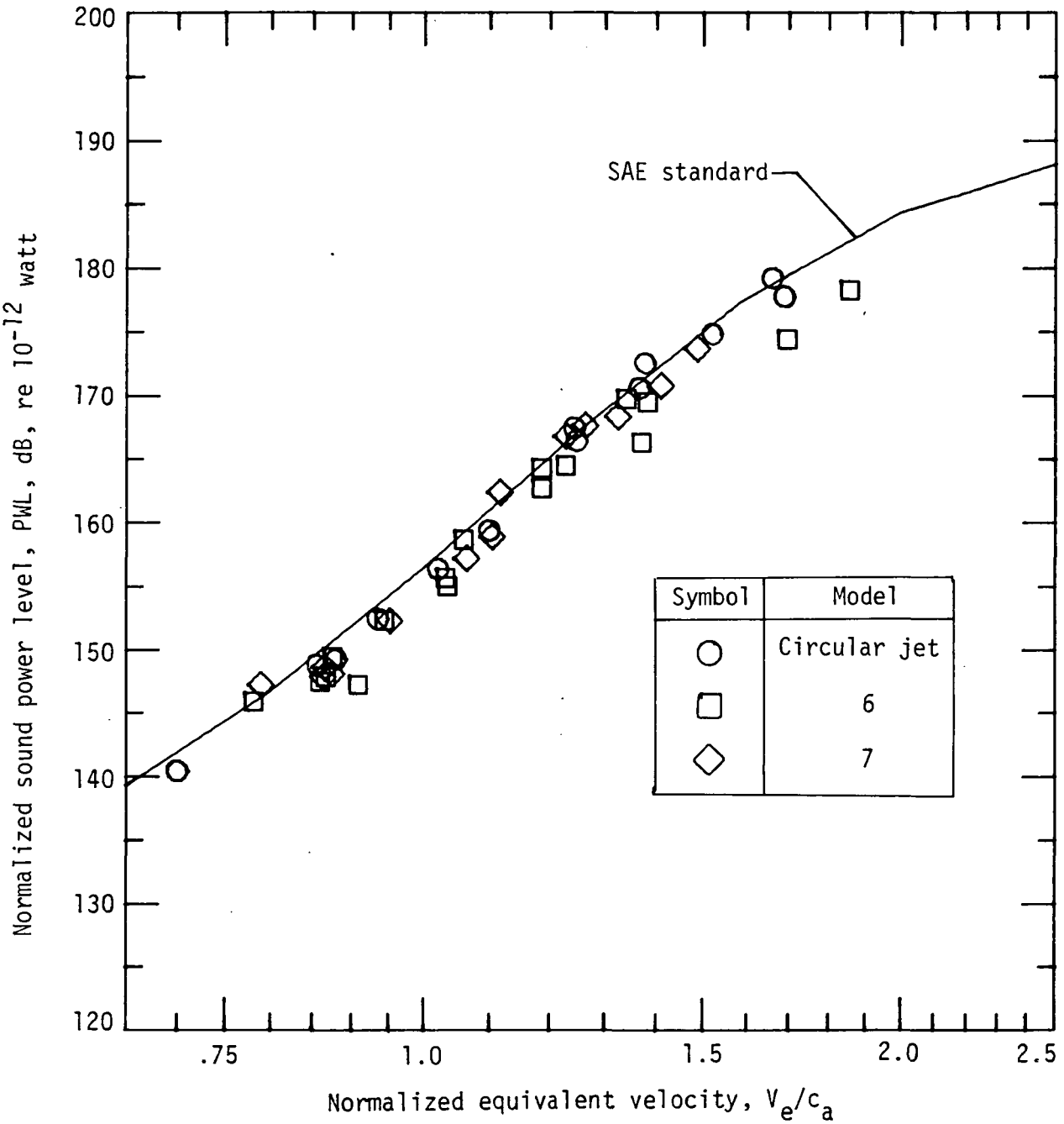

(a) Wind-tunnel velocity V_a near 8 m/s.

Figure 47.- Effect of forward velocity on uncorrected overall acoustic power levels for models 6 and 7.

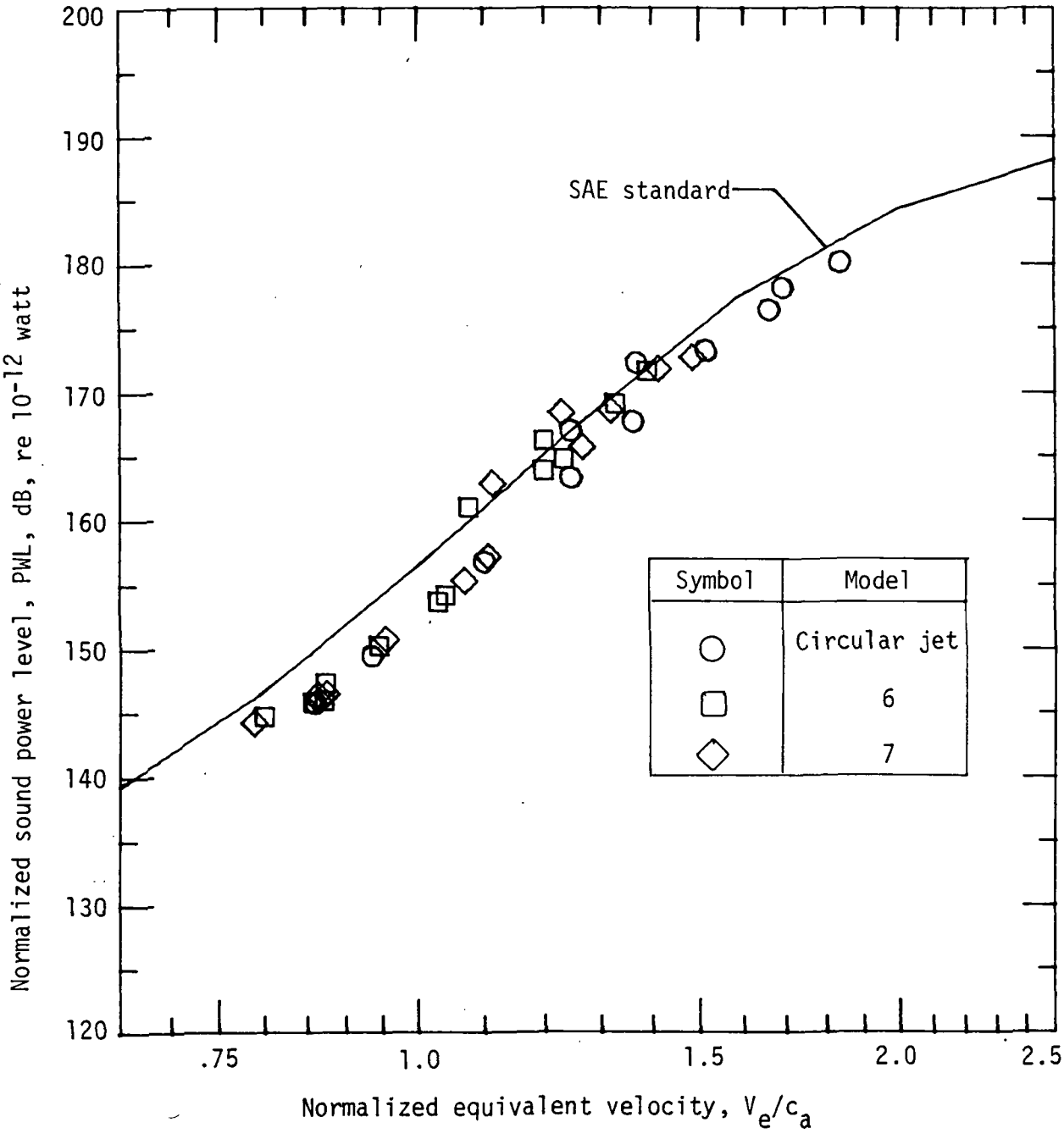

(b) Wind-tunnel velocity V_a near 30 m/s.

Figure 47.- Continued.

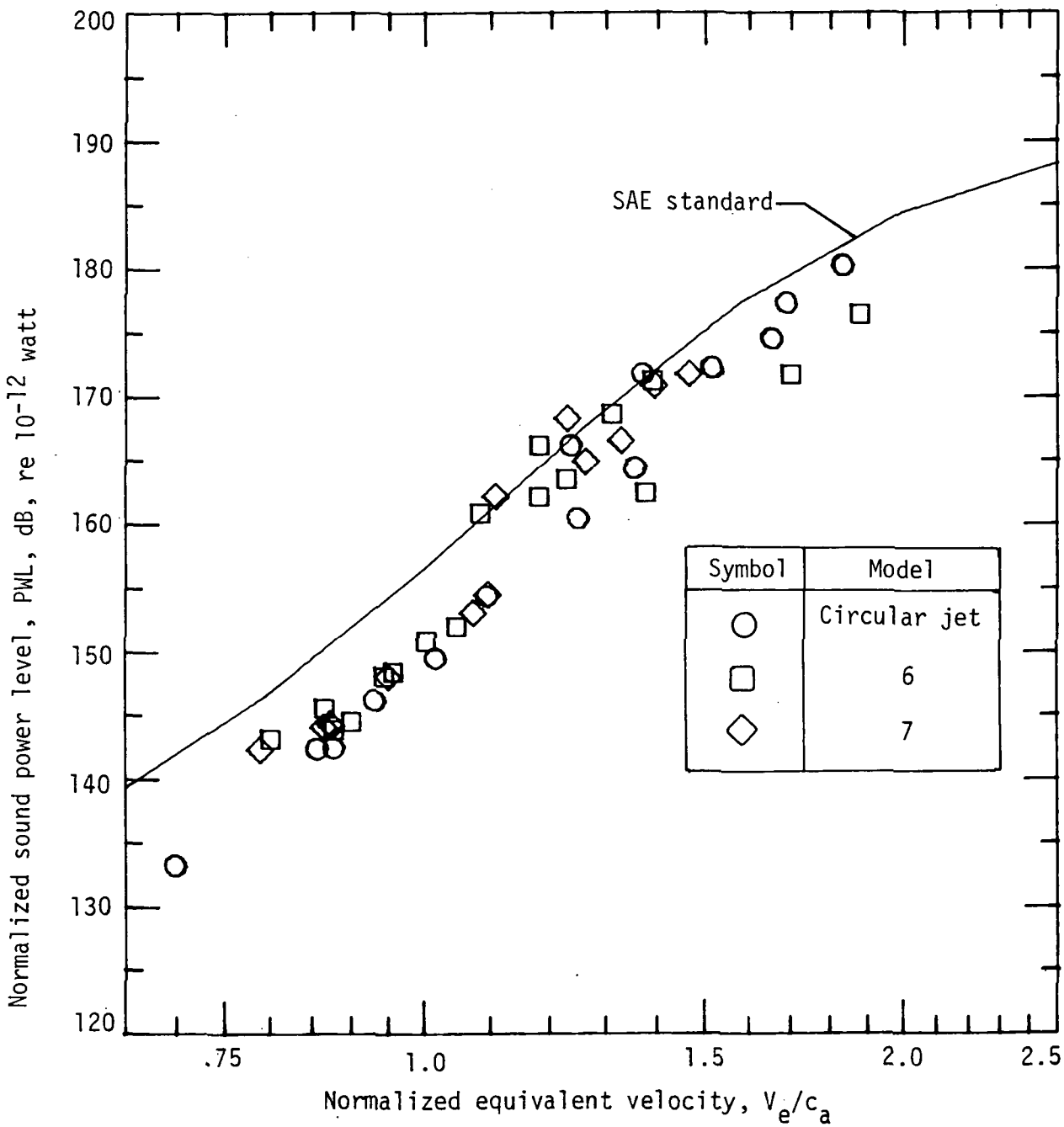

(c) Wind-tunnel velocity V_a near 61 m/s.

Figure 47.- Continued.

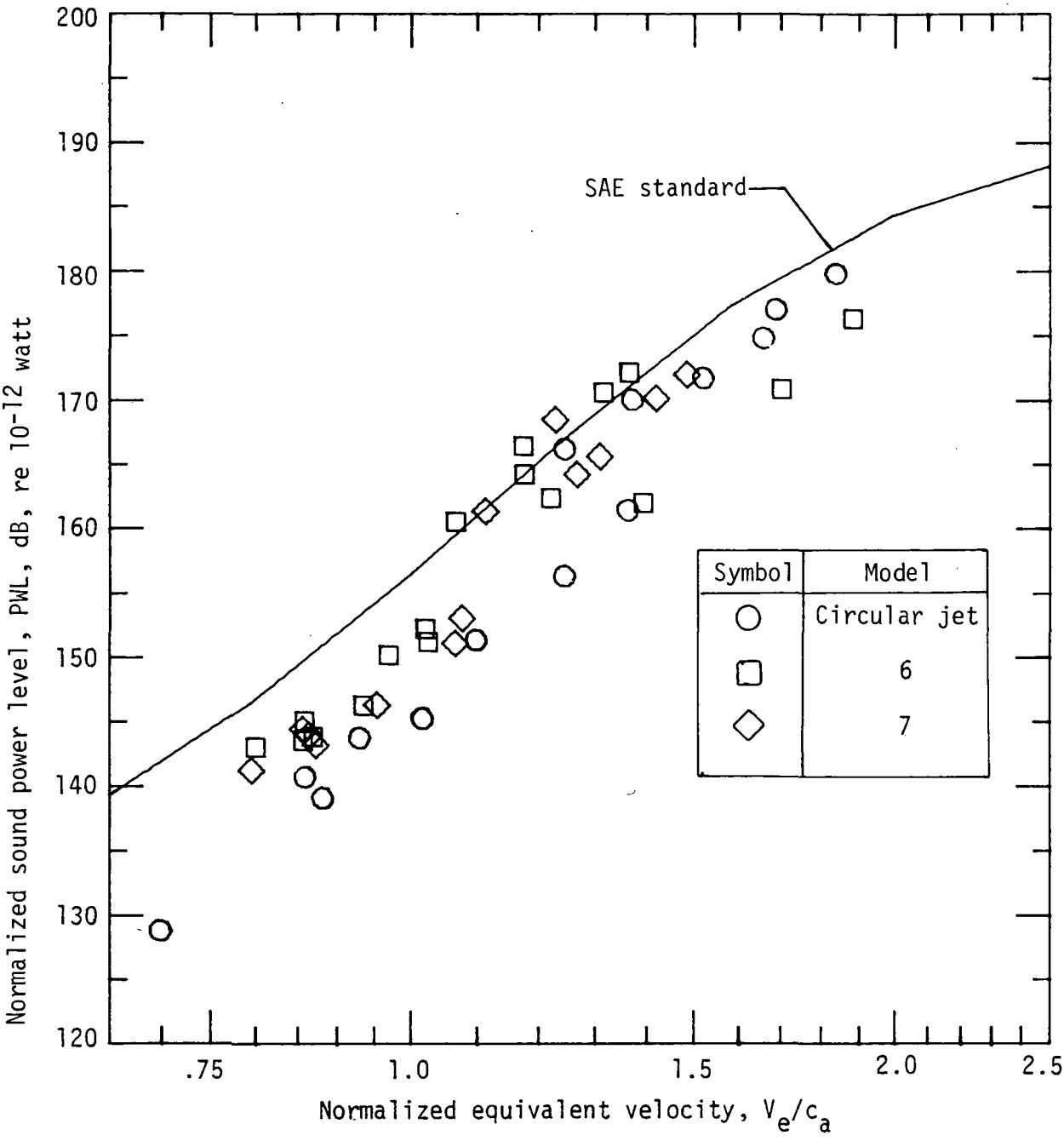

(d) Wind-tunnel velocity V_a near 102 m/s.

Figure 47.- Continued.

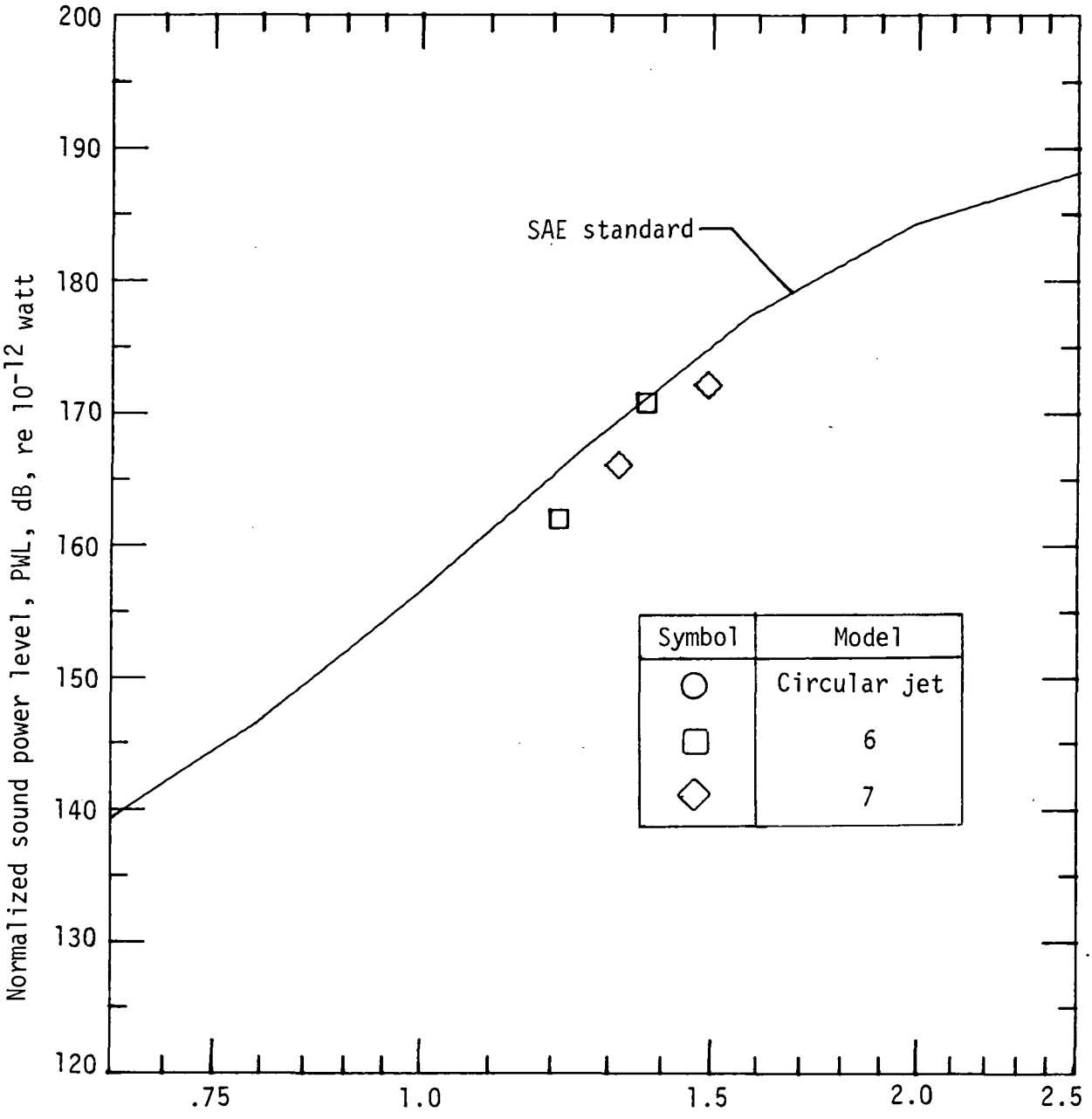

(e) Wind-tunnel velocity V_a near 130 m/s.

Figure 47.- Concluded.

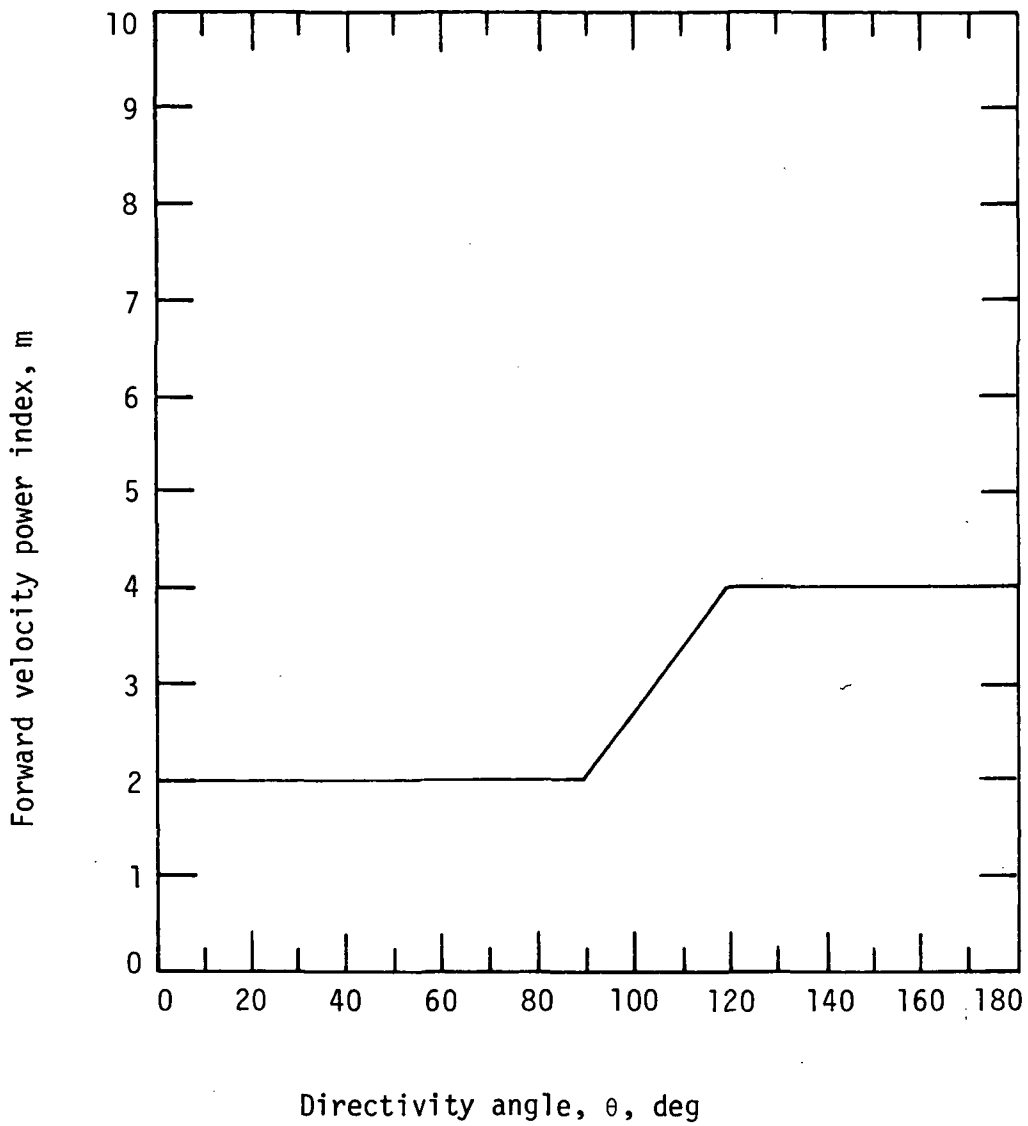

Figure 48.- Modified Stone forward velocity power index (ref. 11).

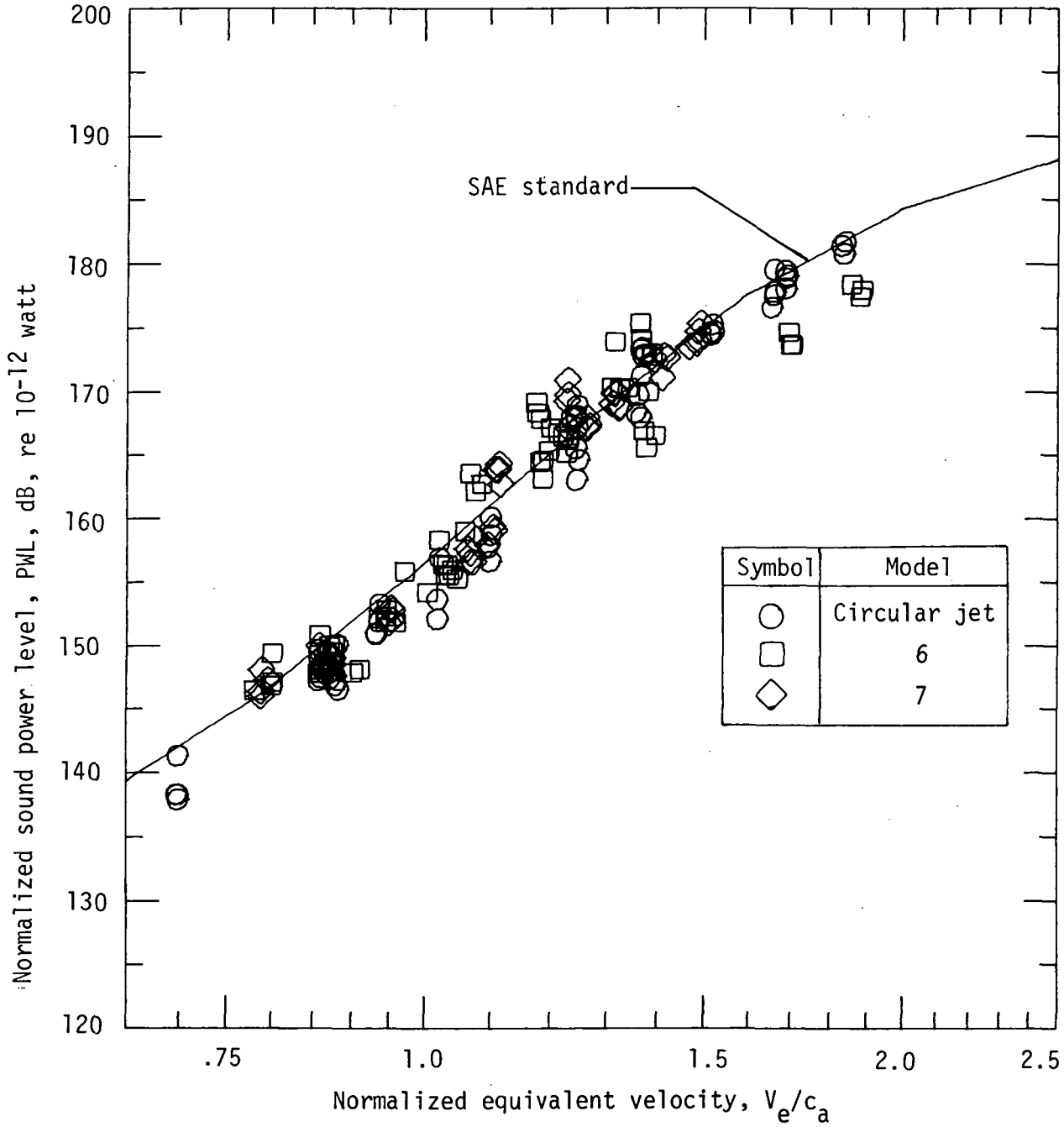

Figure 49.- Models 6 and 7 overall acoustic power levels with modified Stone forward velocity power index.

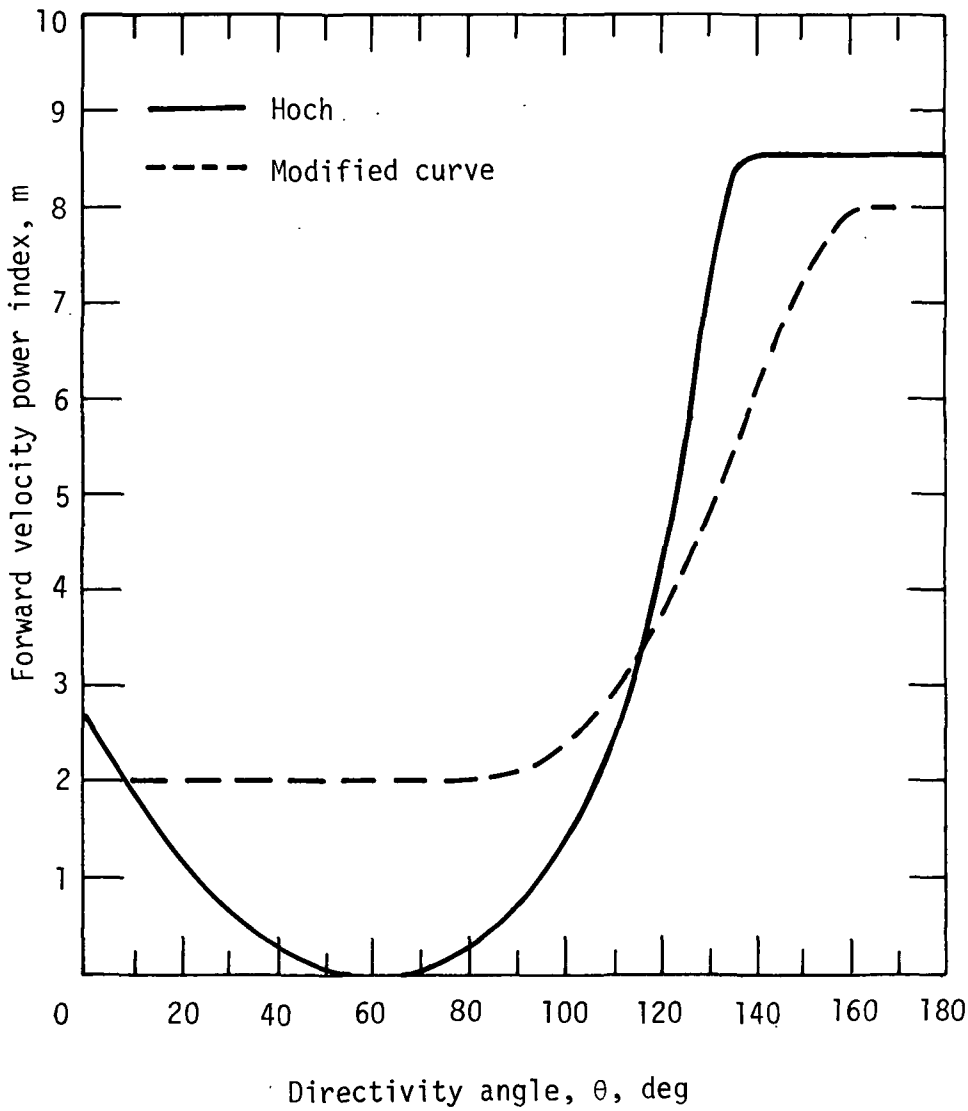

Figure 50.- Hoch forward velocity power index.

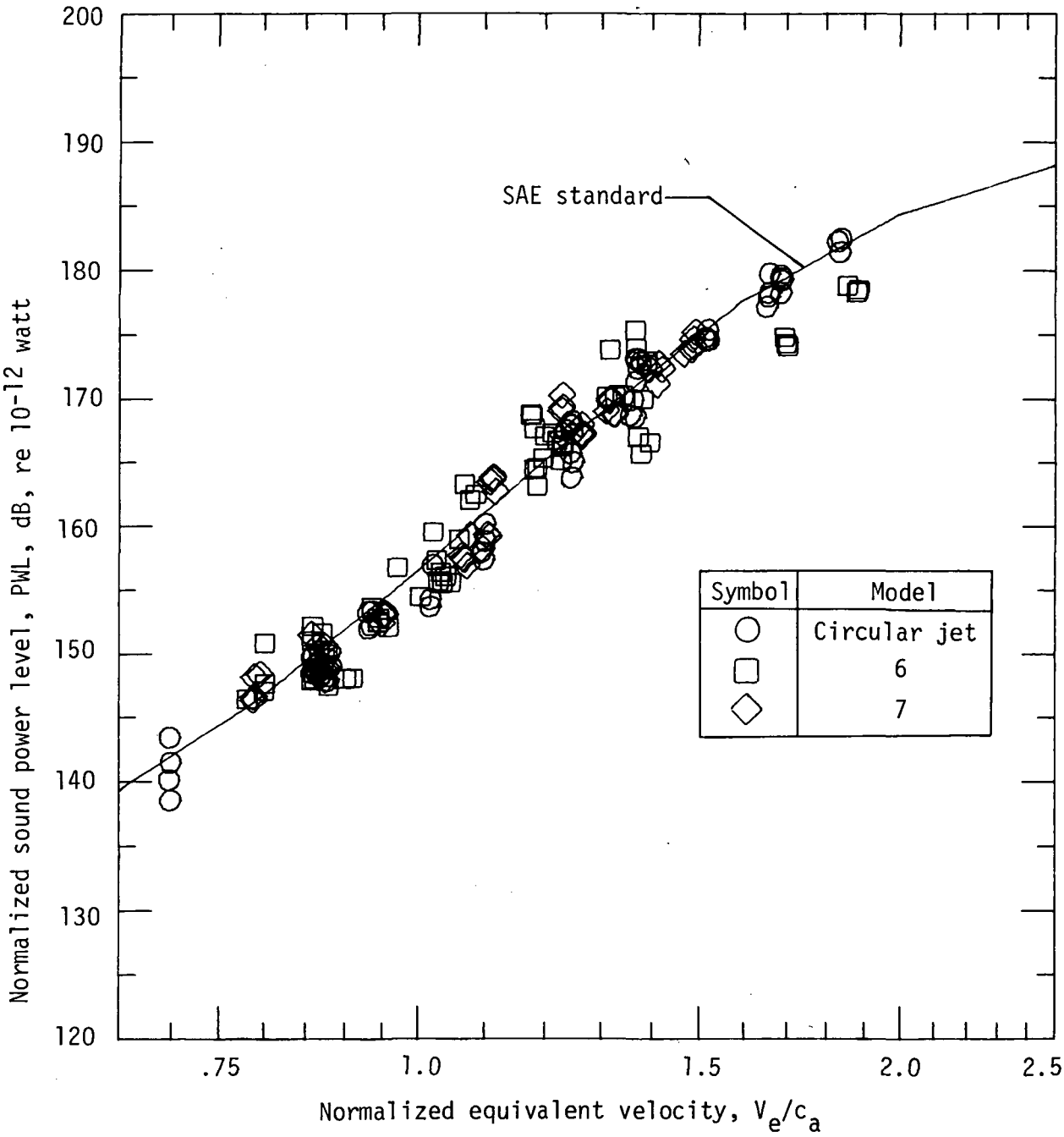

Figure 51.- Models 6 and 7 overall acoustic power levels with Hoch forward velocity power index.

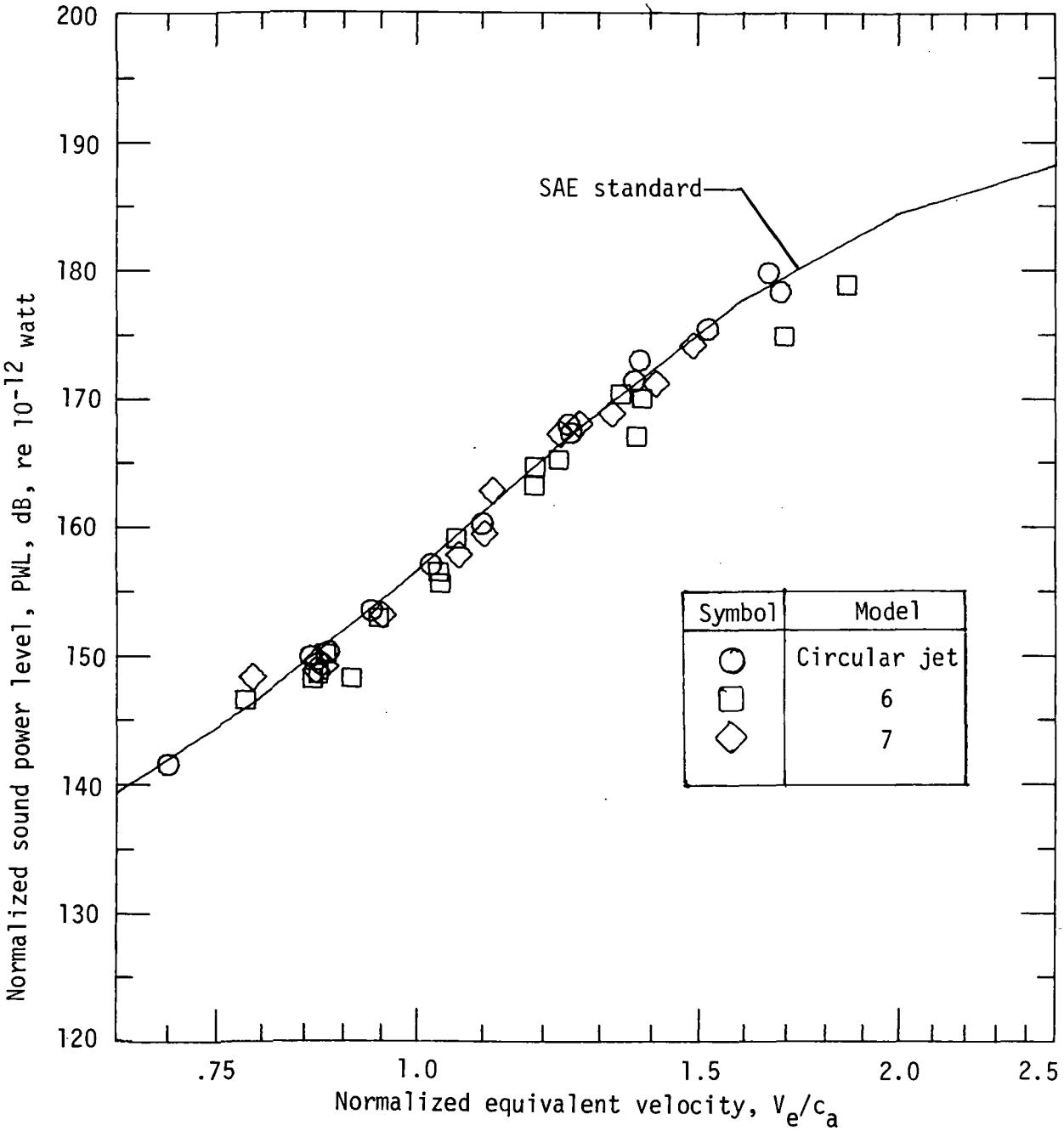

(a) Wind-tunnel velocity V_a near 8 m/s.

Figure 52.- Effect of forward velocity on acoustic power levels with Hoch forward velocity power index for models 6 and 7.

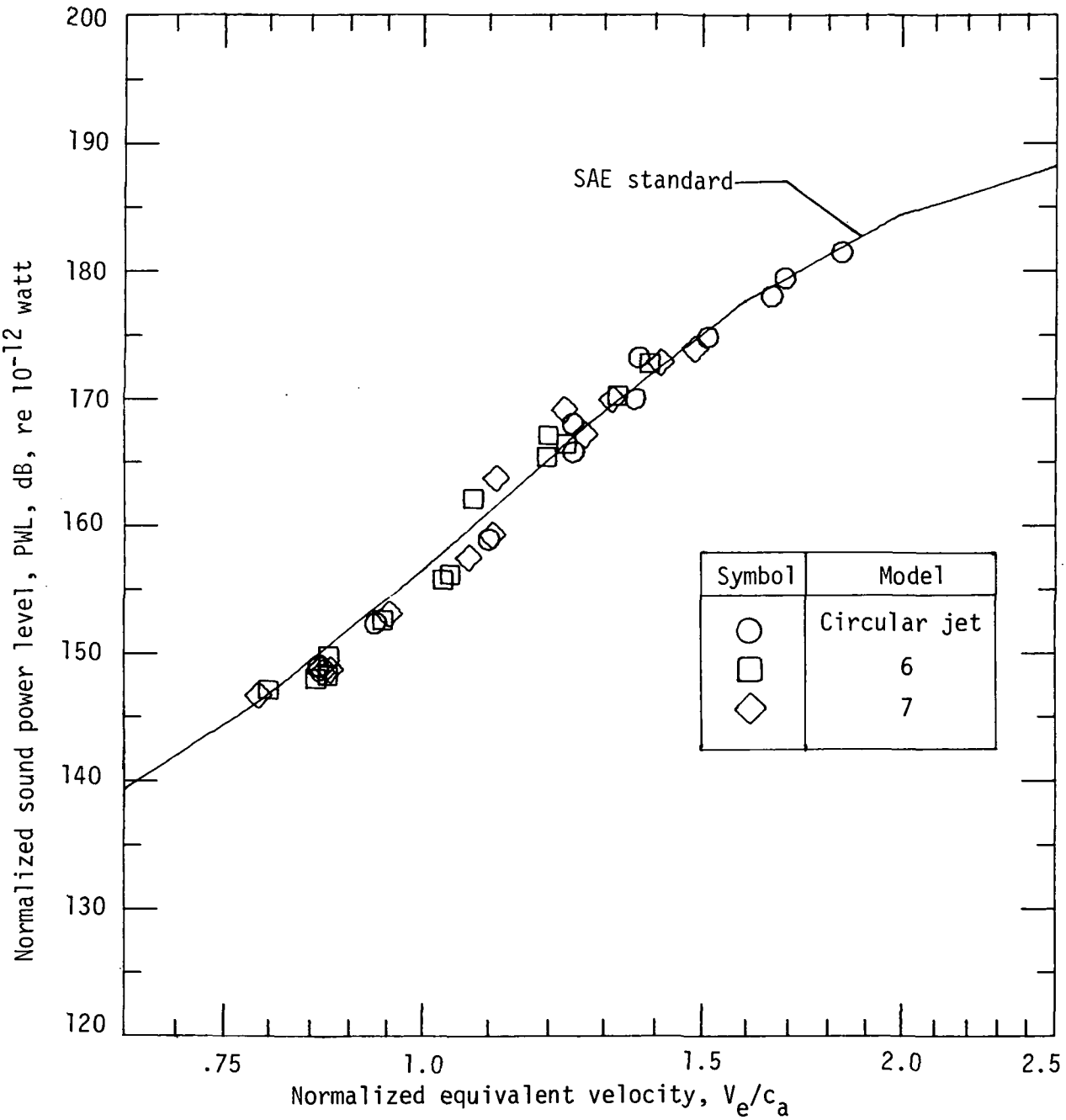

(b) Wind-tunnel velocity V_a near 30 m/s.

Figure 52.- Continued.

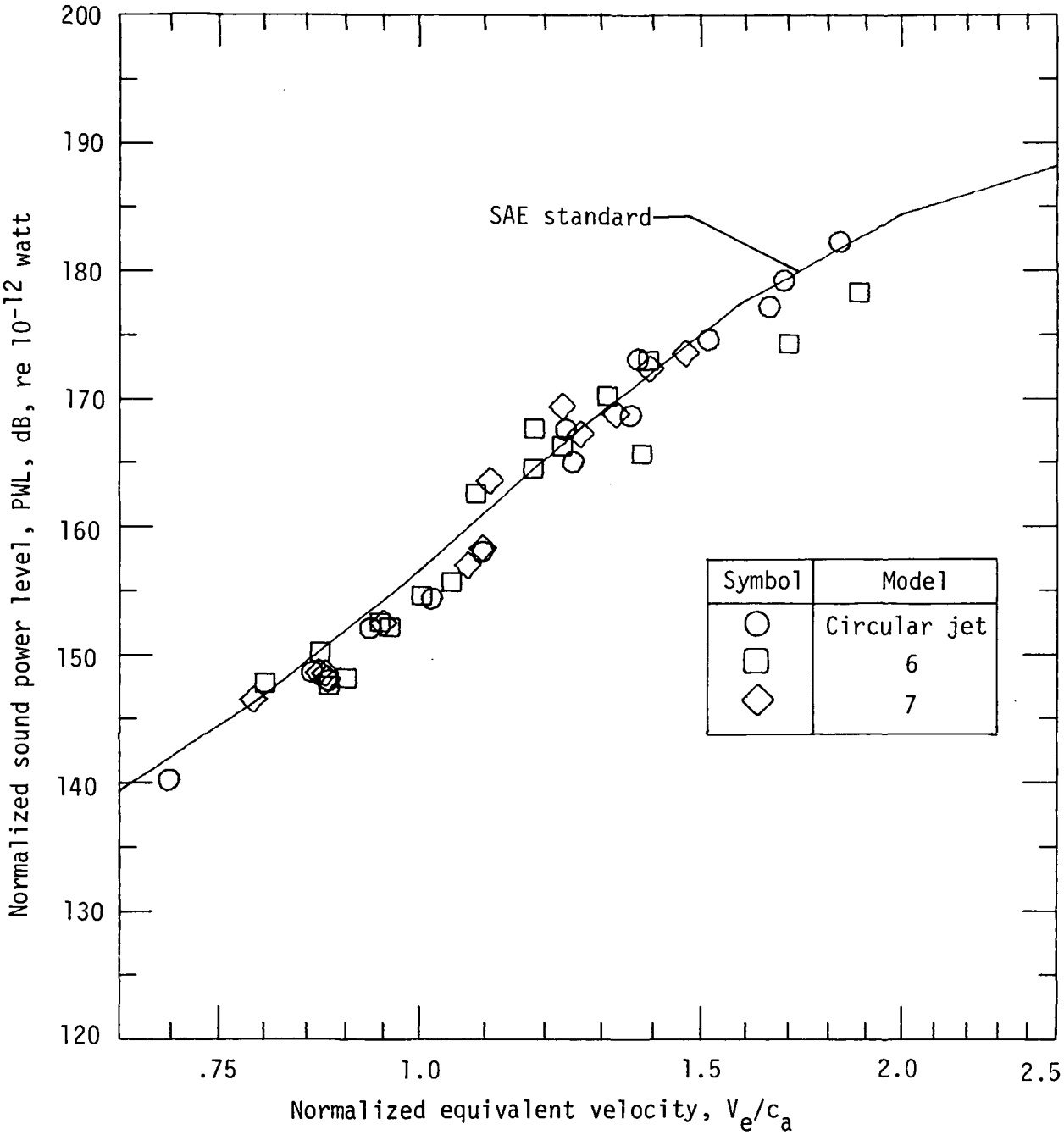

(c) Wind-tunnel velocity V_a near 61 m/s.

Figure 52.- Continued.

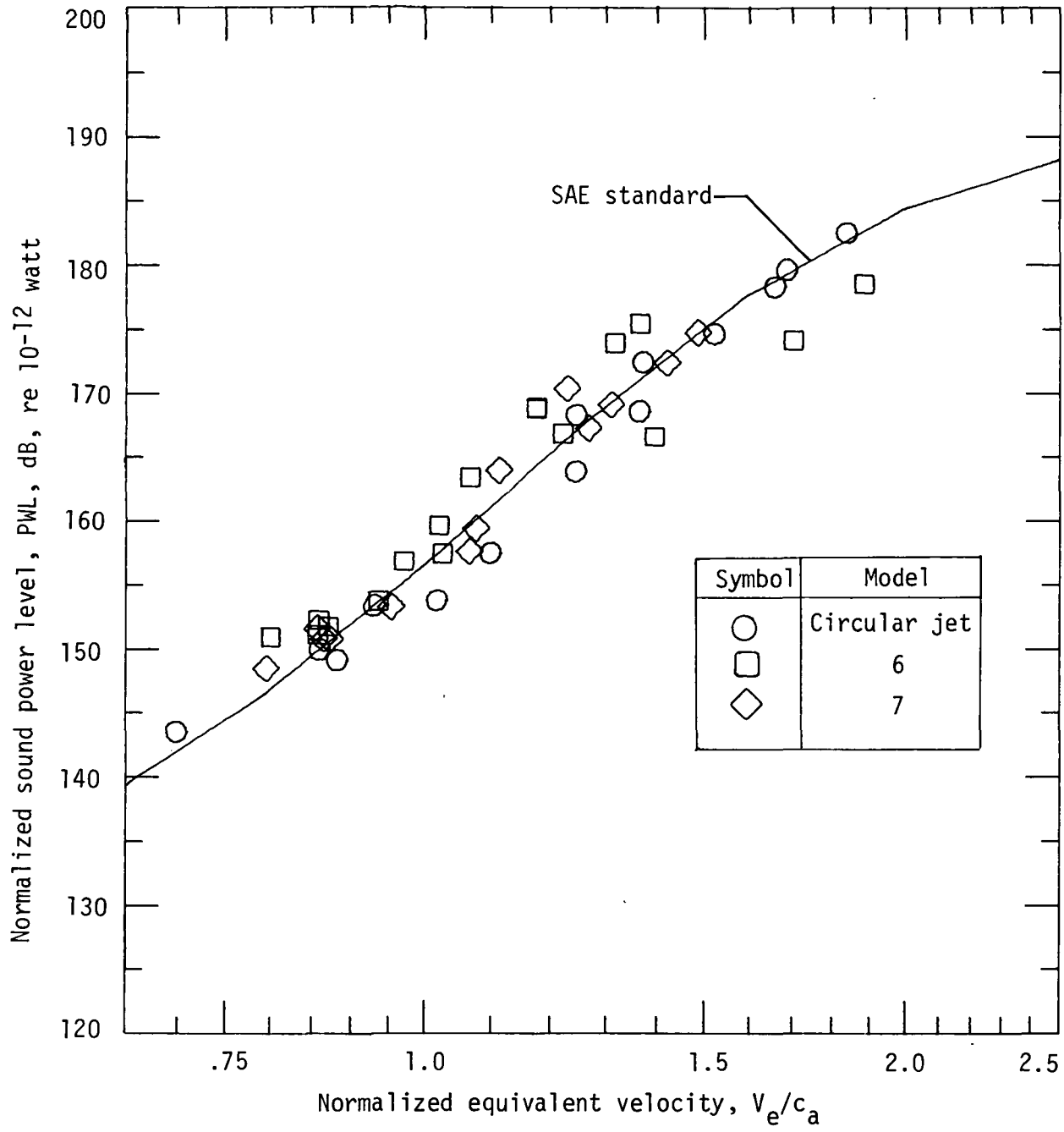

(d) Wind-tunnel velocity V_a near 102 m/s.

Figure 52.- Continued.

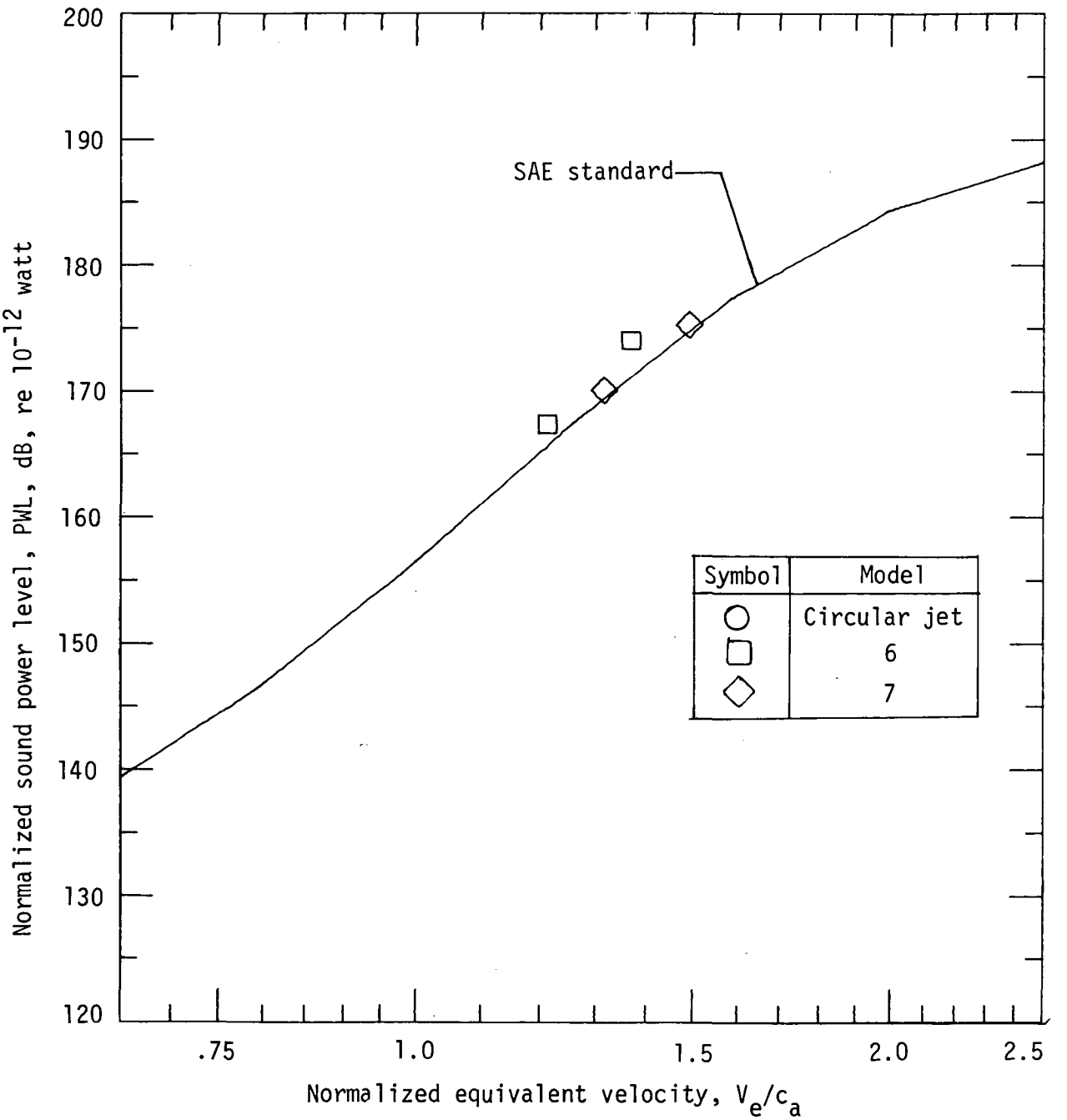

(e) Wind-tunnel velocity V_a near 130 m/s.

Figure 52.- Concluded.

1. Report No.	2. Government Accession No.	3. Recipient's Catalog No.
NASA TP-1301		

4. Title and Subtitle	5. Report Date
A CORRELATION OF MIXING NOISE FROM COANNULAR JETS WITH INVERTED FLOW PROFILES	April 1979
	6. Performing Organization Code
7. Author(s)	8. Performing Organization Report No.
S. Paul Pao	L-12155
	10. Work Unit No.
9. Performing Organization Name and Address	505-03-13-03
NASA Langley Research Center Hampton, VA 23665	11. Contract or Grant No.
	13. Type of Report and Period Covered
12. Sponsoring Agency Name and Address	Technical Paper
National Aeronautics and Space Administration Washington, DC 20546	14. Sponsoring Agency Code

15. Supplementary Notes

16. Abstract

This report correlates data for jet mixing noise from coannular jets with inverted flow velocity profiles (IVP's). The acoustic performance of coannular jets is compared to the performance of a hypothetical single jet with the same total mass flow, thrust, and total enthalpy flow as the coannular jet. The study shows that coannular jets with velocity ratios greater than 1.2 produce less noise than their corresponding equivalent jets and that optimum noise reduction of coannular jets in the data set occurs within a range of equivalent velocities between 500 and 700 meters per second and velocity ratios between 1.6 and 2.3. The maximum sound power reduction is found to be about 4 decibels.

Directivity indices and a special set of spectral curves have been developed to describe the characteristic double peak spectra of coannular jet noise. The temperature ratio between the inner and outer streams has not been found to be important in this acoustic correlation. However, the mean temperature effect has been included in the computations of sound pressure levels. Geometric variation of nozzle configuration and the associated effects on acoustics were not studied for this report.

17. Key Words (Suggested by Author(s))	18. Distribution Statement
Jet noise Variable cycle engine	Unclassified - Unlimited Subject Category 71

19. Security Classif. (of this report)	20. Security Classif. (of this page)	21. No. of Pages	22. Price*
Unclassified	Unclassified	125	$6.50

* For sale by the National Technical Information Service, Springfield, Virginia 22161

NASA-Langley, 1979

National Aeronautics and Space Administration

Washington, D.C.
20546

Official Business
Penalty for Private Use, $300

THIRD-CLASS BULK RATE

Postage and Fees Paid
National Aeronautics and
Space Administration
NASA-451

NASA

POSTMASTER: If Undeliverable (Section 158 Postal Manual) Do Not Return